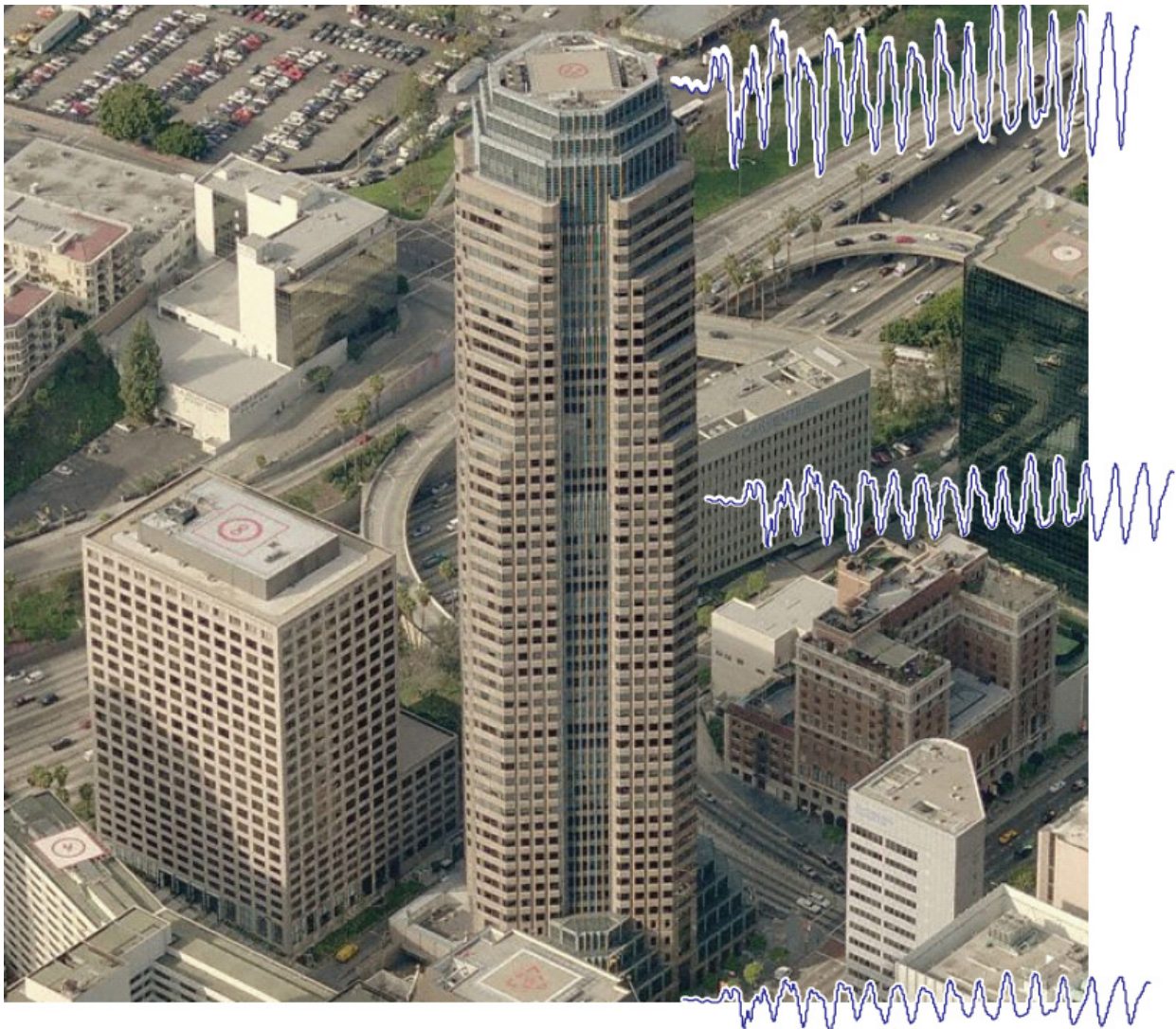


# Practical Guidelines to Select and Scale Earthquake Records for Nonlinear Response History Analysis of Structures

---

By Erol Kalkan and Anil K. Chopra



Open-File Report 2010-1068

U.S. Department of the Interior  
U.S. Geological Survey

**U.S. Department of the Interior**  
KEN SALAZAR, Secretary

**U.S. Geological Survey**  
Marcia K. McNutt, Director

U.S. Geological Survey, Reston, Virginia 2010

For product and ordering information:  
World Wide Web: <http://www.usgs.gov/pubprod/>  
Telephone: 1-888-ASK-USGS

For more information on the USGS—the Federal source for science about the Earth,  
its natural and living resources, natural hazards, and the environment:  
World Wide Web: <http://www.usgs.gov/>  
Telephone: 1-888-ASK-USGS

Suggested citation:  
Kalkan, E., and Chopra, A.K., 2010, Practical guidelines to select and scale earthquake  
records for nonlinear response history analysis of structures: U.S. Geological Survey  
Open-File Report 2010-1068, 124 p. [<http://pubs.usgs.gov/of/2010/1068/>].

Any use of trade, product, or firm names is for descriptive purposes only and does not  
imply endorsement by the U.S. Government.

Although this report is in the public domain, permission must be secured from the  
individual copyright owners to reproduce any copyrighted material contained within this  
report.

# Practical Guidelines to Select and Scale Earthquake Records for Nonlinear Response History Analysis of Structures

By Erol Kalkan<sup>1</sup> and Anil K. Chopra<sup>2</sup>

<sup>1</sup> United States Geological Survey, Earthquake Science Center, Menlo Park, CA, [ekalkan@usgs.gov](mailto:ekalkan@usgs.gov)

<sup>2</sup> University of California, Department of Civil Engineering, Berkeley, CA, [chopra@ce.berkeley.edu](mailto:chopra@ce.berkeley.edu)

## ABSTRACT

Earthquake engineering practice is increasingly using nonlinear response history analysis (RHA) to demonstrate performance of structures. This rigorous method of analysis requires selection and scaling of ground motions appropriate to design hazard levels. Presented herein is a modal-pushover-based scaling (MPS) method to scale ground motions for use in nonlinear RHA of buildings and bridges. In the MPS method, the ground motions are scaled to match (to a specified tolerance) a target value of the inelastic deformation of the first-“mode” inelastic single-degree-of-freedom (SDF) system whose properties are determined by first-“mode” pushover analysis. Appropriate for first-“mode” dominated structures, this approach is extended for structures with significant contributions of higher modes by considering elastic deformation of second-“mode” SDF system in selecting a subset of the scaled ground motions. Based on results presented for two bridges, covering single- and multi-span “ordinary standard” bridge types, and six buildings, covering low-, mid-, and tall building types in California, the accuracy and efficiency of the MPS procedure are established and its superiority over the ASCE/SEI 7-05 scaling procedure is demonstrated.

## **ACKNOWLEDGMENTS**

First author wishes to acknowledge the generous support of the Earthquake Engineering Research Institute in particular Prof. Thalia Anagnos, Mr. Marshall Lew and Prof. Jonathan Bray, the Federal Emergency Management Agency (FEMA) and the National Institute of Standards and Technology (NIST) in particular Dr. John (Jack) Hayes for the 2008 EERI/FEMA NEHRP Professional Fellowship in Earthquake Hazard Reduction.

Special thanks are extended to Prof. Rakesh Goel, Prof. Sashi K. Kunnath, Prof. Carlos Ventura and Dr. Emrah Erduran for their support in computer models. Drs. Roger Borchardt, Christine Goulet, Ayhan Irfanoglu, Farzin Zareian, Praveen Malhotra, Juan Carlos Reyes and Toorak Zokaie reviewed this report (or part of it) and provided their valuable suggestions.

# CONTENTS

- ABSTRACT ..... 1
- ACKNOWLEDGMENTS ..... 2
- 1. INTRODUCTION ..... 4
  - 1.1. RESEARCH OBJECTIVE ..... 6
- 2. MODAL-PUSHOVER-BASED SCALING ..... 7
  - 2.1. MPS PROCEDURE: SUMMARY ..... 7
  - 2.2. ESTIMATING SDF-SYSTEM INELASTIC DEFORMATION ..... 10
- 3. CODE-BASED SCALING PROCEDURE ..... 12
- 4. GROUND MOTION SELECTION PROCEDURE ..... 13
  - Magnitude Dependence ..... 13
  - Distance Dependence ..... 14
  - Soil Condition Dependence ..... 14
  - 4.1 GROUND MOTION ENSEMBLE ..... 14
- 5. EVALUATION OF MPS PROCEDURE: LOW- and MID-RISE BUILDINGS ..... 21
  - 5.1 SELECTED BUILDINGS ..... 21
  - 5.2. SYSTEMS ANALYZED ..... 23
  - 5.3 FIRST-“MODE” SDF-SYSTEM PARAMETERS ..... 24
  - 5.4. EVALUATION OF MPS CONCEPT ..... 24
  - 5.5. EVALUATION OF MPS AND CODE-BASED SCALING PROCEDURES ..... 25
  - 5.6. MULTI-MODE CONSIDERATIONS ..... 28
- 6. EVALUATION OF MPS PROCEDURE: TALL BUILDINGS ..... 53
  - 6.1 BUILDINGS SELECTED ..... 53
  - 6.2 ANALYTICAL MODELS AND CALIBRATION STUDIES ..... 55
  - 6.3. FIRST-“MODE” SDF-SYSTEM PARAMETERS ..... 57
  - 6.4. EVALUATION OF MPS PROCEDURE ..... 57
  - 6.5. MPS CONSIDERING SECOND-“MODE” ..... 59
  - 6.6. COMPARING MPS AND CODE-BASED SCALING PROCEDURES ..... 59
- 7. EVALUATION OF MPS PROCEDURE: SHORT - PERIOD BUILDING ..... 85
  - 7.1 BUILDING DETAILS AND ANALYTICAL MODEL ..... 85
  - 7.2. FIRST-“MODE” SDF-SYSTEM PARAMETERS ..... 86
  - 7.3. EVALUATION OF MPS PROCEDURE ..... 86
- 8. EVALUATION OF MPS PROCEDURE: “ORDINARY STANDARD” BRIDGES ..... 95
  - 8.1 DESCRIPTION OF BRIDGES AND ANALYTICAL MODELS ..... 95
  - 8.2 FIRST-“MODE” SDF-SYSTEM PARAMETERS ..... 98
  - 8.3 EVALUATION OF MPS PROCEDURE ..... 98
- 9. SUMMARY & CONCLUSIONS ..... 115
- 10. REFERENCES CITED ..... 117
- 11. NOTATION ..... 122
- 12. APPENDIX A: COMPUTATION OF MINIMUM SCALE FACTOR ..... 124

# 1. INTRODUCTION

Seismic evaluation of existing structures and of proposed design of new structures is usually based on nonlinear static (or pushover) analysis procedures, but nonlinear response history analysis (RHA) is now being increasingly used. In the latter approach, the seismic demands are determined by nonlinear RHA of the structure for several ground motions. Procedures for selecting and scaling ground motion records for a site-specific hazard are described in building codes (for example, IBC 2006 (ICBO, 2006) and CBC 2007 (ICBO, 2007)) and have been the subject of much research in recent years.

Current performance-based design and evaluation methodologies prefer intensity-based methods to scale ground motions over spectral matching techniques that modify the frequency content or phasing of the record to match its response spectrum to the target (or design) spectrum. In contrast, intensity-based scaling methods preserve the original non-stationary content and only modify its amplitude. The primary objective of intensity-based scaling methods is to provide scale factors for a small number of ground motion records so that nonlinear RHA of the structure for these scaled records is accurate, that is, it provides an accurate estimate in the median value of the engineering demand parameters (EDPs), and is efficient, that is, it minimizes the record-to-record variations in the EDP. Scaling ground motions to match a target value of peak ground acceleration (PGA) is the earliest approach to the problem, which produces inaccurate estimates with large dispersion in EDP values (Nau and Hall, 1984; Miranda, 1993; Vidic and others, 1994; Shome and Cornell, 1998). Other scalar intensity measures (IMs) such as: effective peak acceleration, Arias intensity and effective peak velocity have also been found to be inaccurate and inefficient (Kurama and Farrow, 2003). None of the preceding IMs consider any property of the structure to be analyzed.

Including a vibration property of the structure led to improved methods to scale ground motions, for example, scaling records to a target value of the first mode elastic spectral acceleration,  $A(T_1)$  from the code-based design spectrum or PSHA-based uniform hazard spectrum at the fundamental vibration period of the structure,  $T_1$ , provides improved results for structures whose response is dominated by their first-“mode” (Shome and others, 1998). However, this scaling method becomes less accurate and less efficient for structures responding significantly in their higher vibration modes or far into the inelastic range (Mehanny, 1999; Alavi and Krawinkler, 2000; Kurama and Farrow, 2003). To consider higher mode response, a scalar

IM that combines the spectral accelerations  $A(T_1)$  and  $A(T_2)$  at the first two periods and a vector IM comprised of  $A(T_1)$  and the ratio of  $A(T_1)/A(T_2)$  have been developed (Bazzurro, 1998; Shome and Cornell, 1999). Although this vector IM improves accuracy, it remains inefficient for near-fault records with a dominant velocity pulse (Baker and Cornell, 2006).

To recognize the lengthening of the apparent period of vibration due to yielding of the structure, a scalar IM defined as a combination of  $A(T_1)$  and  $A(cT_1)$  where  $c > 1$ , has been considered (Mehanny 1999; Cordova and others, 2000); alternatively, scaling earthquake records to minimize the difference between its elastic response spectrum and the target spectrum has been proposed (Kennedy and others, 1984; Malhotra, 2003; Alavi and Krawinkler, 2004; Naeim and others, 2004; Youngs and others, 2007).

International Building Code (IBC) (ICBO, 2006) and California Building Code (CBC) (ICBO, 2007) require that earthquake records be scaled according to the ASCE/SEI 7-05 provisions (ASCE, 2005). For two-dimensional analyses of regular structures, ground motions are scaled such that the average value of the 5%-damped elastic response spectra for a set of scaled motions is not less than the design response spectrum over the period range from  $0.2T_l$  to  $1.5T_l$ . For structures having plan irregularities or structures without independent orthogonal lateral load resisting systems where three-dimensional analyses need to be performed, ground motions should consist of appropriate horizontal components.

All the preceding scaling methods utilize IMs based on elastic response of the structure, but do not explicitly consider its inelastic response. They lead to scale factors that depend only on the structural period(s), independent of the structural strength. The elastic-response-based IMs may not be appropriate for near-fault sites where the inelastic spectral deformation can be significantly larger than corresponding elastic spectral deformation (Bozorgnia and Mahin, 1998; Alavi and Krawinkler, 2000; Baez and Miranda, 2000; Chopra and Chintanapakdee, 2004). This limitation has been overcome in recently proposed IMs based on the inelastic deformation spectrum, leading to improved estimate of the median EDPs and reduced dispersion of EDPs (Bazzurro and Luco, 2004; Luco and Cornell, 2007). Through incremental dynamic analyses, response of generic frames to different intensity levels of near-fault ground motions demonstrated that scaling records with the IM defined as the inelastic deformation of the first-“mode” inelastic SDF system is accurate, efficient and sufficient compared to elastic-response-

based IMs (Tothong and Luco, 2007; Tothong and Cornell, 2008). Required in this approach are attenuation relationships for the inelastic deformation with given ground motion properties (magnitude, fault distance, site condition, and so forth) and mean rate of occurrence of the hazard level considered (Tothong and Cornell, 2008).

## **1.1. RESEARCH OBJECTIVE**

The objective of this report is to develop a new practical method for selecting and scaling earthquake ground motion records in a form convenient for evaluating existing structures or proposed designs for new structures. The selection procedure presented considers the important characteristics of the ground motions (for example, pulse, directivity, fling, basin, duration) consistent with the hazard conditions. The scaling procedure presented explicitly considers structural strength and is based on the standard IM of spectral acceleration that is available from the USGS seismic hazard maps, where it is mapped for periods of 0.2 sec and 1.0 sec for the entire U.S. to facilitate construction of site-specific design spectrum (Petersen and others, 2008) or it can be computed from the uniform hazard spectrum obtained by probabilistic seismic hazard analysis (PSHA) for the site.

Based on modal pushover analysis, the procedure presented herein explicitly considers the strength of the structure, obtained from the first-“mode” pushover curve and determines scaling factors for each record to match a target value of the deformation of the first-“mode” inelastic SDF system estimated by established procedures. Appropriate for first-“mode” dominated structures, this approach is extended for structures with significant contributions of higher modes. Based on results presented for computer models of six actual buildings [4-story reinforced concrete (RC), 4-, 6-, 13-, 19- and 52-story steel special moment resisting frame (SMRF)] and two bridges [two span and multi-span], the effectiveness of this scaling procedure is established and its superiority over the ASCE/SEI 7-05 scaling procedure is demonstrated.

## **2. MODAL-PUSHOVER-BASED SCALING**

In the modal pushover-based scaling (MPS) procedure, each ground motion record is scaled by a scale factor selected to ensure that the peak deformation of the first-“mode” inelastic SDF system due to the scaled record is close enough to a target value of the inelastic deformation. The force-deformation relation for the first-“mode” inelastic SDF system is determined from the first-“mode” pushover curve. The target value of the inelastic deformation is the median deformation of the inelastic SDF system for a large ensemble of (unscaled) earthquake records compatible with the site-specific seismic hazard conditions. Nonlinear RHA of the inelastic SDF system provides the peak deformation of the system to each record in the ensemble, and the median of the data set provides the target value. Alternatively, the median deformation of the inelastic SDF system can be estimated as the deformation of the corresponding linearly elastic system, known directly from the target spectrum, multiplied by the inelastic deformation ratio; empirical equations for this ratio are available for systems with known yield-strength reduction factor (Chopra and Chintanapakdee, 2004).

For first-“mode” dominated structures, scaling earthquake records to the same target value of inelastic deformation is expected to be sufficient. Because higher vibration modes are known to contribute significantly to the seismic response of mid-rise and tall buildings, the MPS procedure checks for higher-mode compatibility of each record by comparing its scaled elastic spectral displacement response values at higher-mode vibration periods of the structure against the target spectrum. This approach ensures that each scaled earthquake record satisfies two requirements: (1) the peak deformation of the first-“mode” inelastic SDF system is close enough to the target value of the inelastic deformation; and (2) the peak deformation of the higher-mode elastic SDF system is not far from the target spectrum.

### **2.1. MPS PROCEDURE: SUMMARY**

The MPS procedure is summarized below in a step-by-step form:

1. For the given site, define the target pseudo-acceleration response spectrum either as the PSHA-based uniform hazard spectrum, or code-based design spectrum, or the median pseudo-acceleration spectrum for a large ensemble of (unscaled) earthquake records compatible with the site-specific seismic hazard conditions.

2. Compute the frequencies  $\omega_n$  (periods  $T_n$ ) and mode shape vectors  $\phi_n$  of the first few modes of elastic vibration of the structure.

### First-“mode” Dominated Structures

3. Develop the base shear-roof displacement  $V_{b1}-u_{r1}$  relation or pushover curve by nonlinear static analysis of the structure subjected to gradually increasing lateral forces with an invariant force distribution  $s_j^* = \mathbf{m}\phi_1$ , associated with the first-“mode”, where  $\mathbf{m}$  is the structural mass matrix. Gravity loads, including those present on the gravity frames, are applied before starting the pushover analysis.
4. Idealize the pushover curve and select a hysteretic model for cyclic deformations, both appropriate for the structural system and materials (Han and Chopra, 2005; Bobadilla and Chopra, 2007). Determine the yield-strength reduction factor  $R_y$  (equals strength required for the structure to remain elastic divided by the yield strength of the structure) from:  $R_y = M_1^* \bar{A}_1 / V_{b1y}$ , where  $M_1^*$  is the effective modal mass and,  $\bar{A}_1$  is the target spectral acceleration at the first-“mode” and  $V_{b1y}$  is the yield point value of base shear determined from the idealized pushover curve.
5. Convert the idealized pushover curve to the force-deformation  $F_{s1}/L_1 - D_1$  relation of the first-“mode” inelastic SDF system by utilizing  $F_{s1}/L_1 = V_{b1} / M_1^*$  and  $D_1 = u_{r1} / \Gamma_1 \phi_{r1}$  in which  $L_1 = \ddot{\mathbf{o}}_1 \mathbf{m} \mathbf{t}$ ,  $\phi_{r1}$  is the value of  $\phi_1$  at the roof,  $u_{r1}$  is the deck displacement of a bridge under first-“mode” pushover,  $\Gamma_1 = (\phi_1^* \mathbf{m} \mathbf{t}) / (\phi_1^* \mathbf{m} \phi_1)$  and each element of the influence vector  $\mathbf{t}$  is equal to unity.
6. For the first-“mode” inelastic SDF system, establish the target value of deformation  $\bar{D}_1'$  from  $\bar{D}_1' = C_R \bar{D}_1$ , where  $\bar{D}_1 = (T_1 / 2\pi)^2 \bar{A}_1$  and  $\bar{A}_1$  is the target pseudo-spectral acceleration at period  $T_1$  and  $C_R$  is determined from an empirical equation (shown in Section 2.2) for the inelastic deformation ratio corresponding to the yield-strength reduction factor  $R_y$ , determined in Step 4.

7. Compute the peak deformation  $D_1' = \max |D_1(t)|$  of the first-“mode” inelastic SDF system defined by the force deformation relation developed in Steps 4 and 5 and damping ratio  $\zeta_1$ . The initial elastic vibration period of the system is  $T_1 = 2\pi(L_1 D_{1y} / F_{s1y})^{1/2}$ . For a SDF system with known  $T_1$  and  $\zeta_1$ ,  $D_1'$  can be computed by nonlinear RHA due to one of the selected ground motions  $\ddot{u}_g(t)$  multiplied by a scale factor SF, to be determined to satisfy Step 8, by solving

$$\ddot{D}_1 + 2\zeta_1\omega_1\dot{D}_1 + F_{s1}D_1 / L_1 = -(\text{SF})\ddot{u}_g(t) \quad (2.1)$$

8. Compare the normalized difference between the target value of the deformation  $\bar{D}_1'$  of the first-“mode” inelastic SDF system (Step 6) and the peak deformation  $D_1'$ , determined in Step 7 against a specified tolerance,  $\varepsilon$

$$\Delta_1 = \left| \bar{D}_1' - D_1' \right| / \bar{D}_1' < \varepsilon \quad (2.2)$$

9. Determine the scale factor  $SF$  such that the scaled record  $(SF)\ddot{u}_g(t)$  satisfies the criterion of equation 2.2. Because equation 2.1 is nonlinear, SF cannot be determined *a priori*, but requires an iterative procedure starting with an initial guess. Starting with  $SF = 1$ , Steps 7 and 8 are implemented and repeated with modified values of SF until equation 2.2 is satisfied. Successive values of SF are chosen by trial and error or by a convergence algorithm, for example, Newton-Raphson iteration procedure. For a given ground motion, if equation 2.2 is satisfied by more than one SF, the SF closest to unity should be taken. Repeat Steps 7 and 8 for as many records as deemed necessary; obviously the scaling factor SF will be different for each record. These scaling factors will be shown to be appropriate for structures that respond dominantly in the first-“mode”.

### Second-“mode” Consideration

10. Establish target values of deformation of higher-mode SDF systems, treated as elastic systems, from the target spectrum  $\bar{D}_n = (T_n / 2\pi)^2 \bar{A}_n$ , where the mode number  $n = 2$ . We have found that the second-“mode” is mostly adequate for buildings susceptible to higher-mode effects.

11. By linear RHA, calculate the peak deformation  $D_2 \equiv \max_t |D_2(t)|$  of the *second-“mode”* elastic SDF system with known  $T_2$  and  $\zeta_2$  due to a selected ground motion  $\ddot{u}_g(t)$  multiplied by its scale factor SF determined in Step 9.

12. Compute the normalized difference between the target value of deformation  $\bar{D}_2$  (Step 10) and the peak deformation determined in Step 11.

$$\Delta_2 = |\bar{D}_2 - D_2| / \bar{D}_2 \quad (2.3)$$

and rank the scaled records based on their  $\Delta_2$  value; the record with the lowest  $\Delta_2$  is ranked the highest.

13. From the ranked list, select the final set of records with their scale factors determined in Step 9 to be used in nonlinear RHA of the structure.

## 2.2. ESTIMATING SDF-SYSTEM INELASTIC DEFORMATION

The inelastic deformation ratio  $C_R$  is required in Step 6 to estimate the deformation of the inelastic SDF system. Such equations were first developed by Veletsos and Newmark (1960) as a function of elastic vibration  $T_n$  and ductility factor  $\mu$ . However, in selecting and scaling ground motion records for nonlinear RHA of an existing building or of a proposed design of a new building, the inelastic deformation ratio should be expressed as a function of  $T_n$  and the yield-strength reduction factor  $R_y$ ; these quantities are determined in Steps 7 and 4 of the MPS procedure (Section 2.1), respectively. The inelastic deformation ratio can be expressed as a function of elastic vibration period and yield-strength reduction factor  $R_y$ . Response data for 216 ground motions recorded on NEHRP site classes B, C, and D demonstrated that the mean inelastic deformation ratio is influenced little by soil condition, by magnitude if  $R_y < 4$  (but significantly for larger  $R_y$ ), or by site-to-fault distance so long as it exceeds 10 km (Ruiz-Garcia and Miranda, 2002). Regression analysis of these data led to an equation for the inelastic deformation ratio as a function of  $T_n$  and  $R_y$ ; this equation is restricted to elastic perfectly plastic systems.

Median values of  $C_R$  have been presented for non-degrading bilinear hysteretic systems subjected to seven ensembles of far-fault ground motions (each with 20 records), representing large or small earthquake magnitude and distance, and NEHRP site classes, B, C, or D; and for two ensembles of near-fault ground motions. Regression analysis of these data led to the empirical equation (Chopra and Chintanapakdee, 2004):

$$C_R = 1 + \left[ (L_R - 1)^{-1} + \left( \frac{a}{R_y^b} + c \right) \left( \frac{T_1}{T_c} \right)^d \right]^{-1} \quad (2.4)$$

in which, the limiting value of  $C_R$  at  $T_n = 0$  is given by  $L_R$  as:

$$L_R = \frac{1}{R_y} \left( 1 + \frac{R_y - 1}{\alpha} \right) \quad (2.5)$$

where  $\alpha$  is the post-yield stiffness ratio and  $T_c$  is the period separating the acceleration and velocity-sensitive regions of the target spectrum; the parameters in equation 2.4 are:  $a=61$ ,  $b=2.4$ ,  $c=1.5$ , and  $d=2.4$ .

Equations (2.4) and (2.5) and values of their parameters are valid for far-fault ground motions, independent of (1) earthquake magnitude and distance, and (2) NEHRP site class B, C, and D; and also for near-fault ground motions.

### 3. CODE-BASED SCALING PROCEDURE

The procedures and criteria in the 2006 IBC (ICBO, 2006) and 2007 CBC (ICBO, 2007) for the selection and scaling of ground motions for use in nonlinear RHA of structures are based on the ASCE/SEI 7-05 provisions (ASCE, 2005). According to ASCE/SEI 7-05, earthquake records should be selected from events of magnitudes, fault distance and source mechanisms that comply with the maximum considered earthquake. If the required number of appropriate records is not available, appropriate simulated ground motions may be included to make up the total number required.

For two-dimensional analysis of symmetric-plan buildings, ASCE/SEI 7-05 requires intensity-based scaling of ground motion records using appropriate scale factors so that the average value of the 5%-damped response spectra for the set of scaled records is not less than the design response spectrum over the period range from  $0.2T_1$  to  $1.5T_1$ . The design value of an engineering demand parameter (EDP)—member forces, member deformations or story drifts—is taken as the average value of the EDP over seven (or more) ground motions, or its maximum value over all ground motions, if the system is analyzed for fewer than seven ground motions.

The ASCE/SEI 7-05 scaling procedure does not insure a unique scaling factor for each record; obviously, various combinations of scaling factors can be defined to insure that the average spectrum of scaled records remains above the design spectrum (or amplified spectrum in case of 3-D analyses) over the specified period range. Because it is desirable to scale each record by the scale factor closest to unity, an algorithm is developed (given in Appendix A) and used in applying the code-scaling procedure in Section 4.

## 4. GROUND MOTION SELECTION PROCEDURE

Both record selection and scaling are important processes for success of any nonlinear RHA applied. Appositely selecting records considering the hazard conditions for a given site helps to reduce the dispersion of EDPs and increase accuracy by achieving better estimates of the “true median”. Before scaling ground motions, one needs to define the hazard conditions associated with a given site either through deterministic or probabilistic site-specific hazard analysis or alternatively from the USGS seismic hazard maps. The parameters that need to be considered in identifying the scenario conditions are those that have the most influence on ground motion spectral shape (Graizer and Kalkan, 2009):

- Magnitude range of anticipated significant event(s)
- Distance range of the site from the causative fault(s)
- Site-condition (site-geology generally described by average shear-wave velocity within 30 m of crust)
- Basin effect (if basin exists)
- Directivity effect

Spectral shape (that is, response spectrum normalized by PGA) defines ground motion demand characteristic on MDF systems. Therefore in selecting candidate records for nonlinear RHAs, one needs to carefully identify records whose spectral shapes are close to each other. The dependence of ground motion spectral shape on the first three parameters above is explained in detail in the following:

### **Magnitude Dependence**

In general, events with larger magnitude yield wider response spectra. In order to find the degree of magnitude influence on response spectral shape, average spectral shapes of earthquakes ranging from magnitude 4.9 to 7.9 in the extended NGA database (Graizer and Kalkan, 2009) are plotted in figure 4.1. As shown, the spectral peak gradually shifts from ~0.15 sec for the lowest magnitude earthquake (M4.9) to ~0.5 sec for the largest events (M7.6 - 7.9). Maximum

amplitudes of the average spectral shape are relatively stable varying from 2.3 to 2.6, with higher amplitudes at smaller magnitudes.

### **Distance Dependence**

As reported in previous studies (for example, Abrahamson and Silva 1997), predominant period shifts to higher values with increase in distance from the fault for a given earthquake. Figure 4.2 depicts such a distance dependence on the spectral shape whereby variations of maximum period for different distance bins are plotted for the 1999 M7.6 Chi-Chi earthquake. For this particular event, predominant period shifts from about 0.35 sec at the closest distances (0-20 km bin) to 1.2 sec at farthest fault distances (120-140 km bin).

### **Soil Condition Dependence**

In addition to magnitude and distance dependence, spectral shape also depends on site conditions. Predominant period of spectral shape from a rock site is generally lower than that for a soil site. This tendency is shown in figure 4.3, which compares the average spectral shape in  $V_{S30}$  bin of 180-360 m/sec with that of 540-720 m/sec. At short periods, spectral shape of average rock site remains above that of average soft-soil, while the reverse is observed beyond the spectral period of 0.3 sec. Unlike predominant period shifting to higher values with reduction in  $V_{S30}$ , peak values of spectral shapes remain similar.

## **4.1 GROUND MOTION ENSEMBLE**

In order to test the MPS procedure, a total of twenty-one near-fault strong earthquake ground motions were compiled from the Next Generation Attenuation project earthquake ground motion database (Power and others, 2006). These motions were recorded during seismic events with moment magnitude,  $M \geq 6.5$  at closest fault distances,  $R_{cl} \leq 12$  km and belonging to NEHRP site classification C and D. The selected ground motion records and their characteristic parameters are listed in table 4.1.

Shown in figure 4.4 are the pseudo-acceleration response spectrum for each ground motion and the median of the 21 response spectra. The median spectrum is taken to be the design spectrum for purposes of evaluating the MPS procedure.

The median spectrum of the ground motion ensemble is presented next in figure 4.5 as a four-way logarithmic plot, together with its idealized version (dashed-line). The idealized spectrum is divided into three period ranges: the long-period region to the right of point  $d$ ,  $T_n > T_d$ , is called the displacement-sensitive region; the short-period region to the left of point  $c$ ,  $T_n < T_c$ , is called the acceleration-sensitive region; and the intermediate-period region between points  $c$  and  $d$ ,  $T_c < T_n < T_d$ , is called the velocity-sensitive region (Chopra, 2007; Section 6.8). Note that the nearly constant velocity region is unusually narrow, which is typical of near-fault ground motions.

**Table 4.1 Selected earthquake ground motions**

No.	Earthquake	Year	Station	R <sub>cl</sub>		V <sub>S30</sub> (m/s)	PGA (g)	PGV (cm/s)	PGD (cm)
				M	(km)				
1	Tabas, Iran	1978	Tabas	7.4	2.1	767	0.85	110.3	61.1
2	Imperial Valley	1979	EC Meloland Overpass FF	6.5	0.1	186	0.31	79.3	28.1
3	Imperial Valley	1979	El Centro Array #7	6.5	0.6	211	0.42	80.2	41.0
4	Superstition Hills	1987	Parachute Test Site	6.5	1.0	349	0.46	74.8	36.3
5	Loma Prieta	1989	LGPC	6.9	3.9	478	0.78	77.2	42.7
6	Erzincan, Turkey	1992	Erzincan	6.7	4.4	275	0.49	72.9	24.8
7	Northridge	1994	Jensen Filter Plant	6.7	5.4	373	0.75	77.8	31.9
8	Northridge	1994	Newhall - W Pico Canyon Rd	6.7	5.5	286	0.39	76.6	43.1
9	Northridge	1994	Rinaldi Receiving Sta	6.7	6.5	282	0.63	109.2	28.3
10	Northridge	1994	Sylmar - Converter Sta	6.7	5.4	251	0.75	109.4	45.8
11	Northridge	1994	Sylmar - Converter Sta East	6.7	5.2	371	0.68	87.3	31.7
12	Northridge	1994	Sylmar - Olive View Med FF	6.7	5.3	441	0.71	97.4	22.4
13	Kobe, Japan	1995	Port Island	6.9	3.3	198	0.26	62.3	29.6
14	Kobe, Japan	1995	Takatori	6.9	1.5	256	0.65	118.8	33.4
15	Kocaeli, Turkey	1999	Yarimca	7.4	4.8	297	0.31	60.5	54.7
16	Chi-Chi, Taiwan	1999	TCU052	7.6	0.7	579	0.35	131.9	183.2
17	Chi-Chi, Taiwan	1999	TCU065	7.6	0.6	306	0.68	99.5	81.8
18	Chi-Chi, Taiwan	1999	TCU068	7.6	0.3	487	0.54	206.1	336.3
19	Chi-Chi, Taiwan	1999	TCU084	7.6	11.2	553	0.79	92.7	28.8
20	Chi-Chi, Taiwan	1999	TCU102	7.6	1.5	714	0.24	93.9	65.7
21	Duzce, Turkey	1999	Duzce	7.2	6.6	276	0.42	71.0	46.3

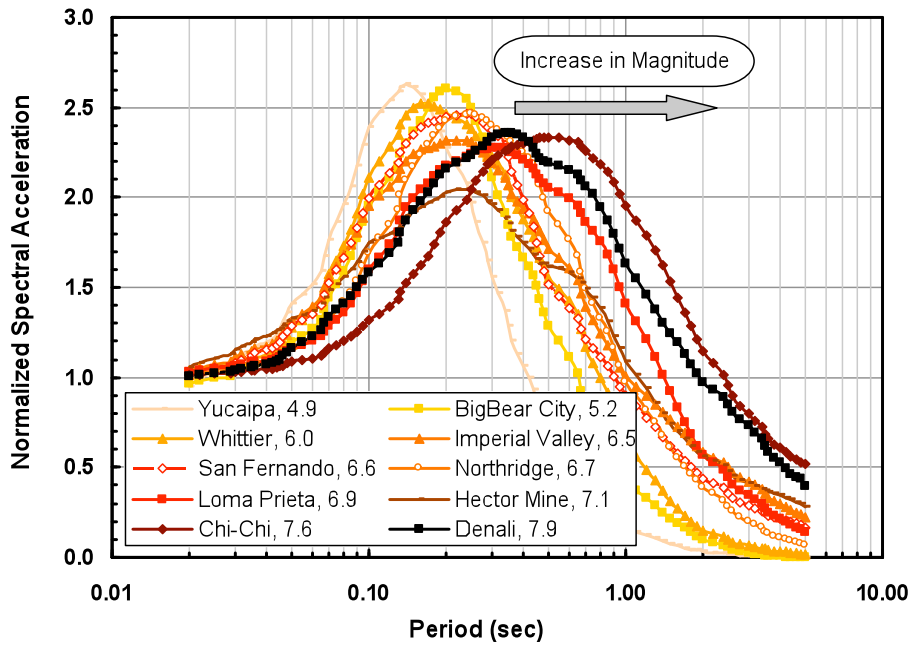


**Figure 4.1** Comparison of average spectral shape of earthquakes in magnitude range of 4.9 to 7.9 (Increase in magnitude shifts the predominant period to higher values).

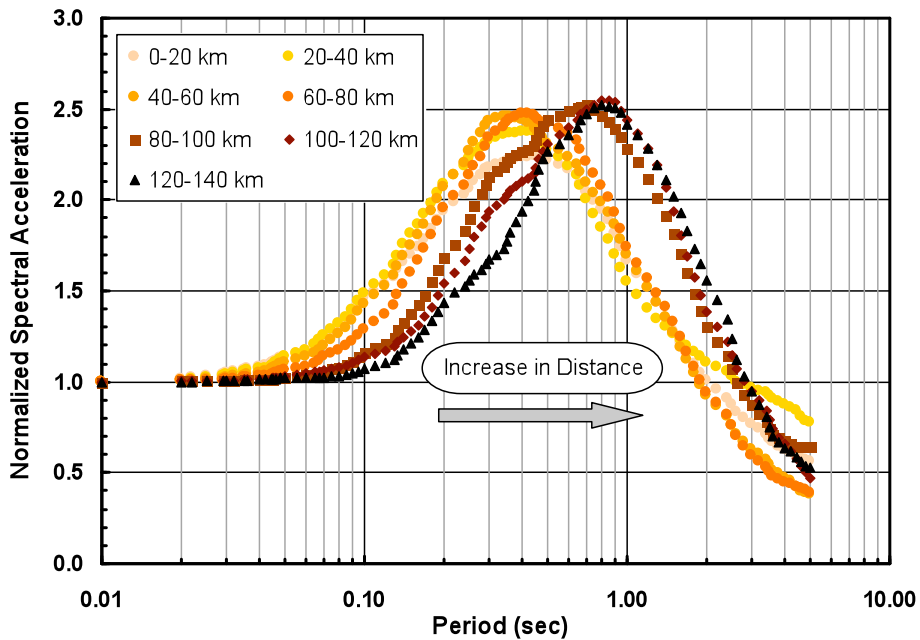


**Figure 4.2** Shift of predominant period of average spectral shape to higher values with increase in average distance within each 20 km distance bin (Data values correspond to the 1999 M7.6 Chi-Chi earthquake).

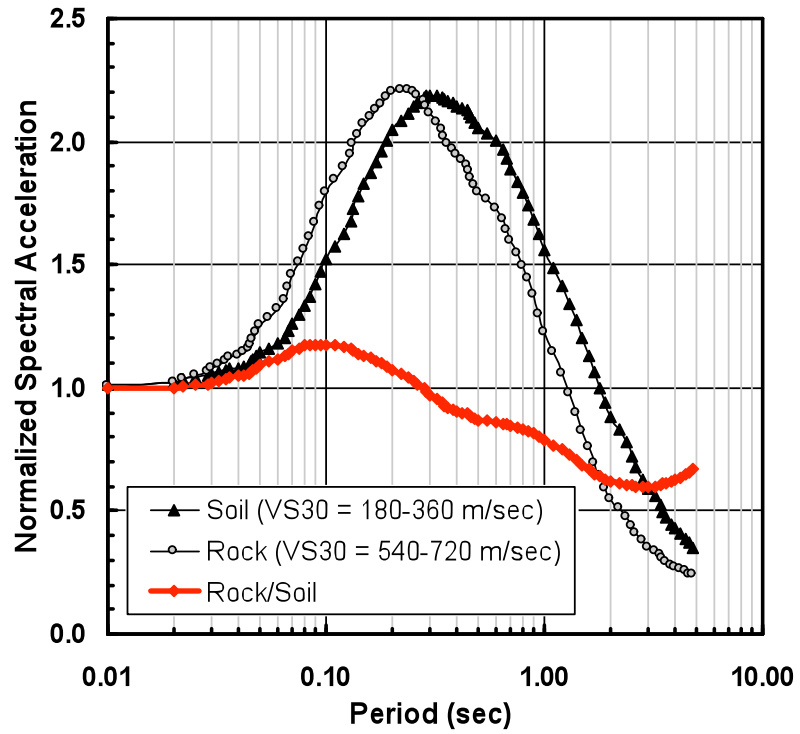


**Figure 4.3** Comparison of average “rock” and “soil” spectral shapes and their transfer function (Rock/Soil).

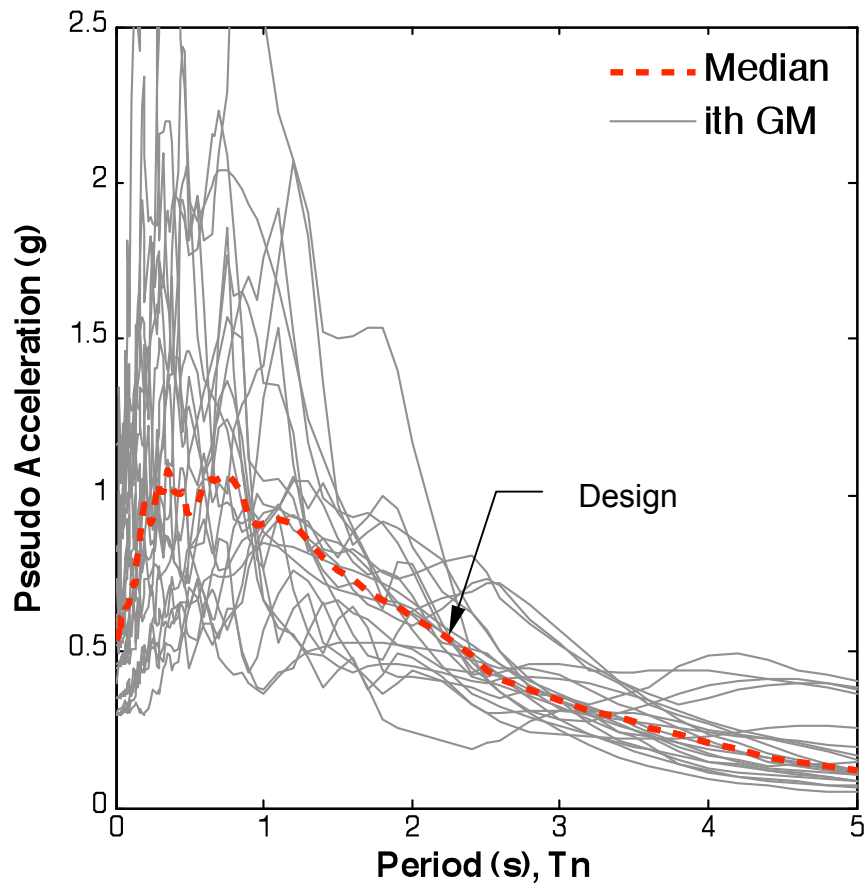


Figure 4.4 Individual response spectra for 21 ground motions and their median response spectrum;  $\zeta = 5\%$ .

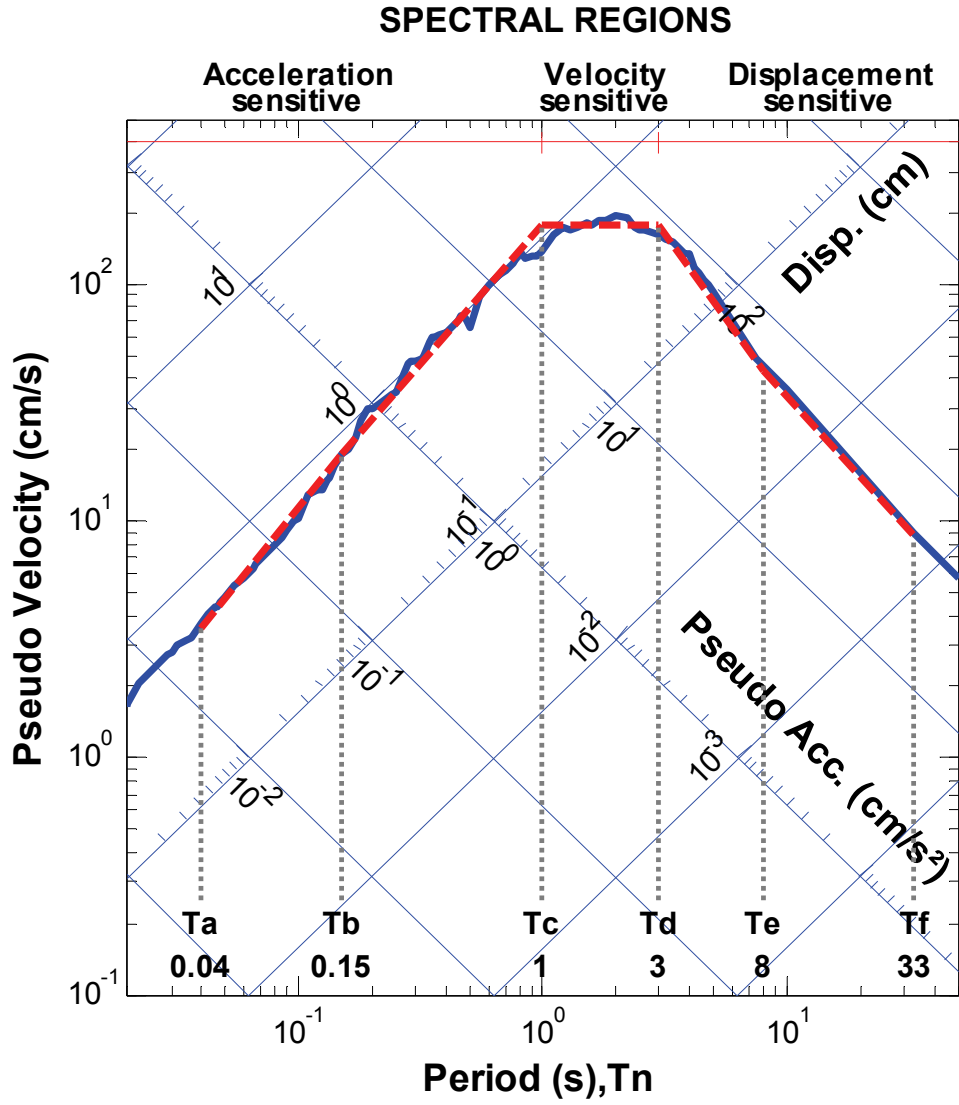


Figure 4.5 Median elastic response spectrum for the selected ensemble of ground motions shown by a solid line, together with its idealized version in dashed line; spectral regions are identified;  $\zeta = 5\%$ .

## 5. EVALUATION OF MPS PROCEDURE: LOW- and MID-RISE BUILDINGS

The efficiency and accuracy of the MPS and ASCE/SEI 7-05 scaling procedures will be first evaluated based on the three steel SMRF buildings representing low- and mid-rise building types in California.

A scaling procedure is considered efficient if the dispersion of EDPs due to the scaled records are small; it is accurate if the median value of the EDPs due to scaled ground motions is close to the benchmark results, defined as the median values of EDPs, determined by nonlinear RHA of the building to each of the twenty-one unscaled ground motions (Chapter 4). In this section, the median values of EDPs determined from a set of seven ground motions, scaled according to MPS and ASCE/SEI 7-05 scaling procedures will be compared. The median value,  $\hat{x}$  defined as the geometric mean and the dispersion measure,  $\delta$  of  $n$  observed values of  $x_i$  are calculated from

$$\hat{x} = \exp \left[ \frac{\sum_{i=1}^n \ln x_i}{n} \right]; \quad \delta = \left[ \frac{\sum_{i=1}^n (\ln x_i - \ln \hat{x})^2}{n-1} \right]^{1/2} \quad (5.1)$$

The EDPs selected are peak values of story drift ratio, that is, peak relative displacement between two consecutive floors normalized by story height; floor displacements normalized by building height; column and beam plastic rotations. These EDPs are computed over the whole time series.

### 5.1 SELECTED BUILDINGS

The first set of buildings selected to evaluate the efficiency and accuracy of the MPS method are existing 4-, 6-, and 13-story steel SMRF buildings. The six and thirteen-story buildings are instrumented, and their motions have been recorded during past earthquakes. A brief description of these buildings and their computer models follow.

### **5.1.1 Four-story Building**

This building, located in Northridge, California, was designed in compliance with 1988 Uniform Building Code (UBC). The structural system is composed of perimeter special moment resisting frames (SMRFs) to resist lateral loads and interior gravity frames. The floor plan and elevation of the building together with beam and column sizes are shown in figure 5.1. In this and subsequent figures, gravity frames are excluded from the plan. The columns are embedded into grade beams and anchored to the top of pile caps; thus, displacements and rotations are essentially restrained in all directions. All columns are made of A-572 grade 50 steel. The girders and beams are made of A-36 steel. The floor systems are composed of 16 cm thick slab (8.3 cm light weight concrete and 7.6 cm composite metal deck). The total seismic weight of the building was estimated to be approximately 10,880 kN.

### **5.1.2 Six-story Building**

The six-story building located in Burbank, California was designed in 1976 in accordance with the 1973 UBC requirements (fig. 5.2). It has a square plan measuring 36.6 m by 36.6 m with a 8.3 cm thick light weight concrete slab over 7.6 cm metal decking. Shear studs between the slab and beams were provided on the interior beams in the North-South direction only. The structural system is essentially symmetrical in plan. Moment continuity of each of the perimeter frames is interrupted at the ends where a simple shear connection is used to connect to the transverse-frame column along its weak axis. The plan view of the building and the elevation of a typical frame together with member sizes are shown in figure 5.3. The interior frames of the building were designed as gravity frames and consist of simple shear connections only. All columns are supported by base plates anchored on foundation beams, which in turn are supported on a pair of concrete piles (9.75 m in length and 0.75 m in diameter). Section properties were computed for A-36 steel with an assumed yield stress of 303 MPa as established from coupon tests (Anderson and Bertero, 1991). The minimum concrete compressive strength at 28 days was 20.7 MPa, except it was 13.8 MPa for the slab on grade. The total seismic weight of the building was estimated to be approximately 34,650 kN. The building was instrumented with a total of 13 strong motion sensors at the ground, 2nd, 3rd and roof levels.

### **5.1.3. Thirteen-story Building**

Located in South San Fernando Valley, 5 km southwest of the epicenter of the 1994 Northridge earthquake, this 13-story building (with one basement) was designed according to the 1973 UBC (fig. 5.4). The footprint of the building is 53.3 by 53.3 m. The exterior frames of the building are moment-resisting frames and interior frames were designed for gravity load bearing. The foundation consists of piles, pile caps and grade beams. The floor plan of the perimeter frames and a typical elevation of one of these frames are shown in figure 5.5; note that member sizes are indicated and that the corner columns are composed of box sections. Floor systems consist of 6.4 cm of 20.7 MPa-concrete fill over 7.5 cm steel decking. The roof system is lighter with 5.7 cm of vermiculite fill on 7.6 cm steel decking. The total seismic weight of the building was estimated to be 68,950 kN. Motions of this building during the 1994 Northridge earthquake were recorded by 7 sensors: three each in the North-South and East-West directions, and one in the vertical direction.

## **5.2. SYSTEMS ANALYZED**

These symmetric-plan buildings may be analyzed as two-dimensional systems for ground motions applied independently along each axis. The frames selected for modeling are: SMRF along Line 1 for the 4-story building, SMRF long Line 1 for the 6-story building, and the SMRF along Line G for the 13-story building. The analytical models were generated in the open source finite element platform, OpenSees (2009) using a force-based nonlinear beam-column element (Neuenhofer and Filippou, 1998). This element utilizes a layered ‘fiber’ section at each integration point, which in turn is associated with uni-axial material models and enforces Bernoulli beam assumptions for axial force and bending. Centerline dimensions were used in element modeling. Included in the frame model was one half of the building mass distributed proportionally to the floor nodes. Special features such as local connection fracture were not simulated; consequently, modeling of members and connections was based on the assumption of stable hysteresis loops derived from a bilinear stress-strain model. The columns were assumed to be fixed at the base level. Complete details of the analytical models and calibration studies for the six- and thirteen-story buildings against the recorded data are reported in Kalkan (2006). The

first three natural vibration periods and modes of each building are shown in figure 5.6 and the first-“mode” pushover curves in figure 5.7, where P-Δ effects are included.

### 5.3 FIRST-“MODE” SDF-SYSTEM PARAMETERS

In order to establish first-“mode” SDF system properties for each building, the global hysteretic behavior of buildings is described by the cyclic pushover curves (Han and others 2004; Chopra and Bobadilla, 2007) as shown in figure 5.8. These were determined by nonlinear static analysis of the buildings subjected to the modal force distribution ( $s_l^* = \mathbf{m}\phi_1$ ) with its magnitude varied and reversed to cause the cyclic roof displacement described by figure 5.9. Comparison of the cyclic and monotonic pushover curve in figure 5.10 indicates cycle-to-cycle deterioration of stiffness due to P-Δ effects.

The force-deformation relation for the first-“mode” SDF system is determined from the base shear – roof displacement relation defined by modal pushover curve by utilizing  $F_{s1}/L_1 = V_{b1} / M_1^*$  and  $D_1 = u_{r1} / \Gamma_1\phi_{r1}$ . The hysteretic force-deformation relation is idealized by the peak-oriented model (Ibarra and Krawinkler, 2005; Ibarra and others, 2005), with the monotonic curve idealized as tri-linear (fig. 5.10). In the hysteretic model, the cyclic behavior is described by a series of deterioration rules. These deterioration parameters are determined from the cyclic force deformation relation  $F_{S1} / L_1 - D_1$  obtained from the cyclic pushover curve (fig. 5.8) by an iterative trial-and-error procedure to obtain a best fit of the model to the actual cyclic curve. The associated hysteretic model provides reasonable representation of the global cyclic behavior of the buildings as shown in figure 5.11.

### 5.4. EVALUATION OF MPS CONCEPT

As a first step in evaluating the concept underlying the MPS procedure, the target value of deformation  $\bar{D}_1'$  is computed not as described in Step 6 of the procedure (Chapter 2) but as the median value of peak deformation of the first-“mode” inelastic SDF system due to twenty-one ground motions determined by nonlinear RHA. The MPS method utilizing this  $\bar{D}_1'$  value is denoted henceforth as MPS\*. The twenty-one ground motions are divided into 3 sets each

containing seven records (table 5.1). The records in each set are selected randomly from at least 3 different earthquakes to avoid any dominant influence of a single event on the ground motion set. An appropriate scale factor for each record is determined by implementing Steps 1-8 of the MPS procedure.

Efficiency and accuracy of the MPS\* procedure are evaluated for each ground motion set separately by comparing the median values of EDPs determined by nonlinear RHA of the building due to the seven scaled records against the benchmark EDPs. Figure 5.12 shows the benchmark EDPs for all three buildings; results from individual records are also included to demonstrate the large dispersion. Almost all of the excitations drive all three buildings well into the inelastic range as shown in figure 5.13 where the roof displacement values due to twenty-one ground motions are identified on the first-“mode” pushover curve. Also shown is the median value. The post-yield branch of the first-“mode” pushover curve exhibits negative slope because of P- $\Delta$  effects.

Comparisons of the EDPs obtained from the MPS procedure with the benchmark results are presented in figures 5.14 through 5.16 for the three buildings. Included are the EDPs due to each of the seven scaled ground motions to show the dispersion of the data. The results are organized for each building in three parts corresponding to the three ground motion sets. These results demonstrate that the MPS procedure is accurate; the median values of EDPs due to every small (7) subset of scaled ground motion closely match the benchmark results, which were determined from a large (twenty-one) set of ground motions. The dispersion of the EDP values due to the seven scaled records about their median value is much smaller compared to the data for the twenty-one unscaled records in figure 5.17. These results collectively demonstrate that the concept underlying the MPS procedure is accurate and efficient in scaling records for nonlinear RHA of buildings.

## **5.5. EVALUATION OF MPS AND CODE-BASED SCALING PROCEDURES**

The preceding implementation of the MPS concept is the same as the MPS procedure described in Section 2 except for how  $\bar{D}_1^I$  was computed. Previously, the “exact” value of  $\bar{D}_1^I$  was determined by nonlinear RHA of the first-“mode” inelastic SDF system, but it will now be

estimated according to Step 6, using an empirical equation for  $C_R$ , in accordance with the MPS procedure. In utilizing the  $C_R$  equation, zero post-yield stiffness is assumed, although the idealized first-“mode” SDF systems (fig. 5.10) have negative post-yield stiffness. This choice is dictated by the fact that the original  $C_R$  equation was determined for stable systems with non-negative post-yield stiffness ratio (Chopra and Chintanapakdee, 2004).

In the  $C_R$  equation, using zero post-yield stiffness seems to be plausible because the variability in the peak displacement demand is not affected significantly by the hysteretic behavior (Kurama and Farrow, 2003; Gupta and Kunnath, 1998). Figure 5.17 compares the “exact” target value of deformation,  $\bar{D}_1^I$  (continuous horizontal line) with estimated target value of deformation,  $\bar{D}_1^I$  (dashed horizontal line) using the  $C_R$  equation with zero post-yield stiffness;  $D_1^I$  values from individual records for each of the three buildings are also included. Notably, “exact” target value of deformation,  $\bar{D}_1^I$  is determined as the median value of  $D_1^I$  from twenty-one ground motions based on first-“mode” inelastic SDF system having peak-oriented hysteretic behavior as shown in figure 5.11. As figure 5.17 indicates, “exact” and estimated values of  $\bar{D}_1^I$  are close to each other; the discrepancy between them becomes less as the initial period,  $T_n$  of the inelastic SDF system prolongs.

Once  $\bar{D}_1^I$  is estimated, an appropriate scale factor for each record is determined based on the inelastic first-“mode” SDF systems (fig. 5.11) by implementing Steps 7-8 of the MPS procedure. Table 5.2 lists the scaled factors computed for each set and for each building. The EDPs determined by nonlinear RHAs of the structure due to a set of seven ground motions scaled according to MPS procedure are compared against the benchmark EDPs. Figures 5.18 - 5.26 present such comparisons for the three buildings and for the three sets of ground motions. These results demonstrate that the MPS procedure is much superior compared to the ASCE/SEI 7-05 procedure for scaling ground motion records. This superiority is apparent in two respects: First, for each building and each ground motion set, the ground motions scaled according to the MPS procedure lead to median values of EDPs that are much closer to the benchmark values than the corresponding results based on the ASCE/SEI 7-05 procedure. The only exception is the combination of 6-story building and Ground Motion Set 3. In this case, the MPS procedure leads to estimates of the EDPs that are only slightly better than results from the ASCE/SEI 7-05

scaling procedure. Second, the dispersion in the EDP values due to the seven scaled records around the median value is much smaller when the records are scaled according to the MPS procedure compared to the ASCE/SEI 7-05 scaling procedure. However, even with the MPS scaling, the dispersion of EDPs for the upper stories of 6- and 13-story buildings is noticeable, particularly for Ground Motion Set 2, indicating that the higher-mode contributions to the seismic demands are significant. These factors are considered for 6- and 13-story buildings in the next chapter.

An alternative way of comparing MPS and ASCE/SEI 7-05 scaling methods is based on the ratio of the EDP value due to a scaled record and the benchmark value. The deviation of the median,  $\Delta$  of this ratio from unity is an indication of the error or bias in estimating the median EDP value, and the dispersion,  $\sigma$  of this ratio (assuming log-normal distribution) is an indication of the scatter in the individual EDPs, determined from the scaled ground motions. Included also in the comparison is the MPS\* procedure based on “exact” values of  $\bar{D}_1'$  instead of Step 6. Figure 5.27 presents the median,  $\Delta$  of the EDP ratio for story drifts determined from records scaled according to the MPS\*, MPS, and ASCE/SEI 7-05 scaling methods. Comparing these  $\Delta$  values against 1.0, it is apparent that the MPS\* method is most accurate (least biased), the MPS method is only slightly less accurate. The bias in the MPS methods is generally less than 20%, except in the case of the 6-story building and Ground Motion Set 3. The ASCE/SEI 7-05 method is least accurate and generally overestimates the EDPs, with the overestimation exceeding 50% in some cases.

Figure 5.28 presents the dispersion of the EDP ratio for story drifts determined from records scaled according to the MPS\*, MPS, and ASCE/SEI 7-05 scaling methods. It is apparent that the MPS\* scaling method leads to the smallest dispersion, and it becomes only slightly larger in the MPS method. Dispersion is largest in the ASCE/SEI 7-05 scaling method, becoming unacceptably large for some combinations of buildings and ground motion sets.

## 5.6. MULTI-MODE CONSIDERATIONS

As demonstrated here, the MPS method based solely on the first-“mode” inelastic SDF system (Steps 1-9 of the method) is superior over the ASCE/SEI 7-05 scaling method. Considering the higher modes of vibration is expected to improve the method further for mid-rise and tall buildings.

To consider the second-“mode” effect into account, the twenty-one records scaled based on the first-“mode” response only (Steps 1-9 of the method) are ranked by accounting for elastic second-“mode” response according to Steps 10-13 of the method. The seven records with the highest ranks (see Step 12) were defined as Ground Motion Set 4. Note that this set is different for each building (table 5.3).

Figure 5.29 compares the median EDPs from ground motions scaled by the MPS method with the benchmark values for the 6- and 13-story building; results of individual ground motions are also shown. It is apparent that considering higher modes in selecting ground motions in the MPS method provides accurate estimates of the median EDPs and reduces the record-to-record variability (compared to the results achieved by Ground Motion Sets 1-3). This improved accuracy and efficiency is demonstrated in figure 5.30, where the  $\Delta$  and  $\sigma$ —the median value of the ratio of the estimated story drift to its benchmark value, and dispersion of this ratio—are plotted for the four set of ground motions. It is apparent that Ground Motion Set 4 is more accurate and efficient than Ground Motion Sets 1 through 3.

The improvement achieved for these buildings is modest because the higher-mode computations are not especially significant in the response of selected buildings. Such improvement is expected to be more pronounced in the case of taller buildings responding significantly in their higher modes.

**Table 5.1 List of records for three ground motion sets**

GM SET - 1		GM SET - 2		GM SET - 3	
Earthquake	Station	Earthquake	Station	Earthquake	Station
Superstition Hills	Parachute Test Site	Tabas, Iran	Tabas	Imperial Valley	El Centro Array #7
Northridge	Jensen Filter Plant	Imperial Valley	EC Meloland Over FF	Loma Prieta	LGPC
Northridge	Sylmar - Converter Sta E	Erzincan, Turkey	Erzincan	Northridge	Newhall - W Pico Can Rd.
Kobe, Japan	Takatori	Northridge	Sylmar - Converter Sta	Northridge	Rinaldi Receiving Sta
Kocaeli, Turkey	Yarimca	Kobe, Japan	Port Island	Northridge	Sylmar - Olive View Med FF
Chi-Chi, Taiwan	TCU065	Chi-Chi, Taiwan	TCU052	Chi-Chi, Taiwan	TCU068
Chi-Chi, Taiwan	TCU102	Chi-Chi, Taiwan	TCU084	Duzce, Turkey	Duzce

**Table 5.2 Scale factors computed for three buildings and for three sets of seven ground motions**

No.	Earthquake	Year	Station	Set No.	Scale Factor		
					4-story	6-story	13-story
1	Superstition Hills	1987	Parachute Test Site	1	0.64	1.04	1.59
2	Northridge	1994	Jensen Filter Plant	1	0.43	0.65	1.37
3	Northridge	1994	Sylmar - Converter Sta East	1	0.99	1.12	1.13
4	Kobe, Japan	1995	Takatori	1	0.52	0.57	1.73
5	Chi-Chi, Taiwan	1999	TCU065	1	0.47	0.76	0.54
6	Chi-Chi, Taiwan	1999	TCU102	1	0.92	1.04	0.99
7	Kocaeli, Turkey	1999	Yarimca	1	1.69	1.91	0.85
1	Erzincan, Turkey	1992	Erzincan	2	0.81	1.15	1.18
2	Imperial Valley	1979	EC Meloland Overpass FF	2	1.20	1.04	1.03
3	Kobe, Japan	1995	Port Island	2	0.92	1.25	0.93
4	Northridge	1994	Sylmar - Converter Sta	2	0.38	1.05	0.90
5	Tabas, Iran	1978	Tabas	2	0.89	1.39	0.91
6	Chi-Chi, Taiwan	1999	TCU052	2	0.93	0.71	0.62
7	Chi-Chi, Taiwan	1999	TCU084	2	0.63	0.64	1.11
1	Duzce, Turkey	1999	Duzce	3	1.14	1.03	1.07
2	Imperial Valley	1979	El Centro Array #7	3	1.07	1.39	1.10
3	Loma Prieta	1989	LGPC	3	1.04	0.95	0.63
4	Northridge	1994	Rinaldi Receiving Sta	3	0.49	0.53	1.14
5	Northridge	1994	Sylmar - Olive View Med FF	3	1.17	1.33	1.51
6	Chi-Chi, Taiwan	1999	TCU068	3	0.92	1.07	0.50
7	Northridge	1994	Newhall - W Pico Canyon Rd	3	0.80	1.02	0.83

**Table 5.3 Scale factors for 6-, and 13-story buildings considering higher-modes**

				<b>Scale Factor</b>
<b>No.</b>	<b>Earthquake</b>	<b>Year</b>	<b>Station</b>	<b>6-story</b>
1	Superstition Hills	1987	Parachute Test Site	1.04
2	Duzce, Turkey	1999	Duzce	1.03
3	Erzincan, Turkey	1992	Erzincan	1.15
4	Kobe, Japan	1995	Takatori	0.57
5	Chi-Chi, Taiwan	1999	TCU102	1.04
6	Northridge	1994	Newhall - W Pico Canyon Rd	1.02
7	Kocaeli, Turkey	1999	Yarimca	1.91
				<b>13-story</b>
1	Superstition Hills	1987	Parachute Test Site	1.59
2	Northridge	1994	Jensen Filter Plant	1.37
3	Loma Prieta	1989	LGPC	0.63
4	Chi-Chi, Taiwan	1999	TCU052	0.62
5	Chi-Chi, Taiwan	1999	TCU068	0.50
6	Chi-Chi, Taiwan	1999	TCU102	0.99
7	Kocaeli, Turkey	1999	Yarimca	0.85

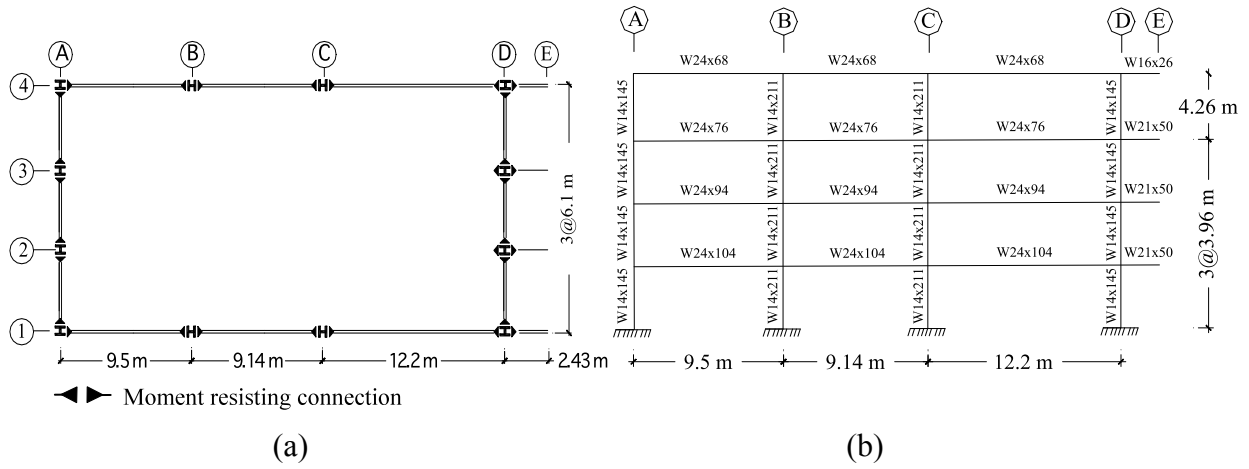


Figure 5.1 4-story building: (a) plan; and (b) elevation of perimeter SMRF.

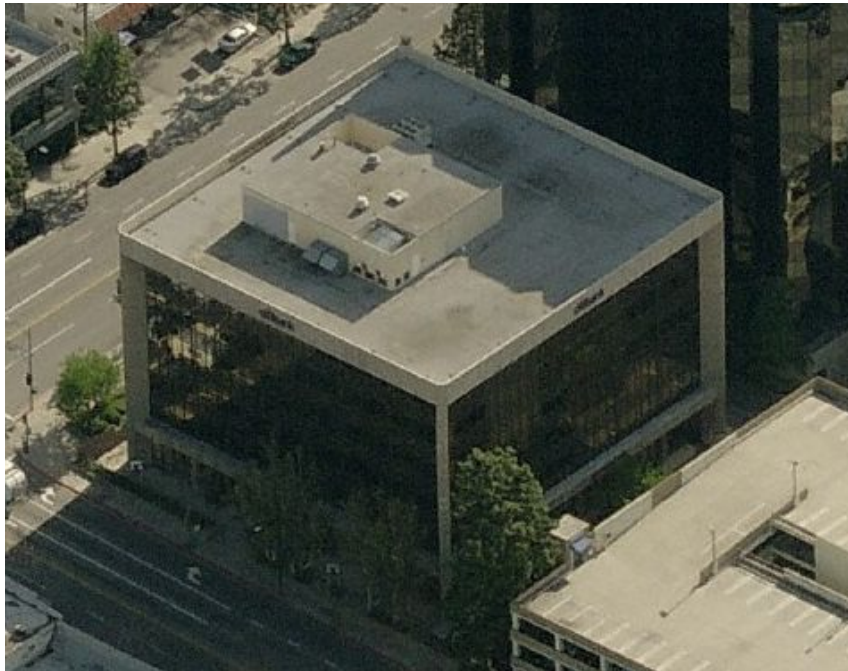
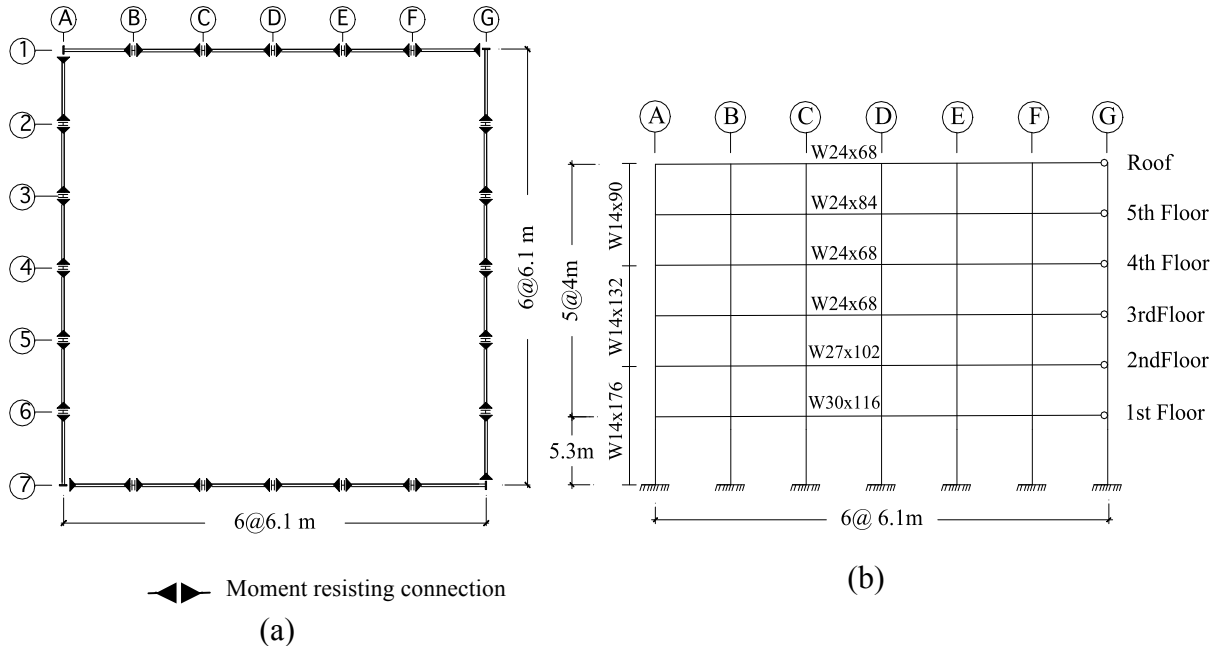
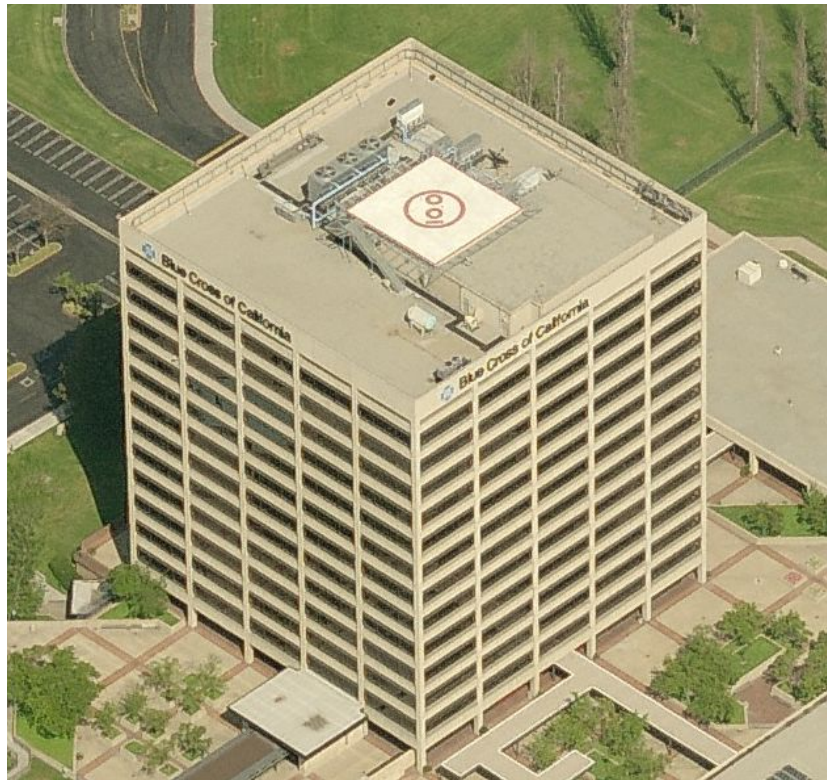


Figure 5.2 Overview of the 6-story steel building in Burbank, CA.



**Figure 5.3 6-story building: (a) plan; and (b) elevation of perimeter SMRF.**



**Figure 5.4 Overview of the 13-story steel building in South San Fernando Valley, CA.**

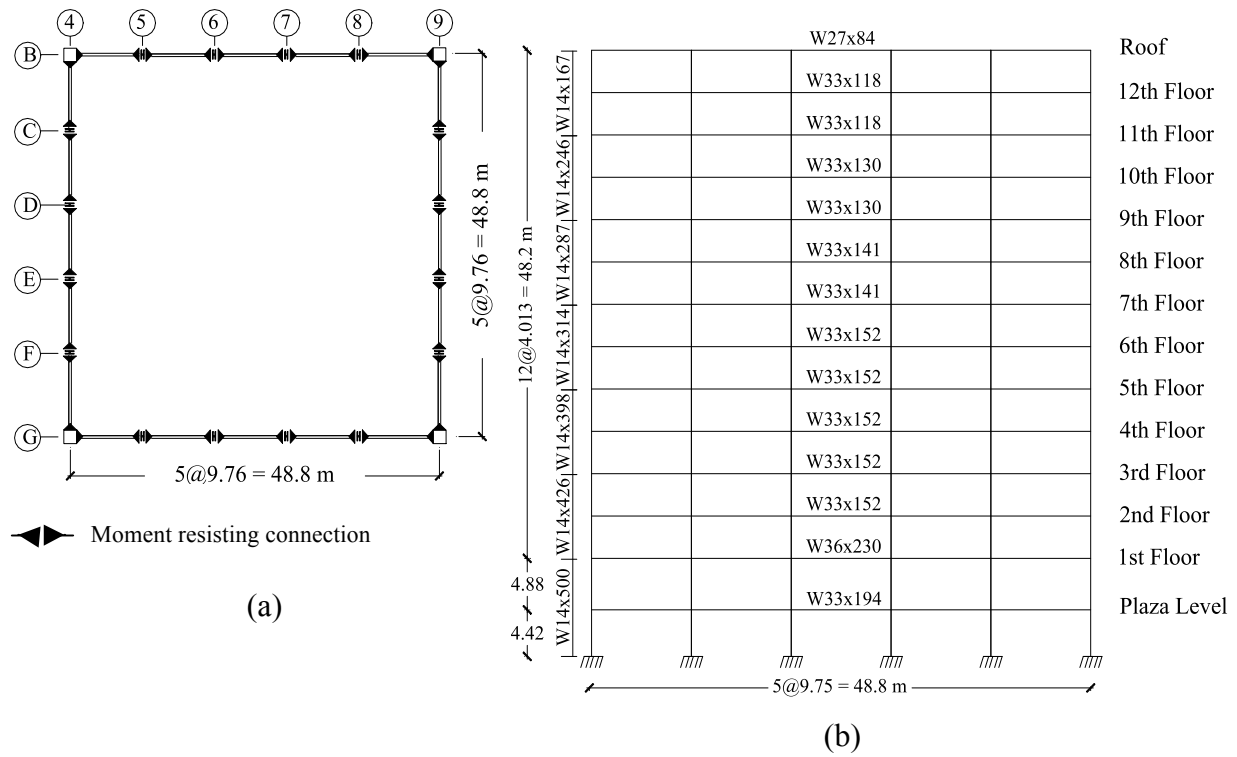


**Figure 5.5 13-story building: (a) plan; and (b) elevation of perimeter SMRF.**

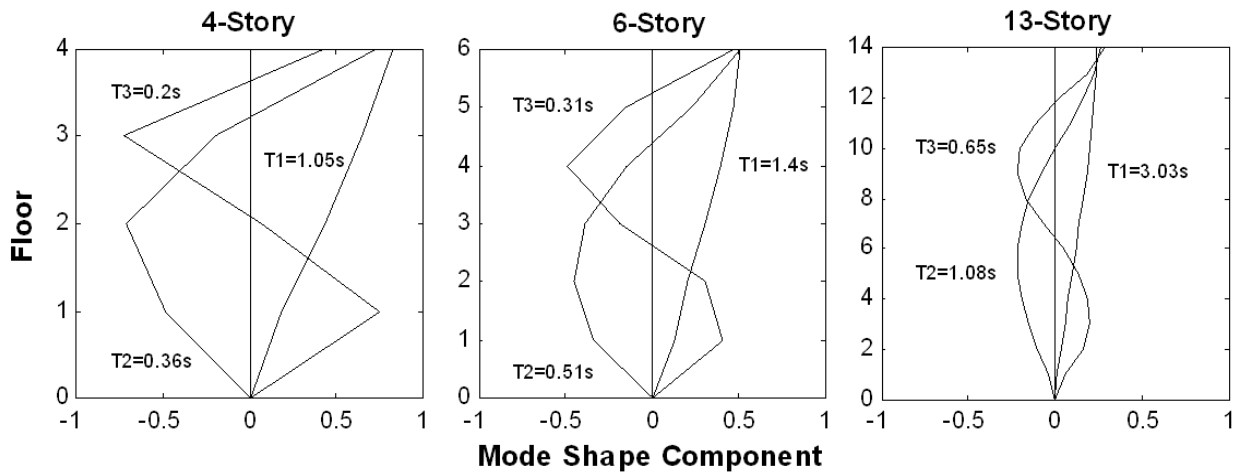


Figure 5.6 Natural vibration periods and modes of 4-, 6-, and 13-story buildings.

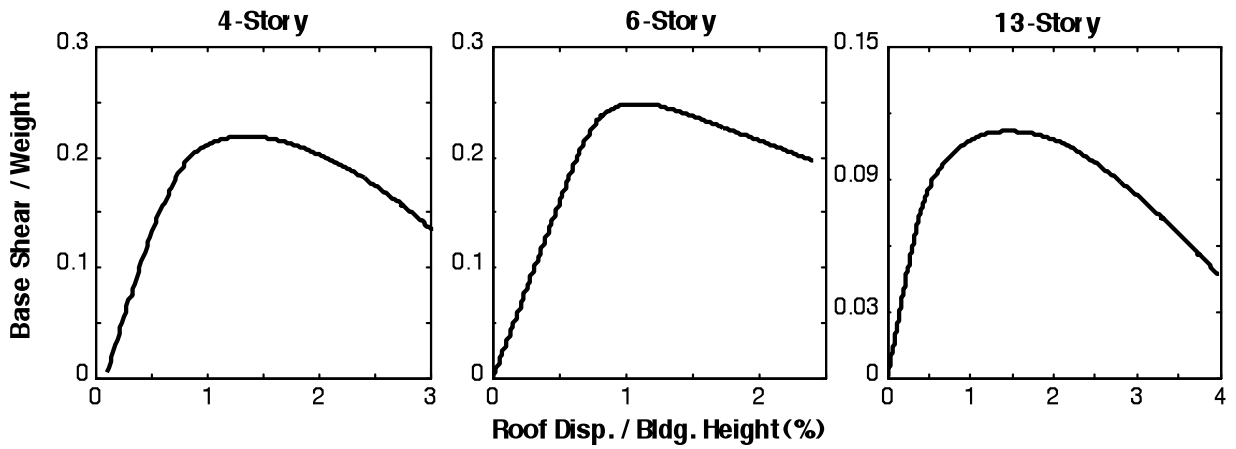


Figure 5.7 First-“mode” pushover curves for 4-, 6-, and 13-story buildings.

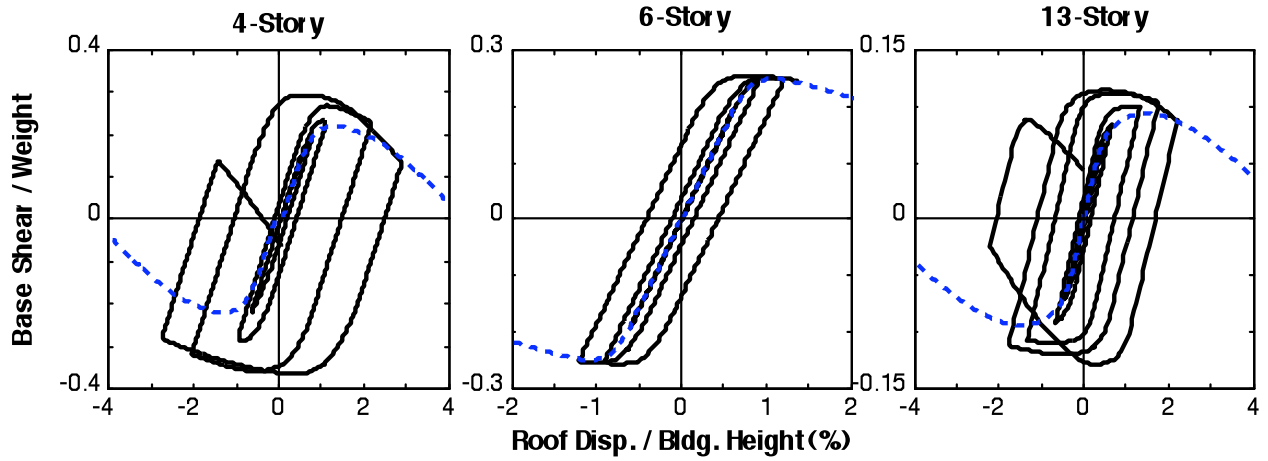


Figure 5.8 First-“mode” cyclic pushover curve (solid line) and monotonic pushover curve (dashed line), for 4-, 6-, and 13-story buildings.

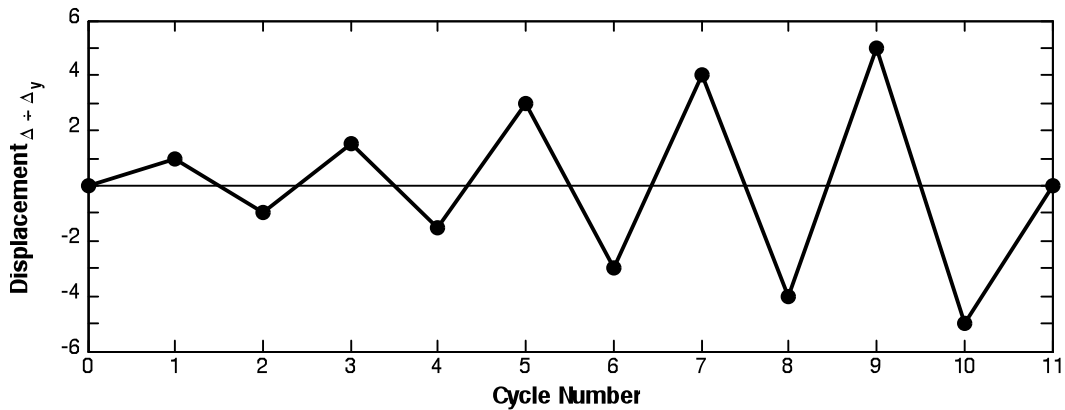


Figure 5.9 Description of roof-displacement amplitudes for cyclic pushover analysis.

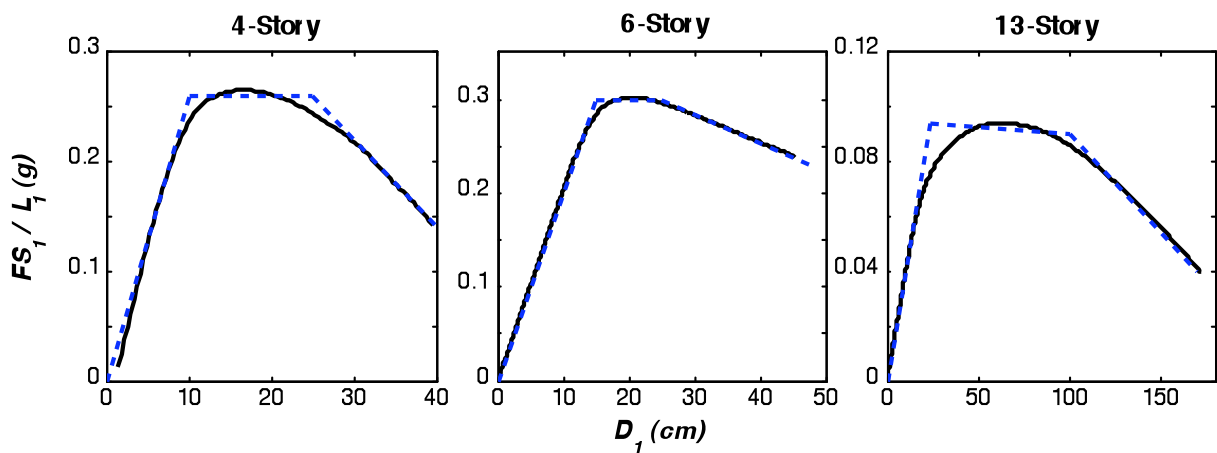


Figure 5.10 Comparison of first-“mode” pushover curve (solid line) and its idealized trilinear model (dashed line) for 4-, 6-, and 13-story buildings.

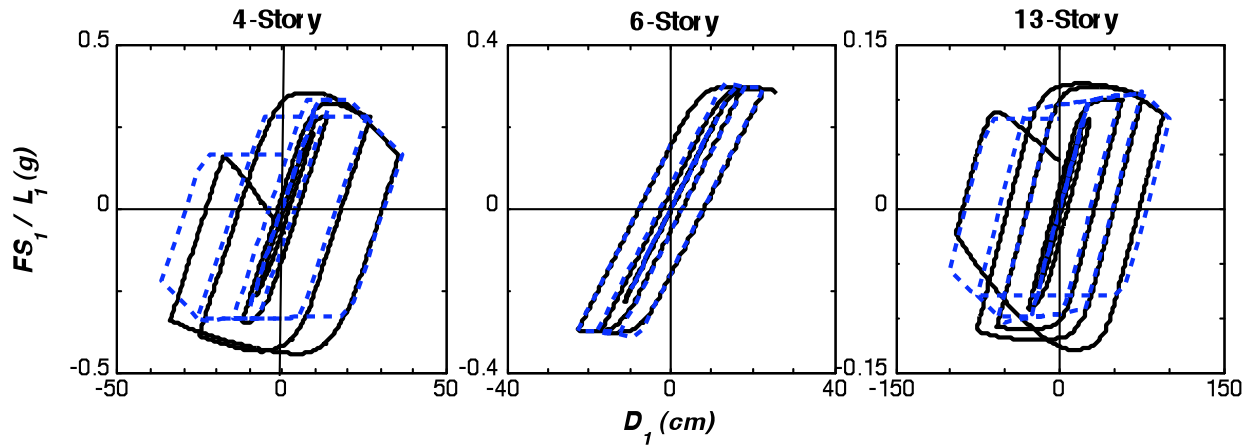


Figure 5.11 Comparison of first-“mode” cyclic pushover curve (solid line) and its hysteretic model (dashed lines), for 4-, 6-, and 13-story buildings.

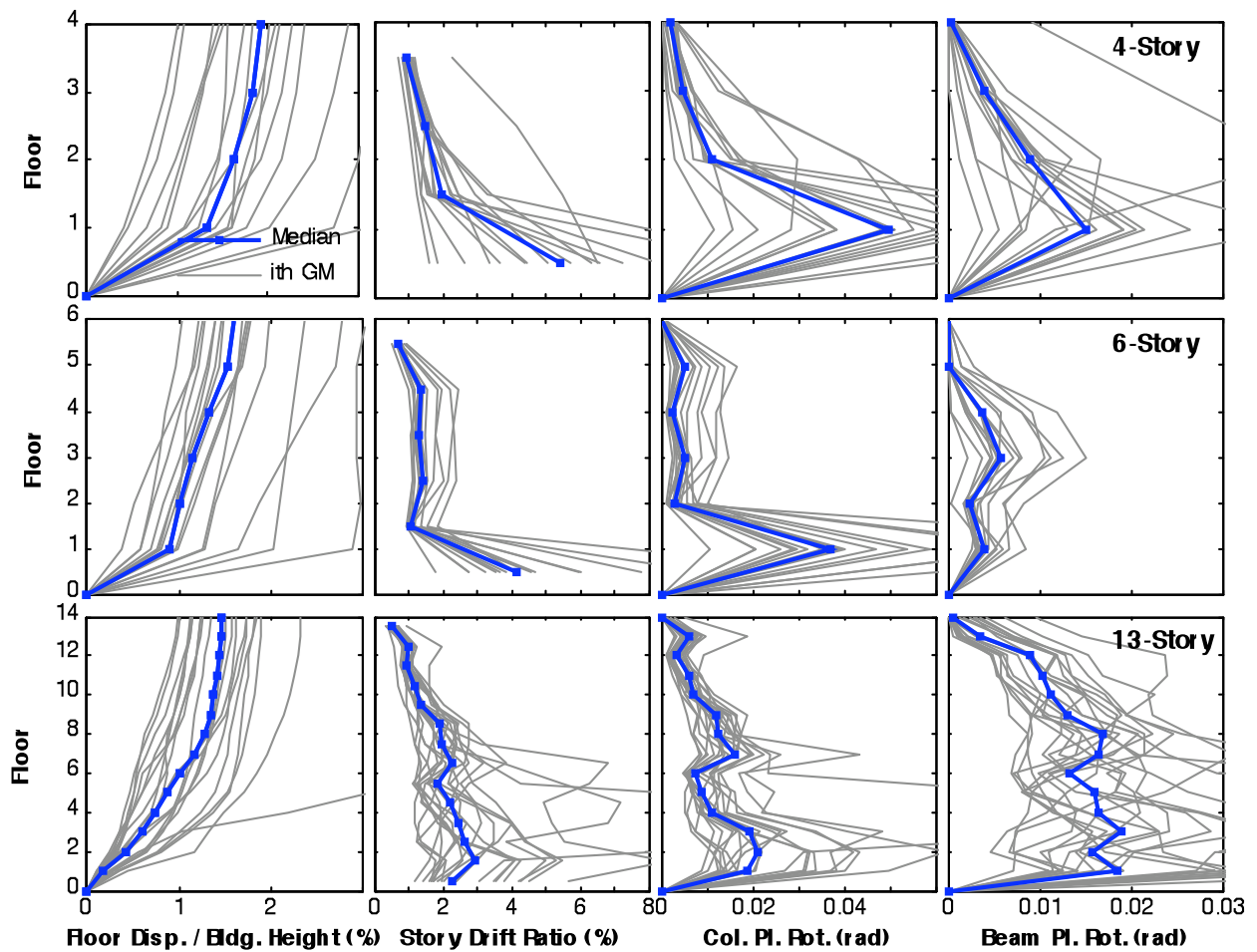


Figure 5.12 Median values of EDPs determined by nonlinear RHA of three buildings for twenty-one ground motions; results for individual ground motions are also included.

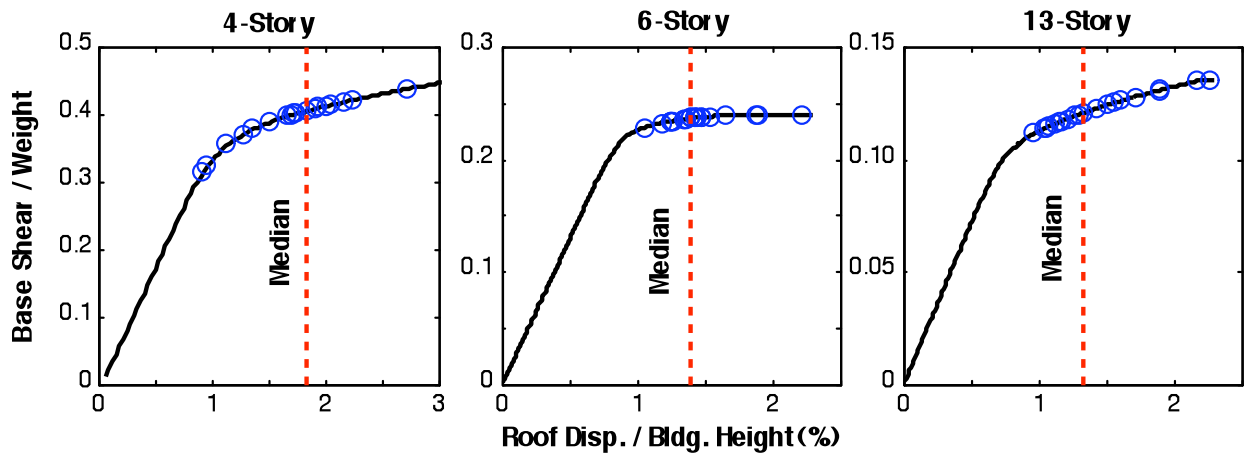


Figure 5.13 Roof displacements determined by nonlinear RHA of three buildings for twenty-one ground motions identified on first-“mode” pushover curves.

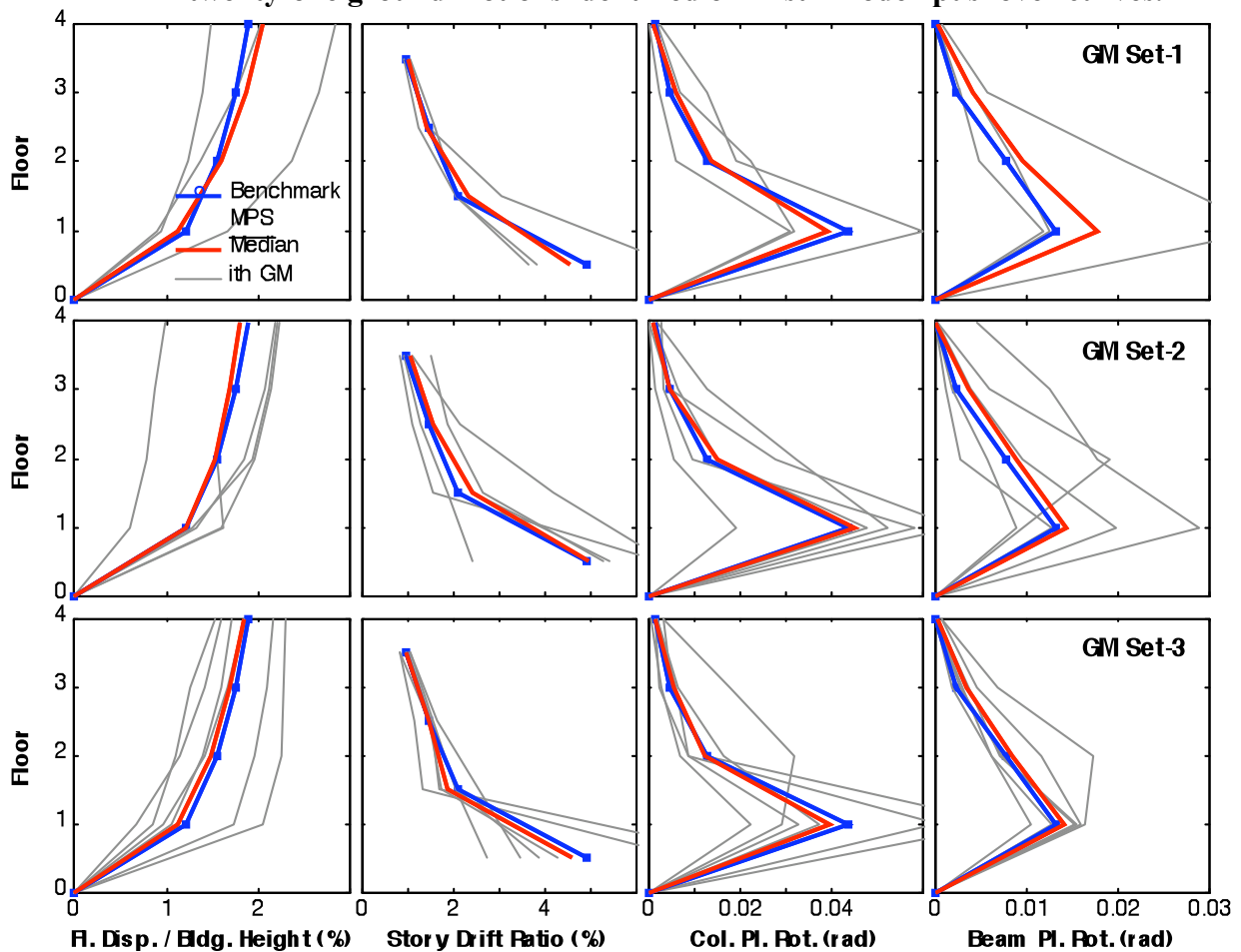
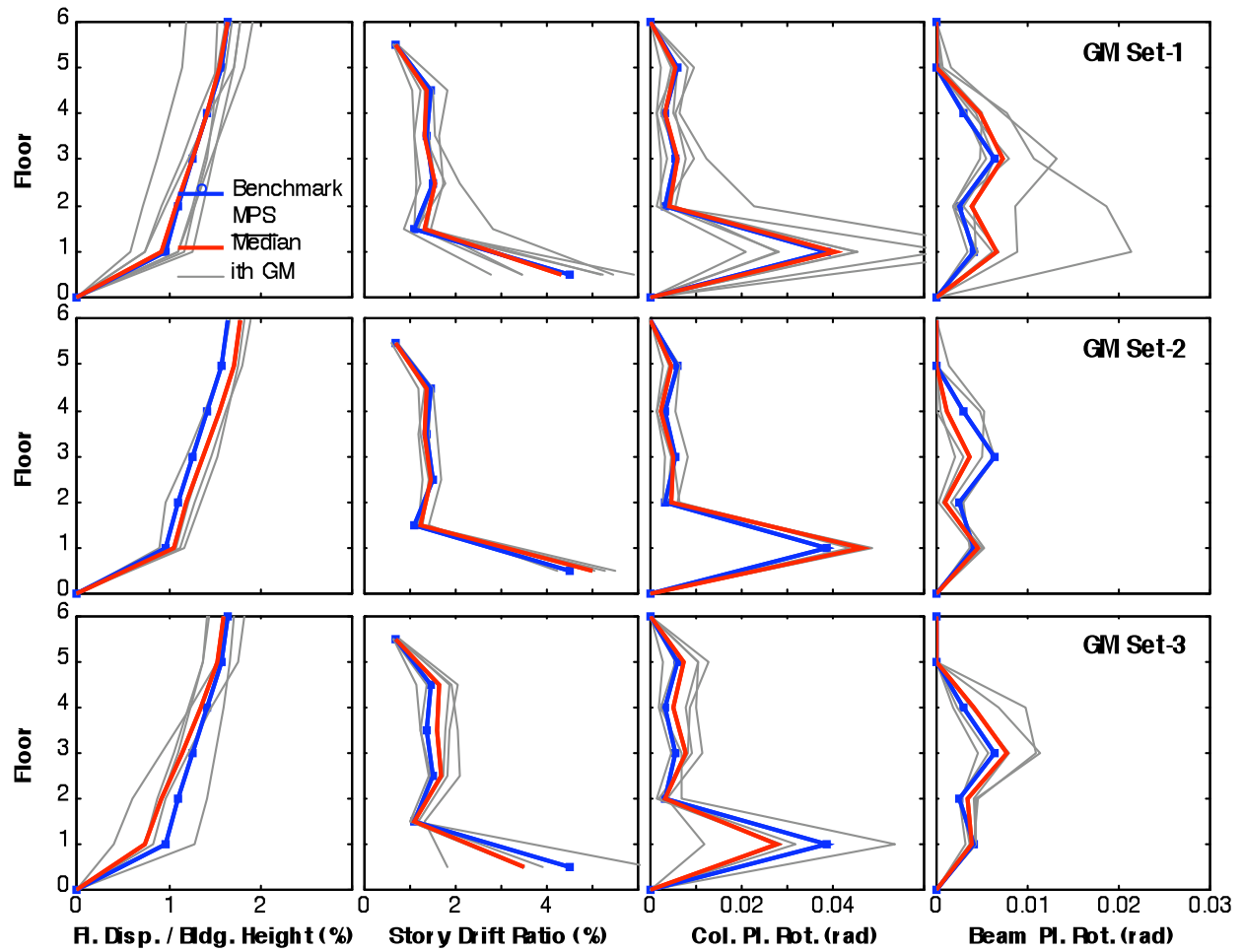
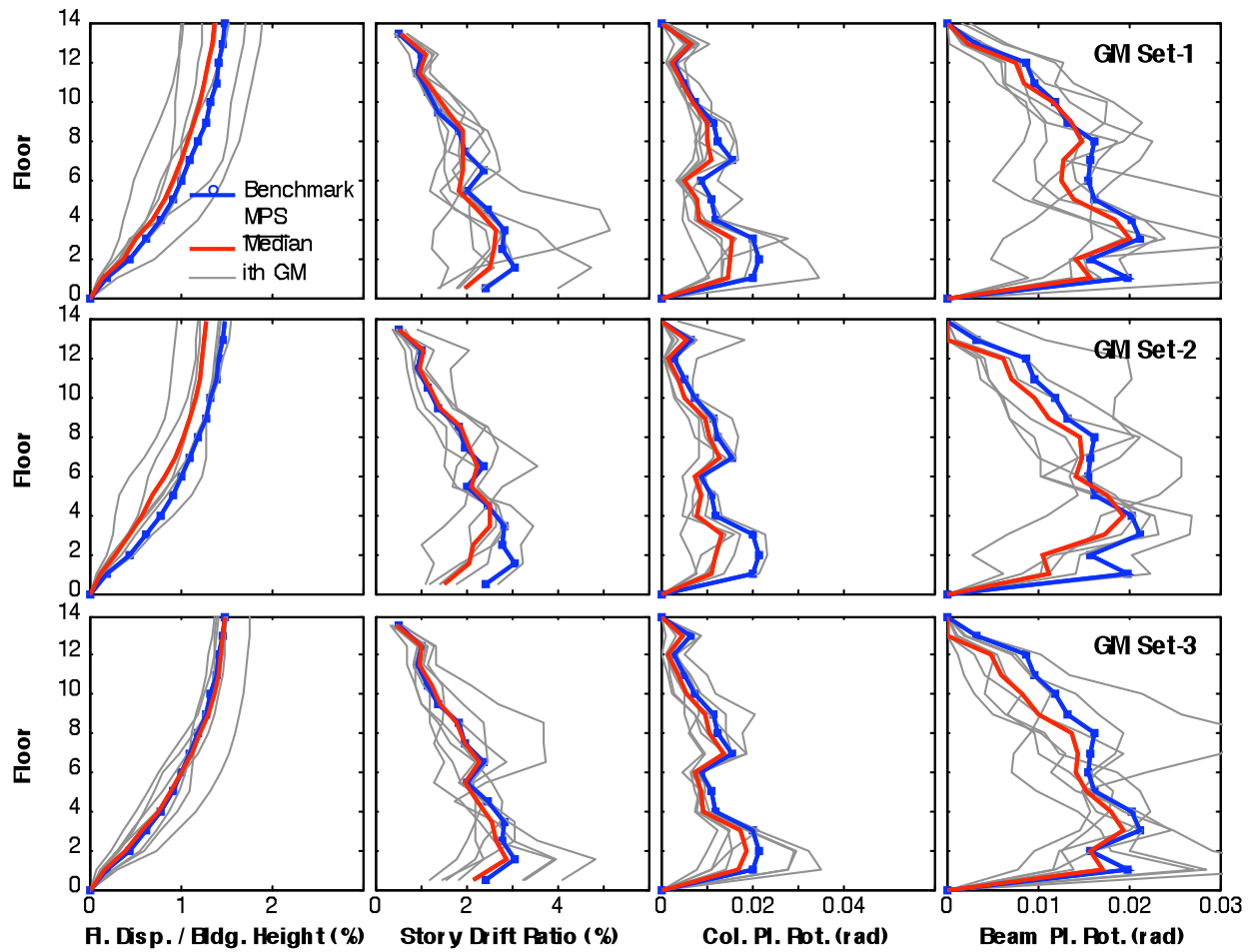


Figure 5.14 Comparison of median EDPs based on the MPS concept with benchmark EDPs for the 4-story building; individual results for each of the seven scaled ground motions are also presented.



**Figure 5.15** Comparison of median EDPs based on the MPS concept with benchmark EDPs for the 6-story building; individual results for each of the seven scaled ground motions are also presented.



**Figure 5.16** Comparison of median EDPs based on the MPS concept with benchmark EDPs for the 13-story building; individual results for each of the seven scaled ground motions are also presented.

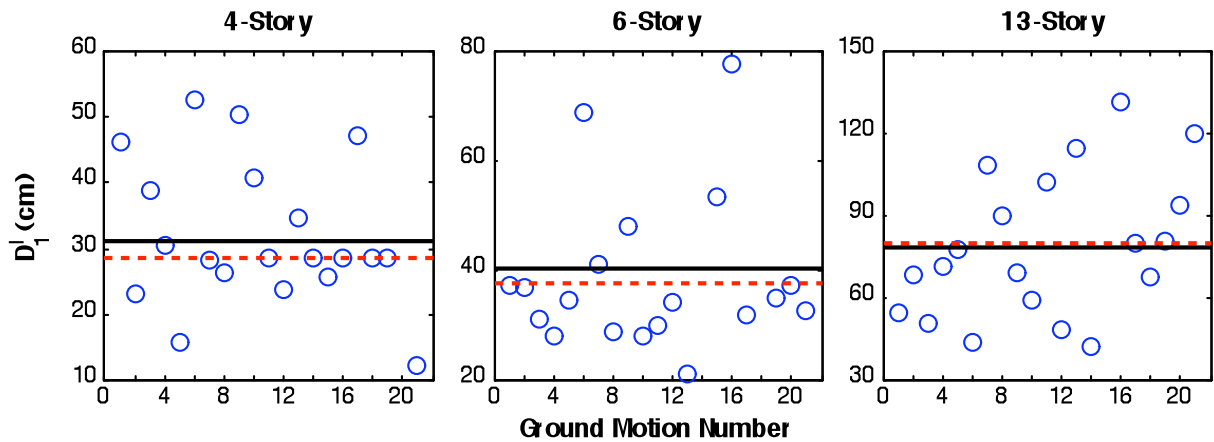


Figure 5.17 Peak deformation  $D_1^l$  values of the first-“mode” inelastic SDF system for twenty-one ground motions for 4-, 6-, and 13-story buildings; “exact” target value of deformation  $\bar{D}_1^l$  is identified by horizontal continuous line; horizontal dashed line indicates target value of deformation  $\bar{D}_1^l$  established by  $C_R$  equation.

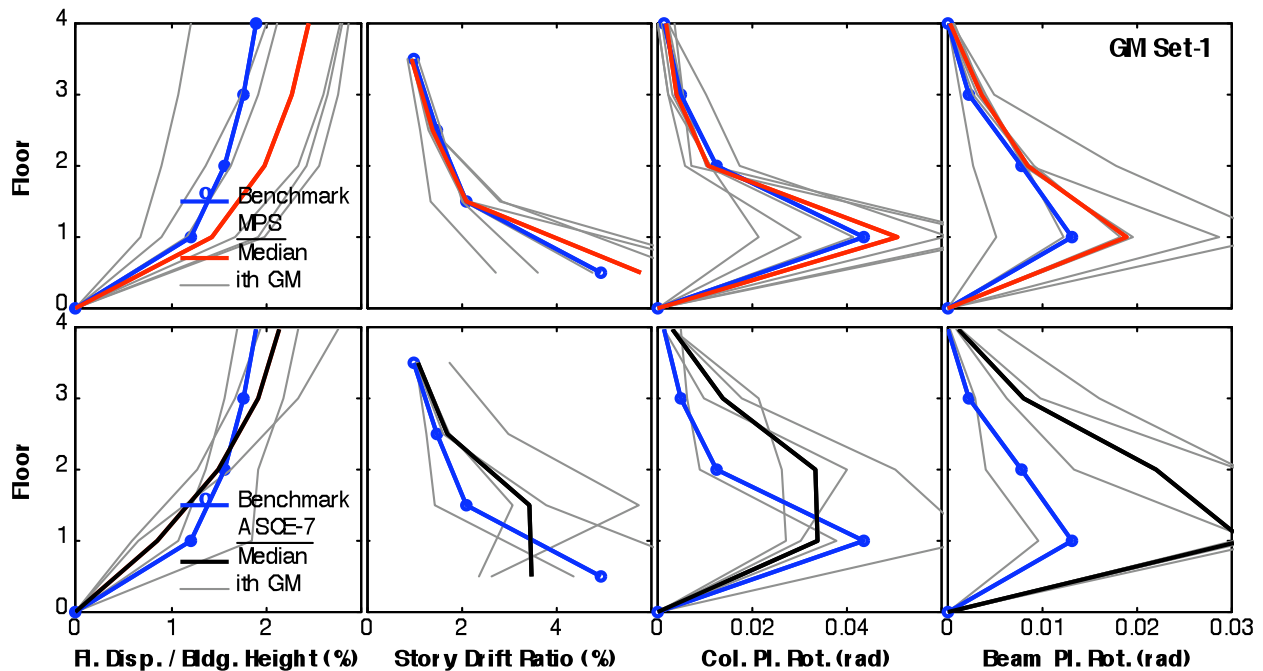
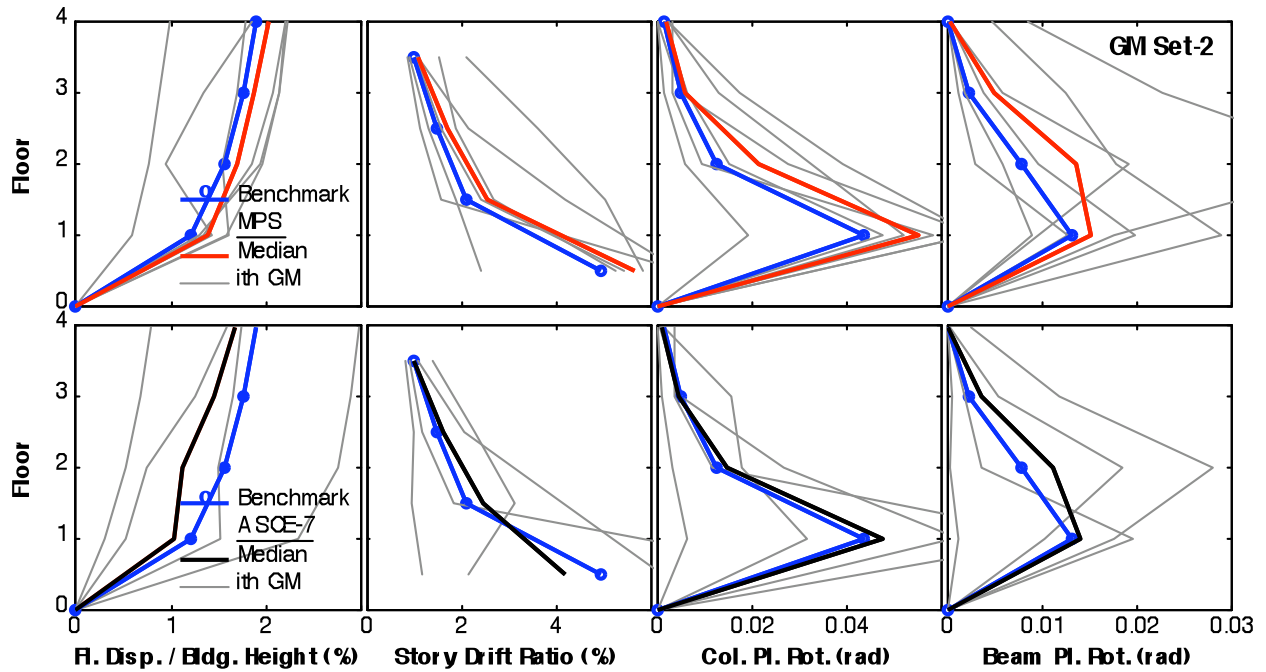
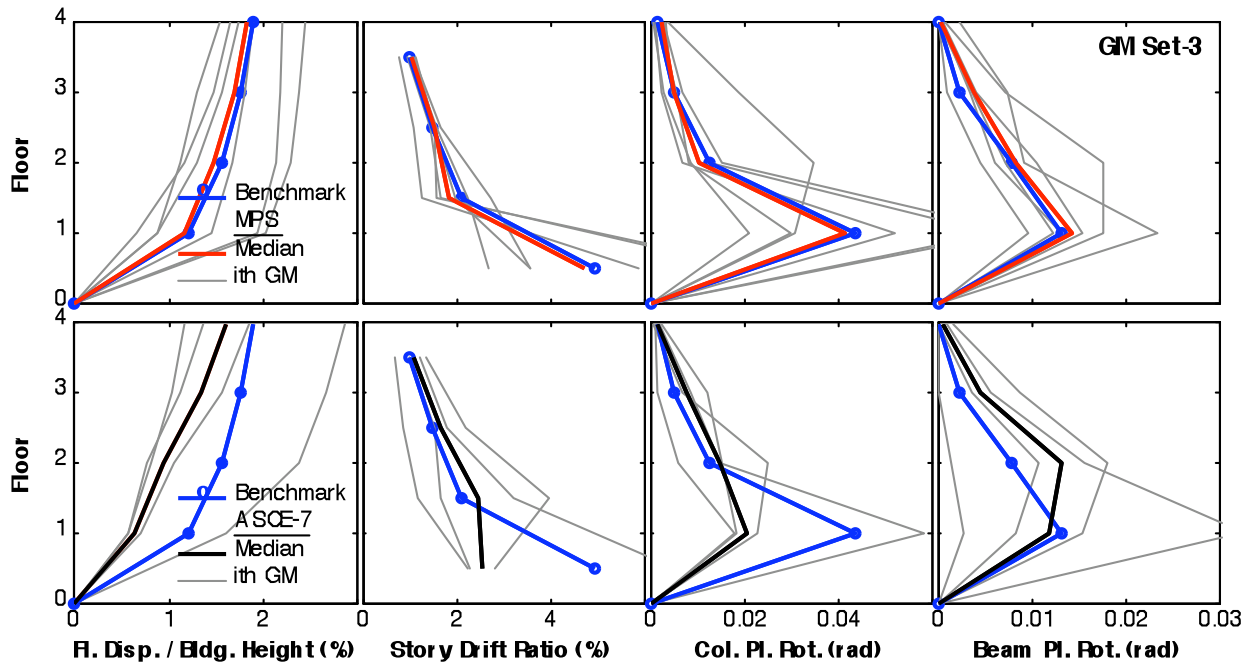


Figure 5.18 Comparison of median EDPs for Ground Motion Set 1 scaled according to MPS (top row) and ASCE/SEI 7-05 (bottom row) scaling procedures with benchmark EDPs; individual results for each of seven scaled ground motions are also presented. Results are for the 4-story building.



**Figure 5.19** Comparison of median EDPs for Ground Motion Set 2 scaled according to MPS (top row) and ASCE/SEI 7-05 (bottom row) scaling procedures with benchmark EDPs; individual results for each of seven scaled ground motions are also presented. Results are for the 4-story building.



**Figure 5.20** Comparison of median EDPs for Ground Motion Set 3 computed for the 4-story building based on the MPS and ASCE/SEI 7-05 earthquake record scaling procedures with benchmark EDPs; individual results for each of seven scaled ground motions are also presented. Results are for the 4-story building.

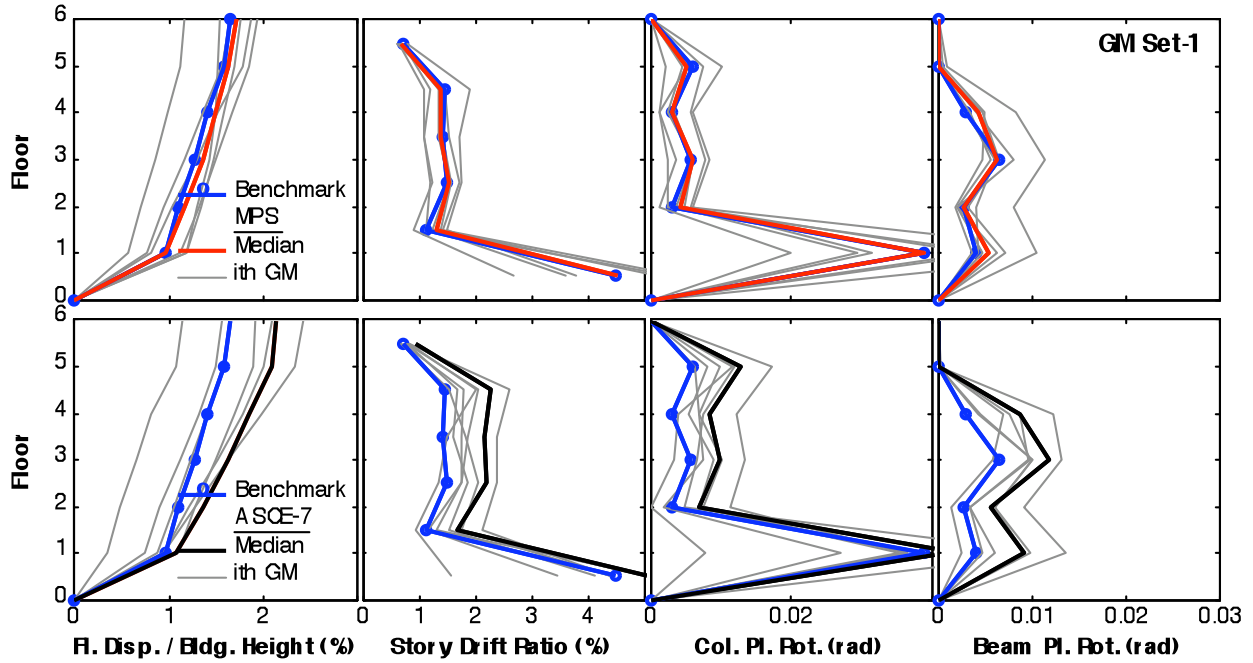


**Figure 5.21** Comparison of median EDPs for Ground Motion Set 1 scaled according to MPS (top row) and ASCE/SEI 7-05 (bottom row) scaling procedures with benchmark EDPs; individual results for each of seven scaled ground motions are also presented. Results are for the 6-story building.

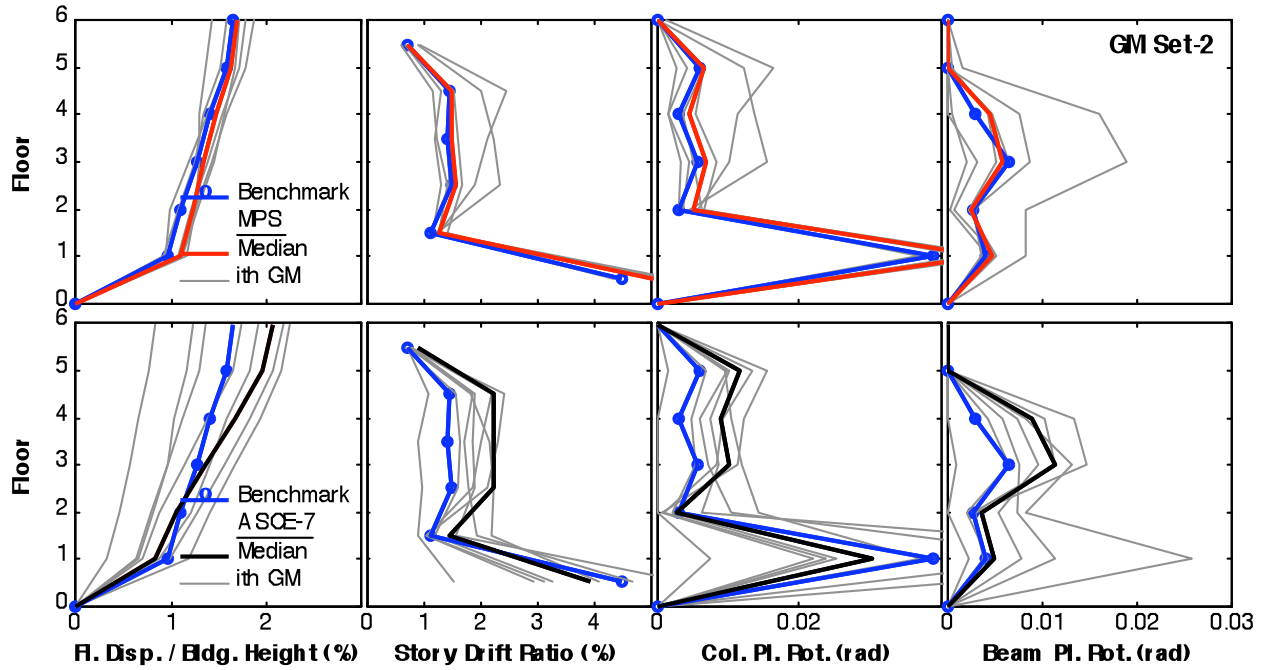


**Figure 5.22** Comparison of median EDPs for Ground Motion Set 2 scaled according to MPS (top row) and ASCE/SEI 7-05 (bottom row) scaling procedures with benchmark EDPs; individual results for each of seven scaled ground motions are also presented. Results are for the 6-story building.

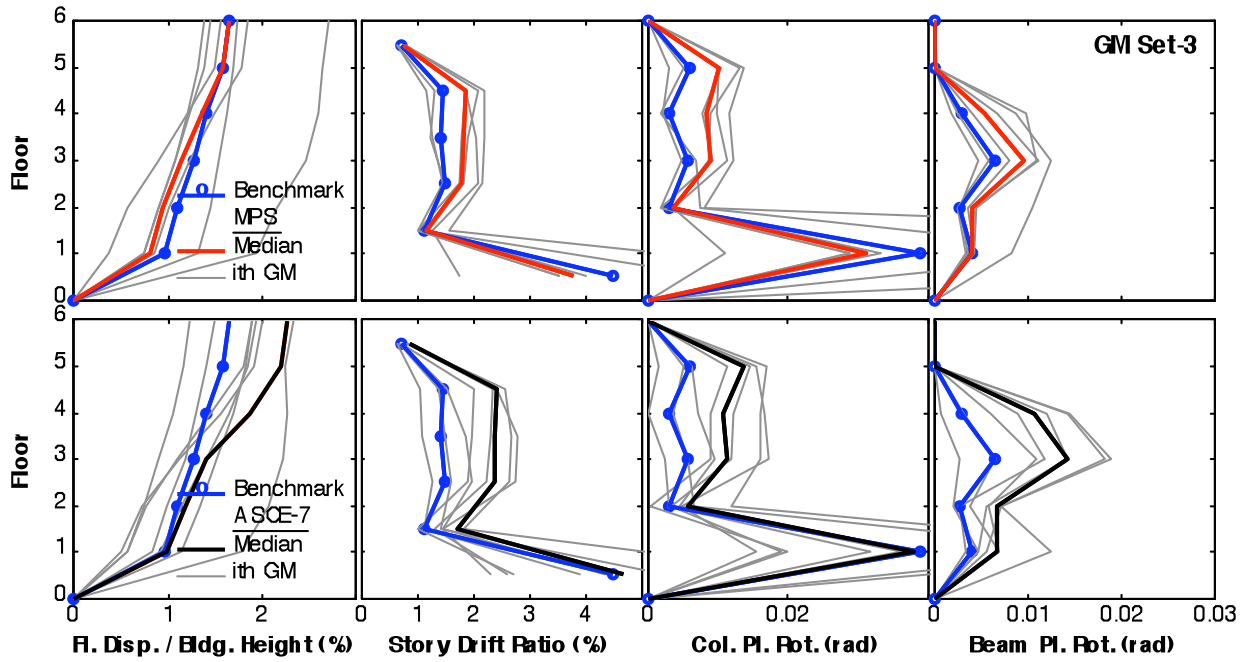


**Figure 5.23** Comparisons of median EDPs for Ground Motion Set 3 scaled according to MPS (top row) and ASCE/SEI 7-05 (bottom row) scaling procedures with benchmark EDPs; individual results for each of seven scaled ground motions are also presented. Results are for the 6-story building.

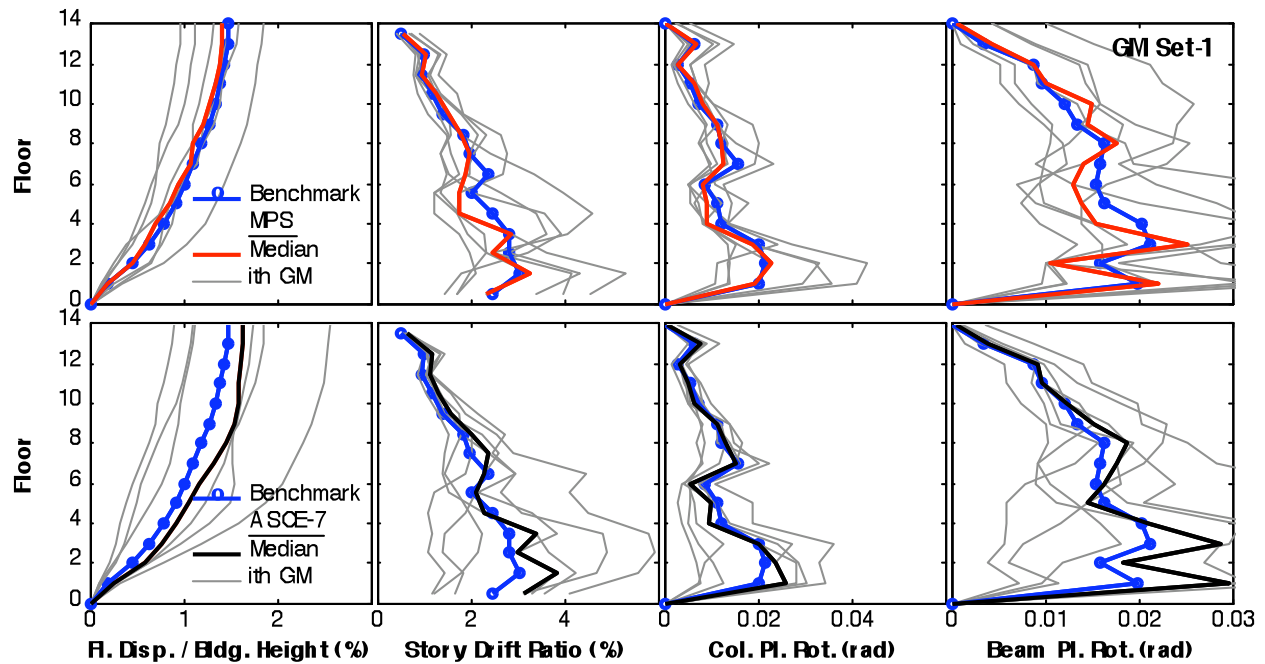


**Figure 5.24** Comparison of median EDPs for Ground Motion Set 1 scaled according to MPS (top row) and ASCE/SEI 7-05 (bottom row) scaling procedures with benchmark EDPs; individual results for each of seven scaled ground motions are also presented. Results are for the 13-story building.

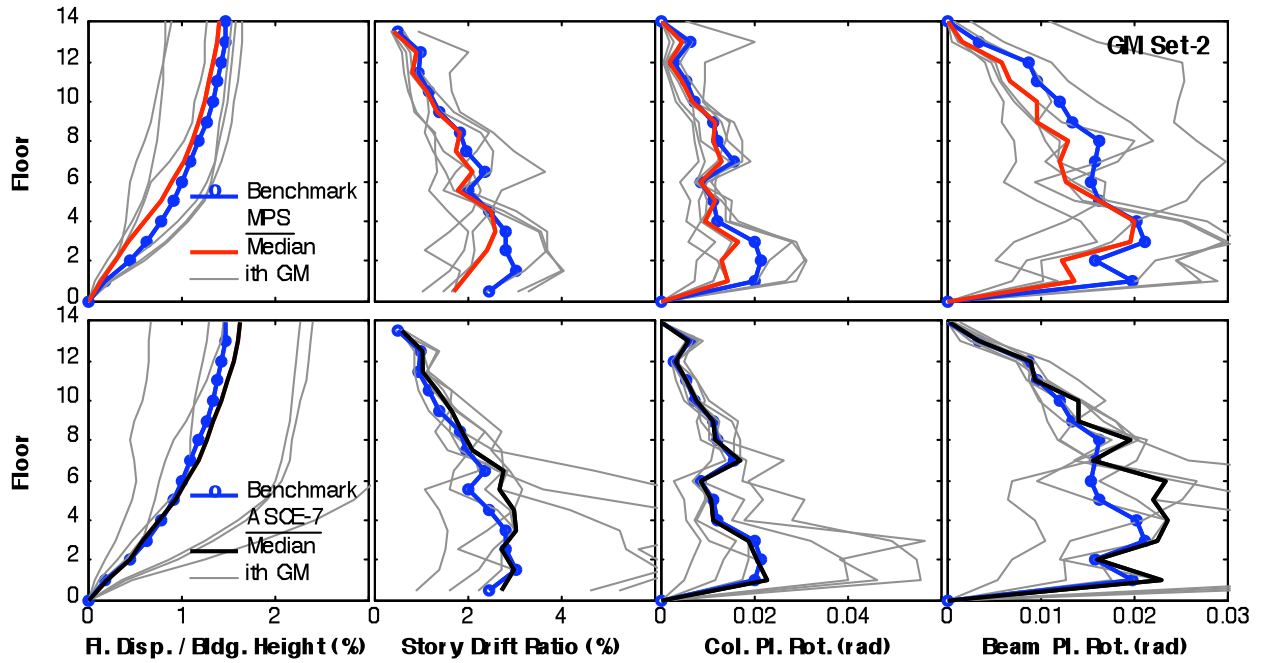


**Figure 5.25** Comparison of median EDPs for Ground Motion Set 2 scaled according to MPS (top row) and ASCE/SEI 7-05 (bottom row) scaling procedures with benchmark EDPs; individual results for each of seven scaled ground motions are also presented. Results are for the 13-story building.

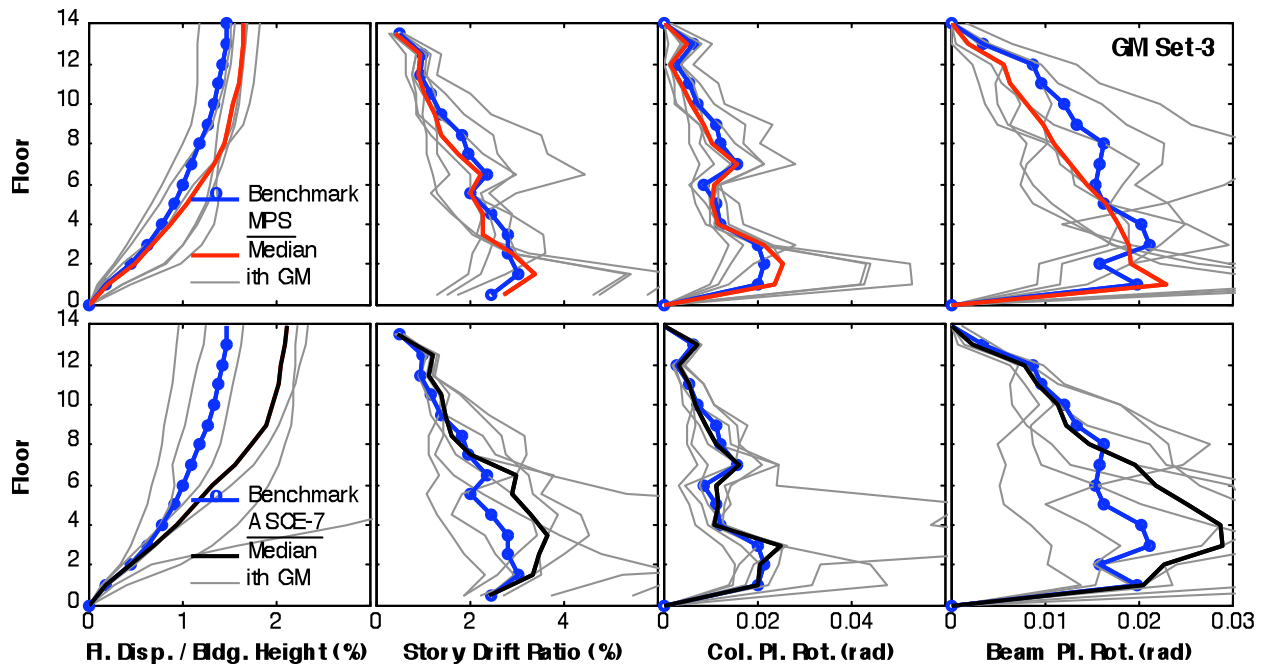


**Figure 5.26** Comparison of median EDPs for Ground Motion Set 3 scaled according to MPS (top row) and ASCE/SEI 7-05 (bottom row) scaling procedures with benchmark EDPs; individual results for each of seven scaled ground motions are also presented. Results are for the 13-story building.

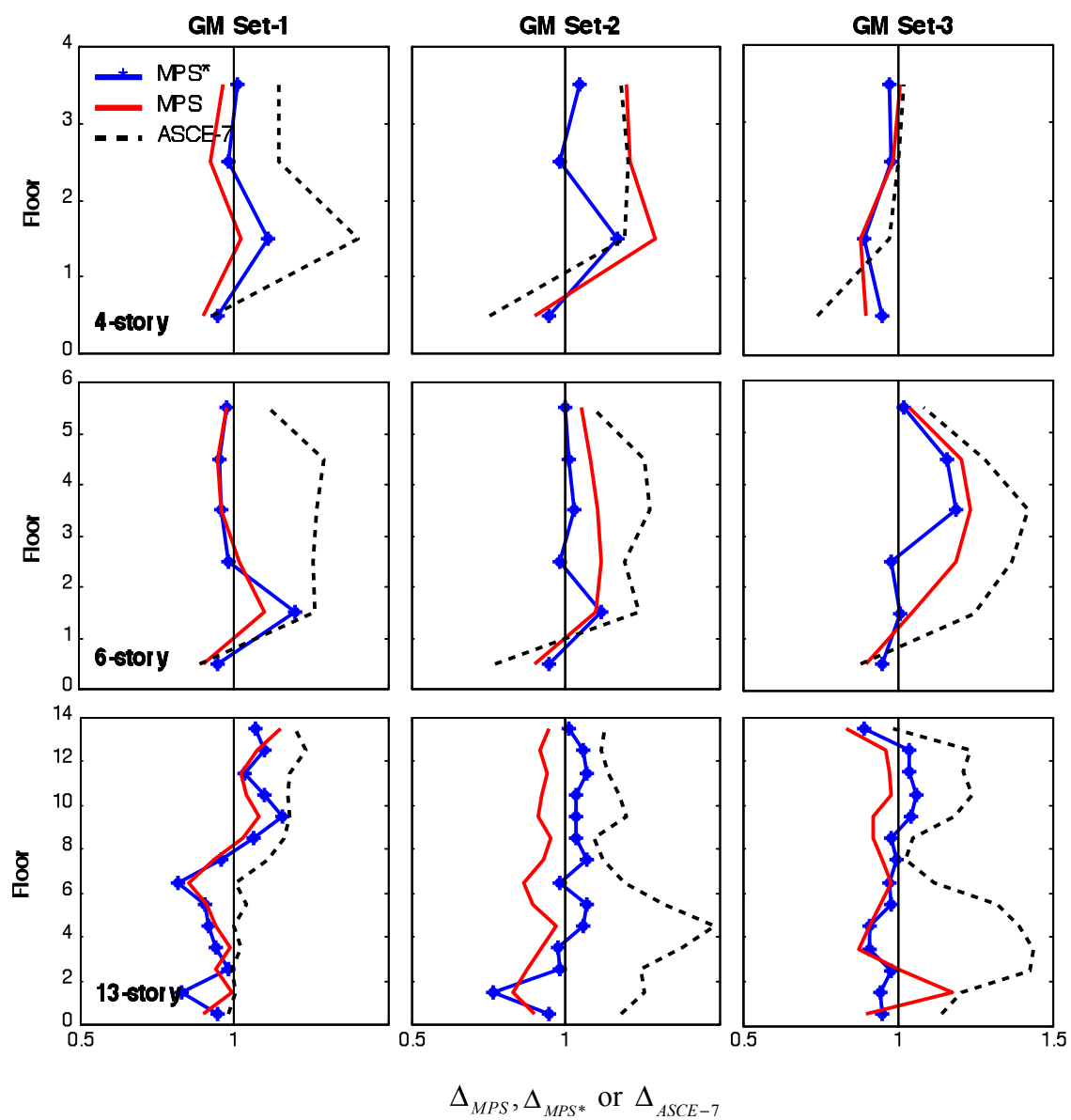


Figure 5.27 Median story drift ratios  $\Delta_{MPS}$ ,  $\Delta_{MPS^*}$  and  $\Delta_{ASCE-7}$  for three ground motions sets and for three buildings.

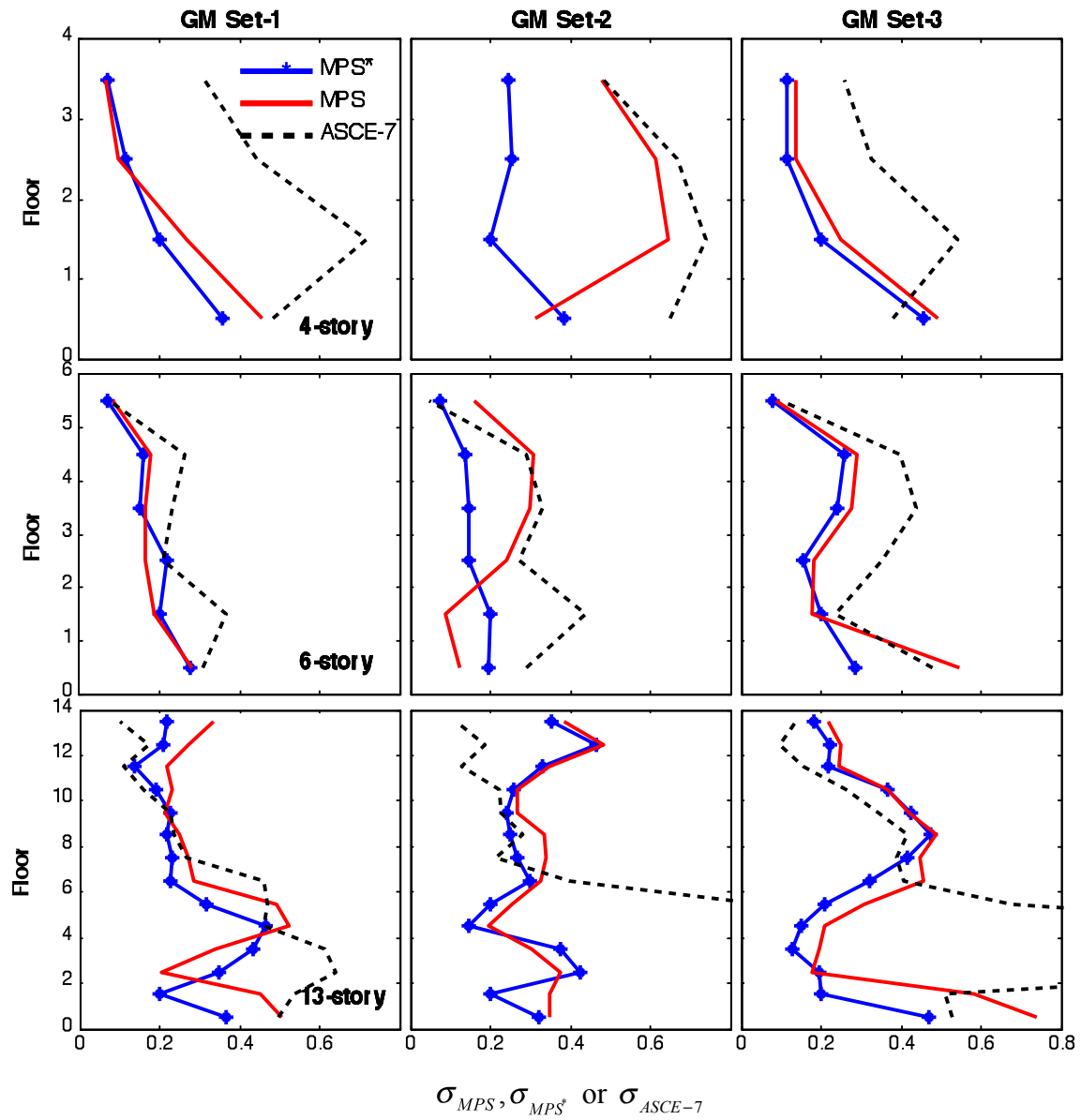
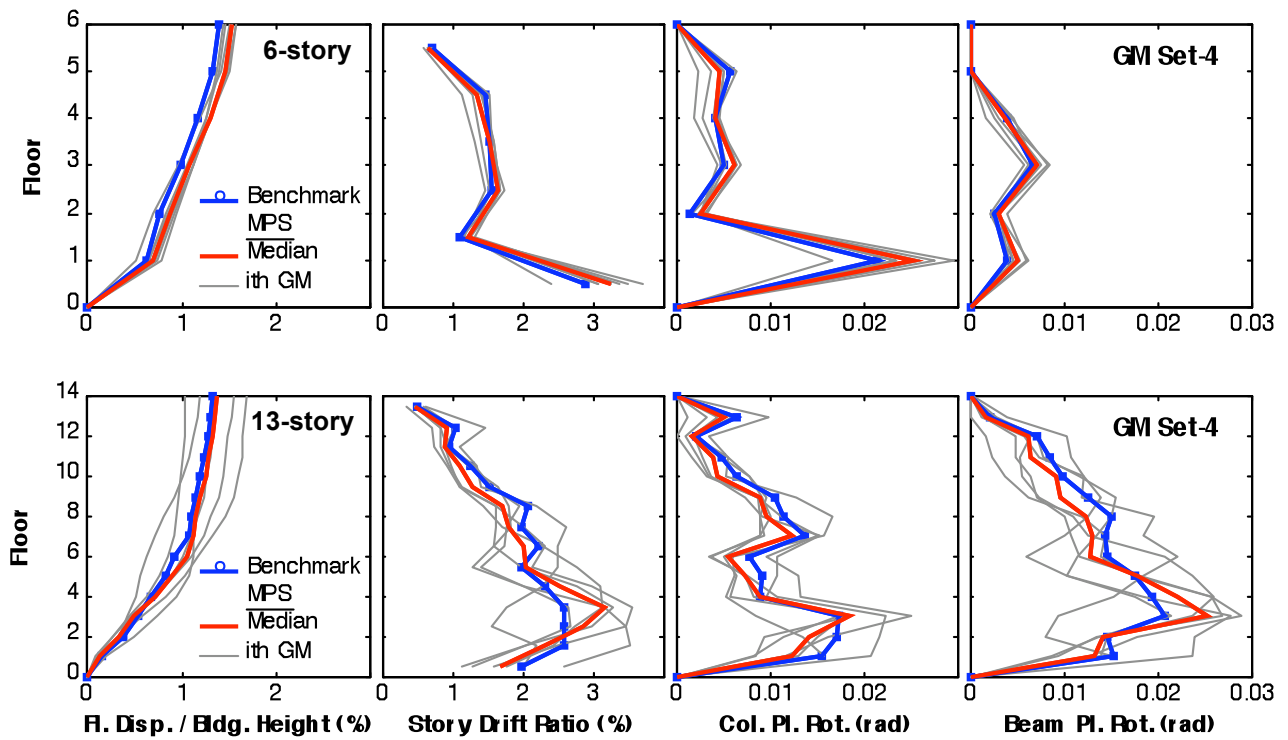
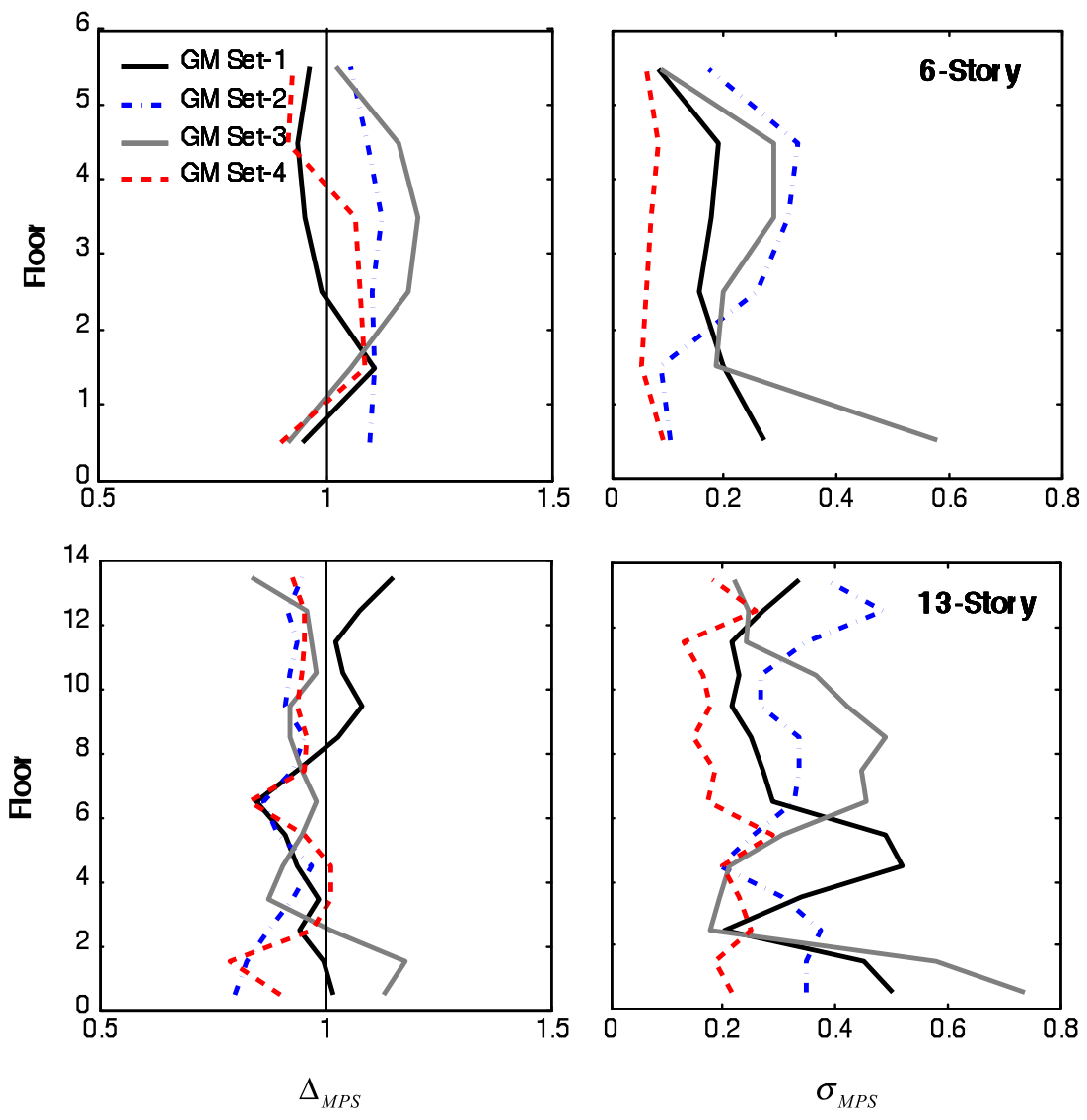


Figure 5.28 Dispersion of story drift ratios  $\sigma_{MPS}, \sigma_{MPS^*}$  and  $\sigma_{ASCE-7}$  for three ground motions sets and for three buildings.



**Figure 5.29** Comparison of median EDPs for Ground Motion Set 4 scaled according to MPS procedure with benchmark EDPs; individual results for each of seven scaled ground motions are also presented. Results are for the 6- (top row), and 13-story building (bottom row).



**Figure 5.30** Median  $\Delta_{MPS}$  and dispersion  $\sigma_{MPS}$  of story drift ratios for four ground motions sets and for two buildings.

## **6. EVALUATION OF MPS PROCEDURE: TALL BUILDINGS**

For tall buildings with unusual configurations, innovative structural systems and high performance materials, the California Building Code (CBC) (ICBO, 2007) and ASCE/SEI 7-05 (ASCE, 2005) documents permit the use of “alternate materials and methods of construction” relative to those prescribed in their seismic requirements with the approval of the regulatory agency. For these buildings, performance-based seismic design (PBSD) concepts are being increasingly employed to ensure their safety, constructability, sustainability and affordability. PBSD often requires nonlinear RHA to validate prescribed performance objective, which is generally *collapse prevention* for tall buildings under a very rare earthquake with a long recurrence interval, on the order of 2,475 years (Lew et al., 2008). The ground motions developed for very rare earthquakes are dominated by aleatoric (that is, source) uncertainties because the strong ground motions recorded from large magnitude earthquakes are scarce. Thus, there is a great need to establish rational procedures for selecting and scaling records to match the target design spectrum.

This chapter investigates the accuracy and efficiency of the MPS procedure for nonlinear RHA of tall buildings where higher-mode effects generally have larger contribution to response. In addition, the accuracy and efficiency of the scaling procedure recommended in the ASCE/SEI 7-05 document is evaluated for selected two tall moment-frame steel buildings.

### **6.1 BUILDINGS SELECTED**

The buildings selected to evaluate the efficiency and accuracy of the MPS method are existing 19- and 52-story steel special moment resisting frame buildings representative of tall building types in California. Both buildings are instrumented, and their recorded motions during past earthquakes were utilized to validate the computer models.

#### **6.1.1 19-story Building**

The building shown in figure 6.1 is located in Century City – Los Angeles, designed in 1966-67 and constructed in 1967. It has 19 stories above ground and 4 stories of parking below the ground level. The vertical load carrying system consists of 11.4 cm thick reinforced concrete slabs supported by steel beams. There is no composite action between the slab and steel beams

due to lack of shear studs. The lateral load resisting system consists of four ductile steel moment frames in the longitudinal direction and five X-braced frames in the transverse direction. Moment resisting connections are used at the intersection of beams and columns. Perimeter columns are standard I-sections except at the first story where columns are built-up box-sections. The foundation system consists of 22 m long driven steel I-beam piles, capped in groups and connected by 61 cm square reinforced concrete tie beams.

The building was initially instrumented with only three sensors at the time of the 1971 San Fernando earthquake. 15 sensors were in place during the 1994 Northridge earthquake (fig. 6.2). During the Northridge event (its epicenter was 20 km away from the site), the recorded peak horizontal accelerations were 0.32 g at the basement, 0.53 g at the ground floor and 0.65 g at the roof; this intensity of shaking resulted in moderate damage in the building in the form of buckling in some braces at upper floor levels in the transverse direction (Naeim, 1997). There was no damage in the perimeter moment frames.

### **6.1.2 52-story Building**

The second building selected is one of the tallest buildings in downtown Los Angeles, designed in 1988 and constructed in 1988–90. This building has a 52-story steel frame office tower and five levels of basement as underground parking. The floor plans of the tower are not perfectly square; the tip of every corner is clipped and the middle third of each side is notched. In groups of about five stories, above the 36<sup>th</sup> story, the corners of the floors are clipped further to provide a setback (fig. 6.3).

The structural system of the building is composed of a braced-core, twelve columns (eight on the perimeter and four in the core), and eight 91.4 cm deep outrigger beams at each floor connecting the inner and outer columns. The core, which is about 17 m by 21 m, is concentrically braced between the level-A (the level below the ground-level) and the 50<sup>th</sup> story. Moment resisting connections are used at the intersection of beams and columns. The outrigger beams, about 12 m long, link the four core columns to the eight perimeter columns to form a ductile moment resisting frame. The outrigger beams are laterally braced to prevent lateral torsional buckling and are effectively connected to the floor diaphragm by shear studs to transmit the horizontal shear force to the frame. Perimeter columns are standard I-sections, while the core

columns are built-up sections with square cross section at the lower floor and crucifix section at the upper floors. The interior core is concentrically braced. The building foundation is concrete spread footings (2.74 to 3.35 m thick) supporting the steel columns with 13 cm thick concrete slab on grade (Ventura and Ding, 2000).

The building is instrumented with twenty accelerometers to record its translational and torsional motions (fig. 6.4). During the Northridge earthquake (its epicenter was 30 km away from the site), the recorded values of peak horizontal accelerations were 0.15 g at the basement, 0.17 g at the level-A, and 0.41 g at the roof; no structural damage was observed. The latest recorded event, the 2008 Chino-Hills earthquake (its epicenter is 47 km away from the site), generated a PGA of 0.06 g at the ground and 0.26 g at the roof level.

## **6.2 ANALYTICAL MODELS AND CALIBRATION STUDIES**

### **6.2.1 19-story Building**

Three dimensional (3-D) computer model of the building was developed. Steel columns, beams, and braces were modeled by force-based nonlinear beam-column element in the open source finite element platform, OpenSees (2009). To properly model the buckling response of the brace, a slight imperfection is modeled at the brace's mid-span. Centerline dimensions were used in element modeling. The building weight, including estimates of non-structural elements such as partition walls and the mechanical equipments on the roof, was estimated to be 102,309 kN. Nodes at each floor were constrained to have the same lateral displacement to simulate rigid diaphragm behavior. The estimated floor mass and mass moment of inertia were lumped at the centre of mass at each floor. Panel zone deformations and local connection fracture were not considered therefore modeling of members and connections was based on the assumption of stable hysteresis loops derived from a bilinear stress-strain model with 3% strain hardening. The expected yield stress for steel members equal to ~250 MPa was used. The columns were assumed to be fixed at the base level. The P- $\Delta$  effects were included in the global system level.

As shown in figure 6.5, the first six natural vibration periods of the building are identified by frequency domain analysis of the motion of the roof relative to base motion recorded during the Northridge event. The computer model was able to match the measured periods (table 6.1).

Figure 6.6 plots the computed mode shapes for the first six modes; although the motion is dominantly in the transverse direction, a slight torsional component exists. Rayleigh damping was selected to be 3% of critical for the first and sixth modes (fig. 6.7) Nonlinear RHA of the building subjected to the three components of the motion recorded at the base level during the Northridge event leads to the relative displacement response in two horizontal directions at the roof, eighth and second floors shown in figure 6.8, where it is compared with the motions derived from records. The excellent agreement between the computed and recorded displacements indicates that the computer model is adequate.

### **6.2.2 52-story Building**

The 3-D model of the 52-story building in OpenSees (2009) included 58 separate column types and 23 different beam types. The building weight, including estimates of non-structural elements such as partition walls and the mechanical equipment in the roof, was estimated to be 235,760 kN. The material model is based on stable hysteresis loops derived from a bilinear stress-strain model with 2% strain hardening. All steel framing including columns are ASTM A-572 (grade 50) with a nominal yielding strength of 345 MPa.

The first nine natural vibration periods of the building identified from the recorded relative roof motions with respect to base during the Northridge and Chino-Hills events are shown in figure 6.9. The computer model was able to match the measured periods reasonably well (table 6.2). Figure 6.10 plots the mode shapes for the first nine modes; torsional modes are well separated from translational modes. Rayleigh damping was selected to be 4% of critical for the first and ninth modes (fig. 6.11). Nonlinear RHA of the building subjected to the three components of the motion recorded at the base level during the Northridge event leads to the relative displacement response in two horizontal directions at the roof, thirty fifth, twenty-second and fourteenth floor shown in figure 6.12. The excellent agreement between the computed and recorded displacements indicates that the computer model is adequate, at least in the elastic range.

### 6.3. FIRST-“MODE” SDF-SYSTEM PARAMETERS

The force-deformation relation  $F_{SI} / L_I - D_I$  for the first-“mode” SDF system for each building is determined from the base shear – roof displacement relation defined by first-“mode” pushover curve by utilizing  $F_{s1}/L_1 = V_{b1} / M_1^*$  and  $D_1 = u_{r1} / \Gamma_1 \phi_{r1}$ . For both buildings, only the E-W direction is considered in the pushover analysis. The resulting force-deformation relations for the first-“mode” SDF system are shown in figure 6.13. For the 19-story building, a bilinear hysteretic force-deformation relation is found to be adequate, while for the 52-story building, the hysteretic force-deformation relation is idealized by the peak-oriented model (Ibarra and Krawinkler, 2005; Ibarra and others, 2005) with the monotonic curve idealized as tri-linear.

### 6.4. EVALUATION OF MPS PROCEDURE

The efficiency and accuracy of the MPS procedure will be evaluated for each of three ground motion sets (table 5.1) separately by comparing the median values of EDPs determined by nonlinear RHA of each building due to the seven scaled records against the benchmark EDPs. Although the twenty-one records selected are the most intense records in the NGA database consistent with the seismic hazard defined in Chapter 4.3, the 19- and 52-story buildings remain essentially within their linearly elastic range. To impose significant inelastic deformations, these twenty-one ground motion records were amplified by a factor of three and their median response spectrum (fig. 6.14) is treated as the target spectrum. Nonlinear RHAs under scaled records indicates significant nonlinearity from both buildings as shown in figure 6.15, where the resultant peak roof displacement values are identified on the first-“mode” pushover curve; and their median values are marked as vertical dashed line. The median deformation exceeds the yield deformation by factors of 3.3 and 2.6, respectively for the 19- and 52-story buildings. Figure 6.16 shows the benchmark EDPs for the two buildings: maximum values of floor displacements (normalized by building height), story drift ratios (story drift ÷ story height), and plastic rotations of the beams and columns. Results from individual records are also included to demonstrate the large dispersion or record-to-record variability. The peak values of story drift ratios range from 1.2% to 12.5% for the 19-story building, and 0.4% to 5.8% for the 52-story building.

In evaluations of the MPS, “exact” value of first-“mode” target inelastic spectral displacement (that is,  $\bar{D}_1^I$ ) was assumed to be unknown and it was estimated using an empirical  $C_R$  equation (Chopra and Chintanapakdee, 2004). This estimate is compared in figure 6.17 against the “exact” value of  $\bar{D}_1^I$  (dashed horizontal line) determined by nonlinear RHAs of the first-“mode” inelastic SDF system for twenty-one “unscaled” records; values from individual records are also included to show its record-to-record variability. The empirical equation for  $C_R$  overestimates “exact” value of  $\bar{D}_1^I$  by only 8% for the 19-story building, and under estimates “exact” value of  $\bar{D}_1^I$  by only 1% for the 52-story building.

Once  $\bar{D}_1^I$  is estimated, an appropriate scale factor for each record is determined based on the inelastic first-“mode” SDF systems (fig. 6.13) by implementing Steps 7-8 of the MPS procedure. The scale factors established for each record in each of the three sets are presented in table 6.3 for both buildings. The EDPs determined by nonlinear RHAs due to three sets of seven ground motions scaled according to the MPS procedure are compared against the benchmark EDPs. Figures 6.18 and 6.19 present such comparisons respectively for the 19- and 52-story buildings considering the three sets of ground motions. Also included are the EDP values due to each of the scaled ground motions to show dispersion of the data. The values of EDPs due to a small (7) subset of scaled ground motions are close to the benchmark results. The median values of the peak floor displacements, story drift ratios and column plastic rotations are well estimated. The height-wise average errors in estimating the median values of peak floor displacements and drifts are 7% and 3%, respectively for the 19-story building, 9% and 8%, respectively for the 52-story building. These are the errors averaged over GM Sets 1-3.

The dispersion of the EDP values due to the seven scaled records is reduced as compared to the dispersion associated with the original records (fig. 6.16), but this reduction is less at intermediate and upper floors, suggesting that second-“mode” responses should also be considered in the MPS procedure.

## 6.5. MPS CONSIDERING SECOND-“MODE”

Next, the second vibration “mode” is considered in selecting the most appropriate set of seven ground motions out of the twenty-one records scaled based on the first-“mode” response only by implementing Steps 10-13 (Chapter – 2.1) of the MPS method. The seven records with the highest ranks (see Step 12) were defined as Ground Motion Set 4; this set is different for each building (see Table 6.4).

Figure 6.20 compares the median EDPs from ground motions scaled by the MPS method with the benchmark values for the two buildings. Considering the second-“mode” in selecting ground motions provides a more accurate estimate of the median EDPs; the height-wise average errors in estimating the median values of peak floor displacements and drift ratios are reduced to 6% and 2%, respectively for the 19-story building, 6% and 7%, respectively for the 52-story building. The height-wise average errors in beam plastic rotations are reduced from 34% (averaged over GM Sets 1-3) to 15% for GM Set 4 for the 52-story building where higher-mode contributions to response are more pronounced; however, the errors in case of the 19-story building remain essentially unchanged. For both buildings considering the second-“mode” in ground motion selection significantly reduces record-to-record variability (compared to the results achieved by Ground Motion Sets 1-3 as shown in figs. 6.18 and 6.19). The enhanced accuracy and efficiency are demonstrated in figure 6.21, where the  $\Delta$  and  $\sigma$ —the median value of the ratio of the estimated story drift to its benchmark value, and dispersion of this ratio—are plotted for the four sets of ground motions. Ground Motion Set 4 is more accurate (that is, height-wise distribution of  $\Delta$  is in average closer to unity) and efficient (that is,  $\sigma$  is closer to zero) than Ground Motion Sets 1 through 3.

## 6.6. COMPARING MPS AND CODE-BASED SCALING PROCEDURES

The EDPs determined by nonlinear RHA of the structure due to a set of seven ground motions scaled according to the ASCE/SEI 7-05 scaling method are compared against the benchmark EDPs. Figures 6.22 and 6.23 present such comparisons for the two buildings and for the three sets of seven ground motions. The ground motions scaled according to the ASCE/SEI 7-05 scaling method overestimate the median EDPs with the height-wise average overestimation of floor displacements and story drifts by 15% and 10% respectively, for the 19-story building,

93% and 130% respectively, for the 52-story building; obviously this overestimation in the latter case is unacceptably large. Errors in beam and column plastic rotations are also considerable. As evident by comparing figures 6.18 and 6.19 with figures 22-23, the MPS method leads to much smaller dispersion compared to the ASCE/SEI 7-05 scaling method. The large dispersion associated with the ASCE/SEI 7-05 scaling method suggests that ground motion records should not be selected randomly from a large set of records that conforms to the site-specific hazard conditions (that is, magnitude, distance and site geology), but their spectral shape should also be considered.

To demonstrate the importance of spectral shape of selected records on the accuracy and efficiency of the ASCE/SEI 7-05 scaling criteria, we deliberately selected a set of seven records (out of twenty-one) such that their scaled spectral accelerations,  $A(T_1)$  and  $A(T_2)$  at the first two vibration periods of the building,  $T_1$  and  $T_2$ , are significantly higher than the design spectrum; this final set is identified as Ground Motion Set 5. Figure 6.24 compares the average spectrum of scaled records in Set 5 with the design spectrum for the 19- and 52-story buildings; also shown are the individual spectra. For both buildings, the average value of  $A(T_1)$  and  $A(T_2)$  are significantly larger than the design spectrum values at these periods.

The median values of EDPs due to GM Set 5 are compared with the benchmark values in Figure 6.25 for the two buildings. Clearly the ASCE/SEI 7-05 scaling method grossly overestimates EDPs at almost all floors, for example, floor displacements are overestimated by as much as 100% for the 19-story building, and almost 200% for the 52-story building. The dispersion in responses due to Ground Motion Set 5 is much larger compared to Sets 1-3. To obtain acceptable estimates of EDPs using records scaled by the ASCE/SEI 7-05 scaling method, the selected records must satisfy the requirement that their scaled response spectra are close to the design spectrum values at  $T_1$  and  $T_2$ . In contrast, the MPS method (with scaling based on “first”-mode only) is effective in scaling the records in GM Set 5 to achieve good estimates of EDPs. This is demonstrated in figure 6.26 where the floor displacements and story drifts differ from the benchmark results by less than 10%; however the errors in plastic hinge rotations are larger. It is reassuring to observe that the MPS procedure is effective in scaling even records with spectral shape significantly different than the design spectrum.

**Table 6.1 Measured and computed natural periods for 19-story building**

Mode No.	Direction	Period (sec)	
		1994 Northridge	OpenSees
1	E-W	3.7	3.7
2	N-S + Torsion	3.4	3.4
3	E-W	1.4	1.4
4	N-S + Torsion	1.1	1.1
5	N-S + Torsion	0.8	0.8
6	E-W	0.6	0.6

**Table 6.2 Measured and computed natural periods for 52-story building**

Mode No.	Direction	Period (sec)		
		1994 Northridge	2008 Chino-Hills	OpenSees
1	E-W	5.9	5.6	5.8
2	Torsional	4.7	-	5.5
3	N-S	5.6	5.3	5.4
4	E-W	1.8	1.7	1.9
5	Torsional	1.7	1.7	1.8
6	N-S	1.7	1.7	1.7
7	E-W	0.9	0.9	1.1
8	Torsional	0.9	0.9	1.0
9	N-S	0.9	0.9	0.9

**Table 6.3 Scale factors for 19- and 52-story buildings and for three sets of seven ground motions**

No.	Earthquake	Station	Set	Scale Factor	
				19-story	52-story
1	Superstition Hills	Parachute Test Site	1	4.76	3.36
2	Northridge	Jensen Filter Plant	1	4.26	8.27
3	Northridge	Sylmar - Converter Sta East	1	3.86	4.41
4	Kobe, Japan	Takatori	1	6.57	5.42
5	Chi-Chi, Taiwan	TCU065	1	1.98	1.16
6	Chi-Chi, Taiwan	TCU102	1	3.28	1.99
7	Kocaeli, Turkey	Yarimca	1	3.51	3.40
1	Erzincan, Turkey	Erzincan	2	6.55	7.28
2	Imperial Valley	EC Meloland Overpass FF	2	3.46	5.01
3	Kobe, Japan	Port Island	2	2.71	4.90
4	Northridge	Sylmar - Converter Sta	2	3.03	3.06
5	Tabas, Iran	Tabas	2	2.38	1.09
6	Chi-Chi, Taiwan	TCU052	2	1.53	0.82
7	Chi-Chi, Taiwan	TCU084	2	4.53	6.11
1	Duzce, Turkey	Duzce	3	3.04	3.59
2	Imperial Valley	El Centro Array #7	3	3.08	3.39
3	Loma Prieta	LGPC	3	4.60	4.34
4	Northridge	Rinaldi Receiving Sta	3	3.43	5.39
5	Northridge	Sylmar - Olive View Med FF	3	4.43	4.80
6	Chi-Chi, Taiwan	TCU068	3	1.19	0.54
7	Northridge	Newhall - W Pico Canyon Rd	3	3.26	3.58

**Table 6.4 Scale factors for 19- and 52-story buildings considering second-“mode”**

No.	Earthquake	Station	Scale Factor
			19-story
1	Superstition Hills	Parachute Test Site	4.76
2	Duzce, Turkey	Duzce	3.04
3	Erzincan, Turkey	Erzincan	6.55
4	Loma Prieta	LGPC	4.60
5	Northridge	Sylmar - Converter Sta	3.03
6	Chi-Chi, Taiwan	TCU102	3.28
7	Northridge	Newhall - W Pico Canyon Rd	3.36
			52-story
1	Superstition Hills	Parachute Test Site	3.36
2	Duzce, Turkey	Duzce	3.59
3	Imperial Valley	El Centro Array #7	3.39
4	Imperial Valley	EC Meloland Overpass FF	5.01
5	Northridge	Sylmar - Converter Sta	3.06
6	Northridge	Newhall - W Pico Canyon Rd	3.58
7	Kocaeli, Turkey	Yarimca	3.40

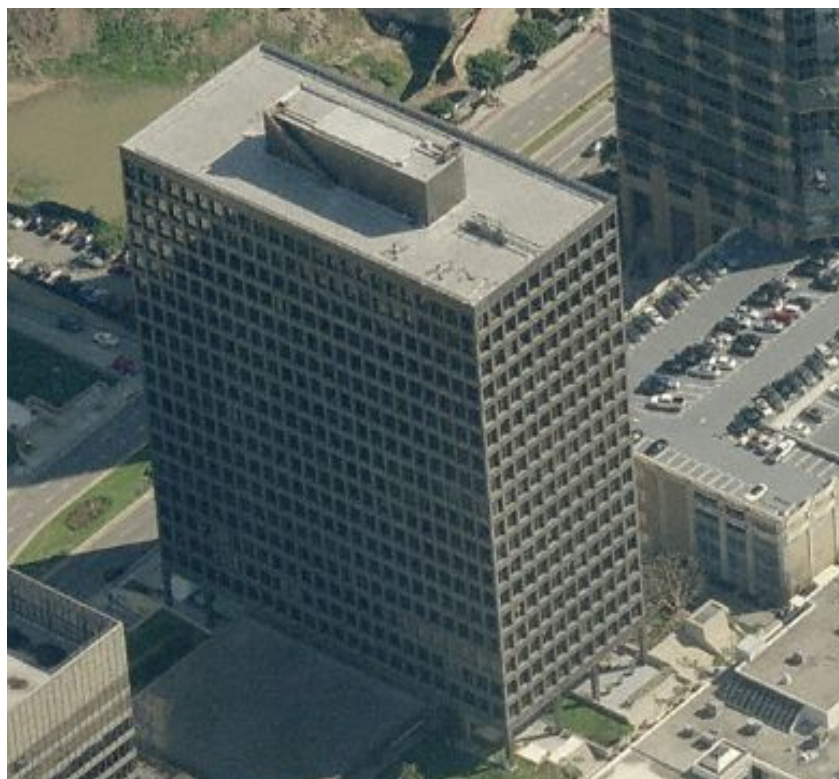


**Figure 6.1 Overview of the 19-story building in Century City, Los Angeles, CA.**

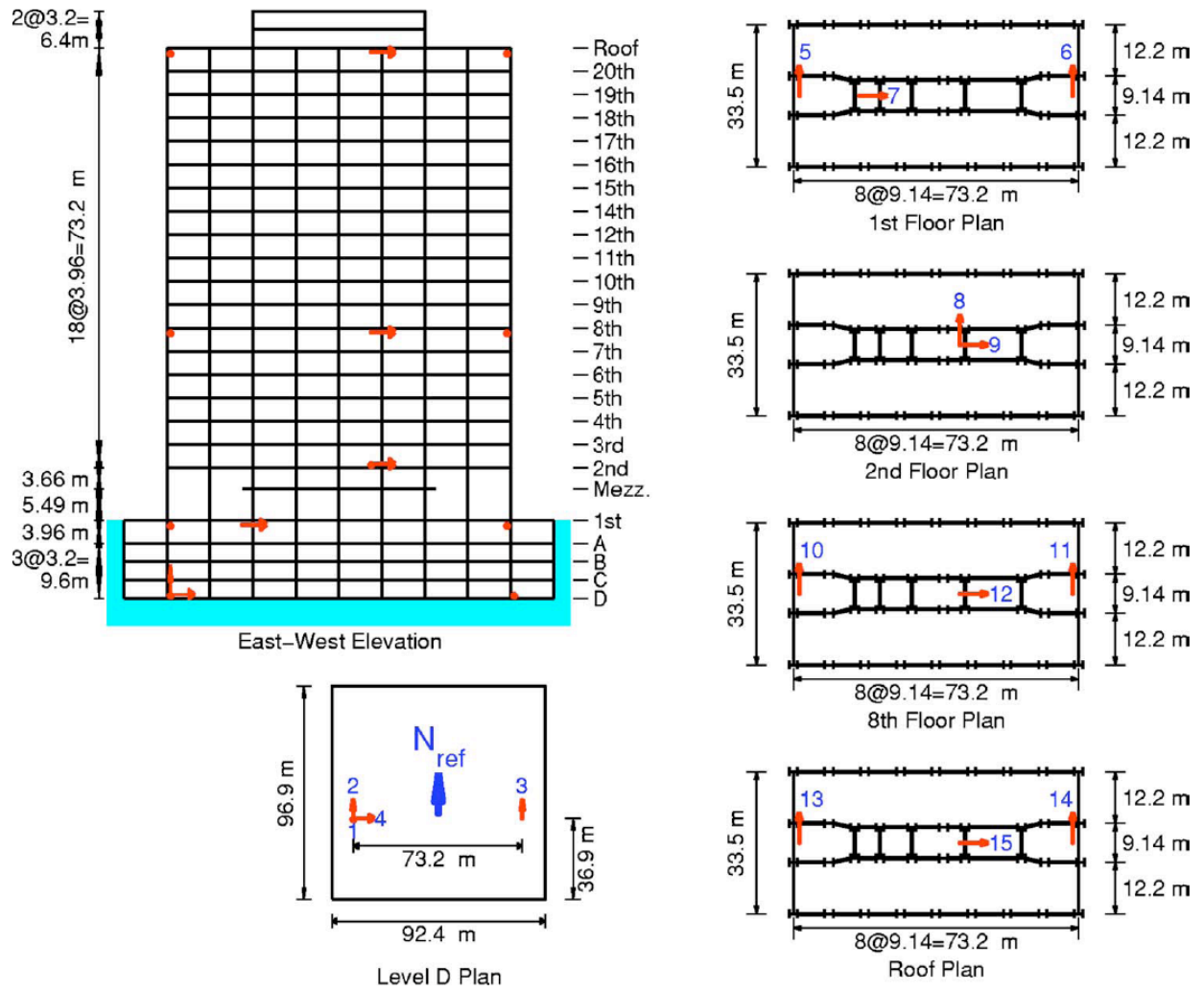


**Figure 6.2 Instrumentation lay out of the 19-story building.**



**Figure 6.3** Overview of the 52-story building in downtown, Los Angeles, CA.

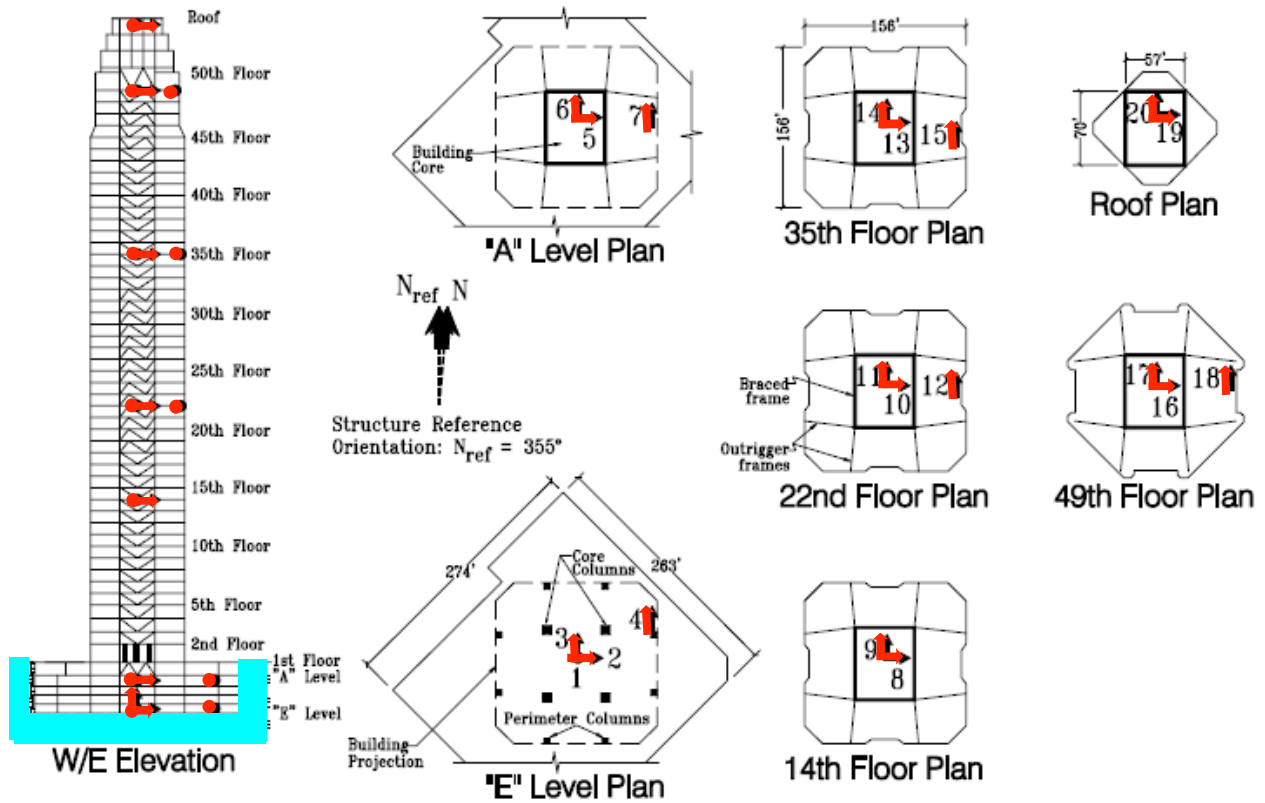


Figure 6.4 Instrumentation lay out of the 52-story building.

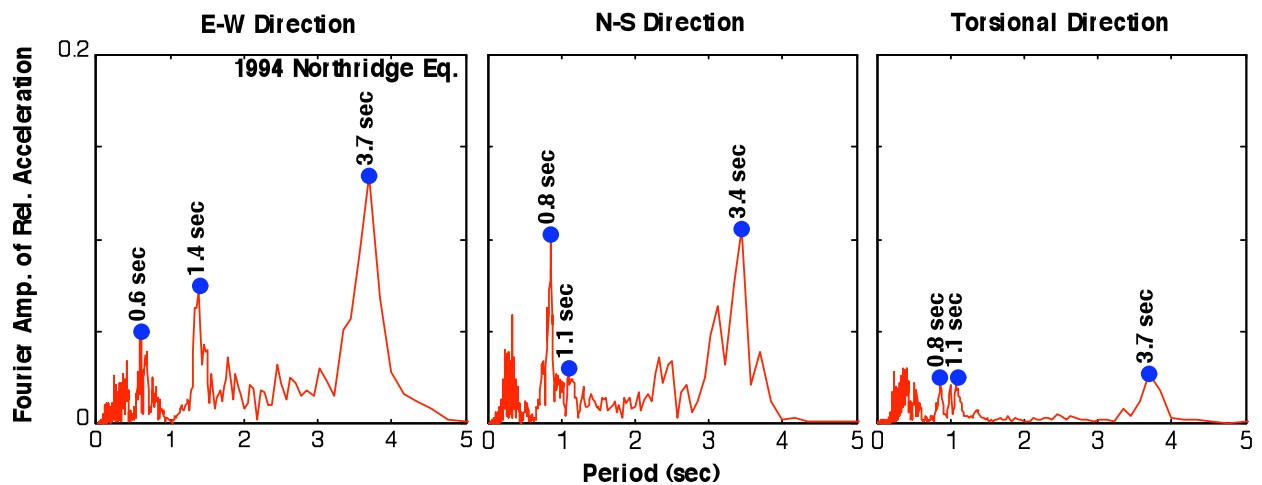


Figure 6.5 Identification of natural periods for the 19-story building using recorded relative motion at the roof level during the 1994 Northridge earthquake.

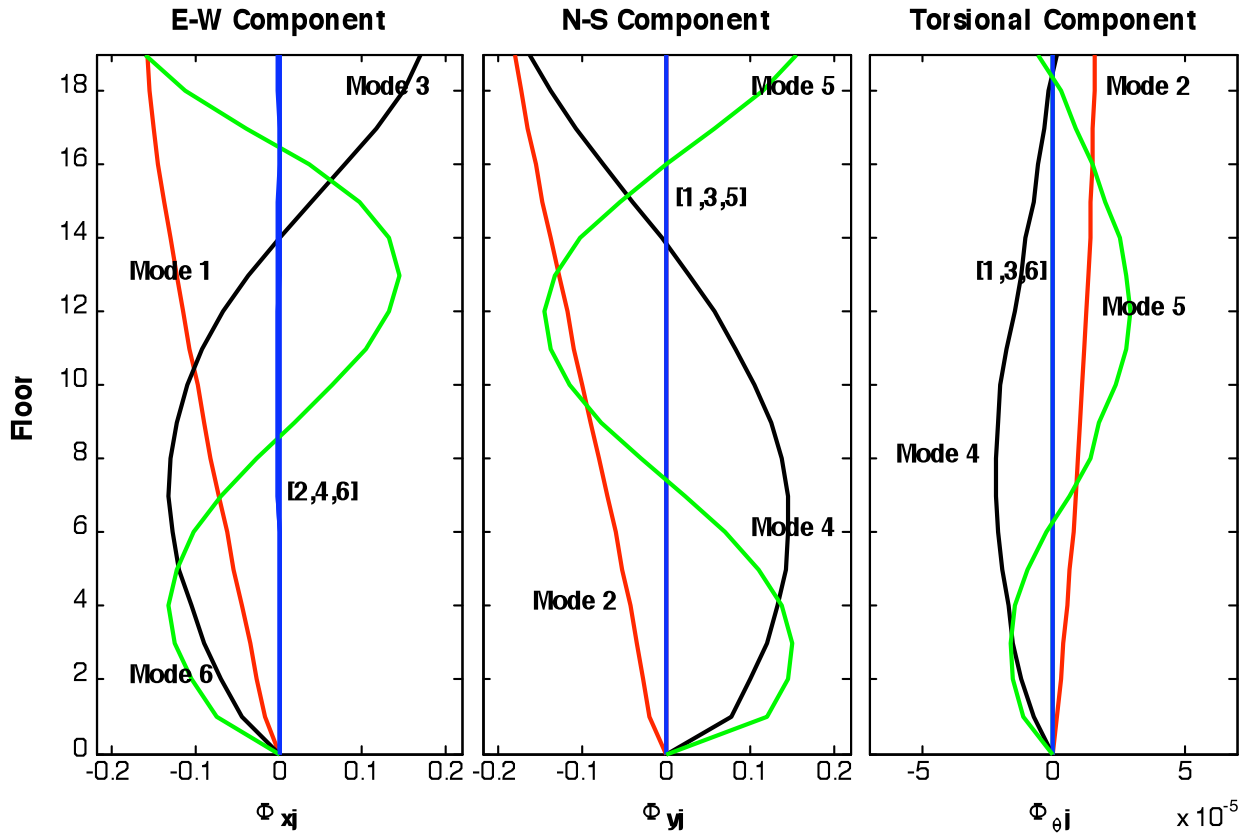


Figure 6.6 Natural vibration modes of the 19-story building.

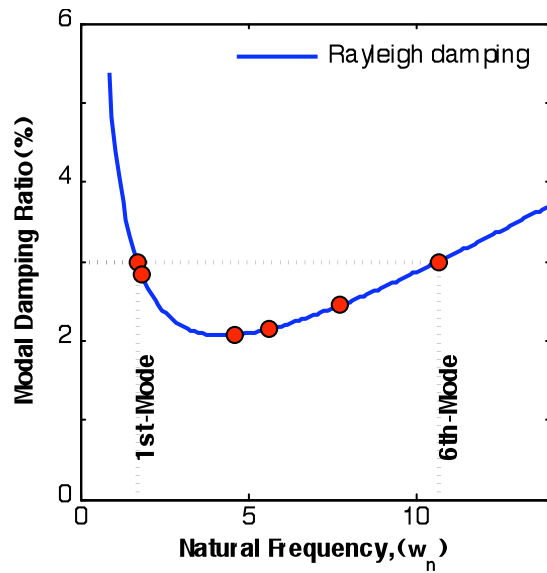
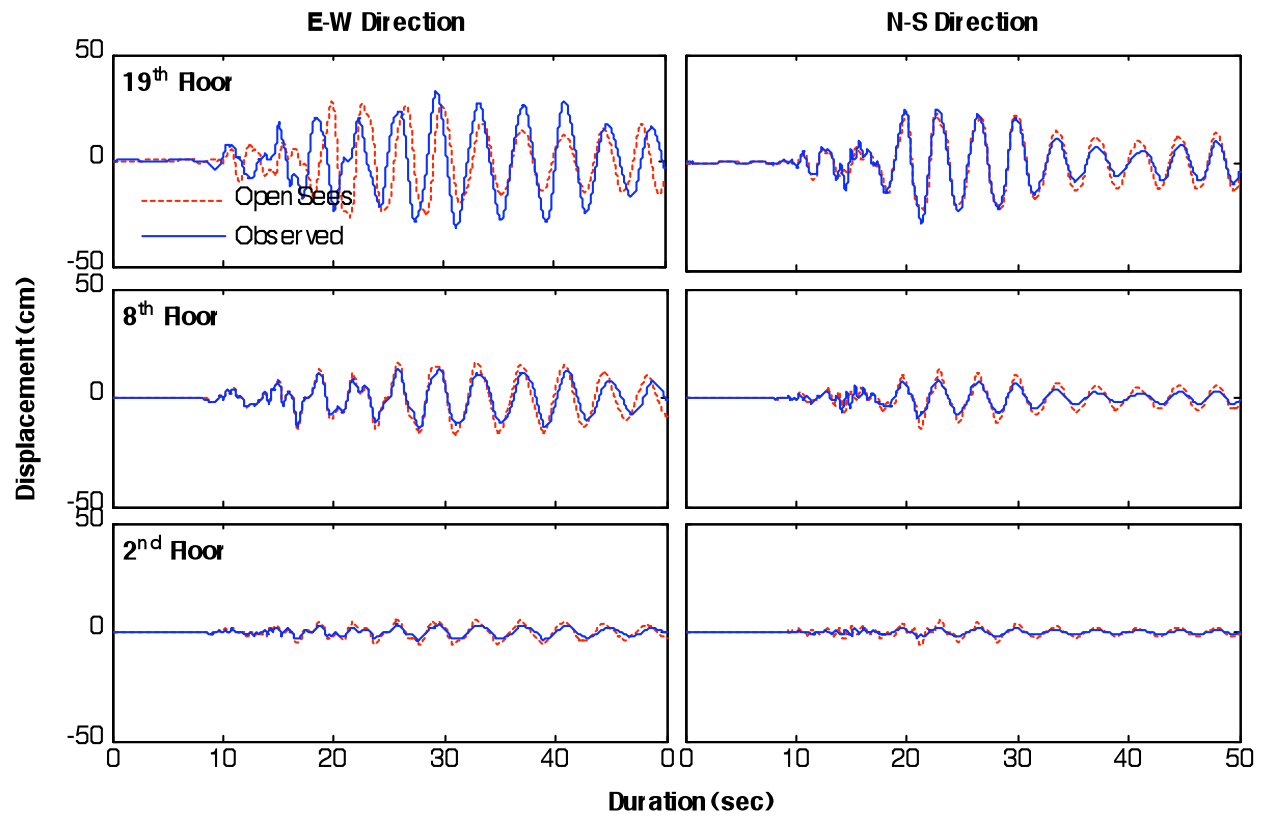
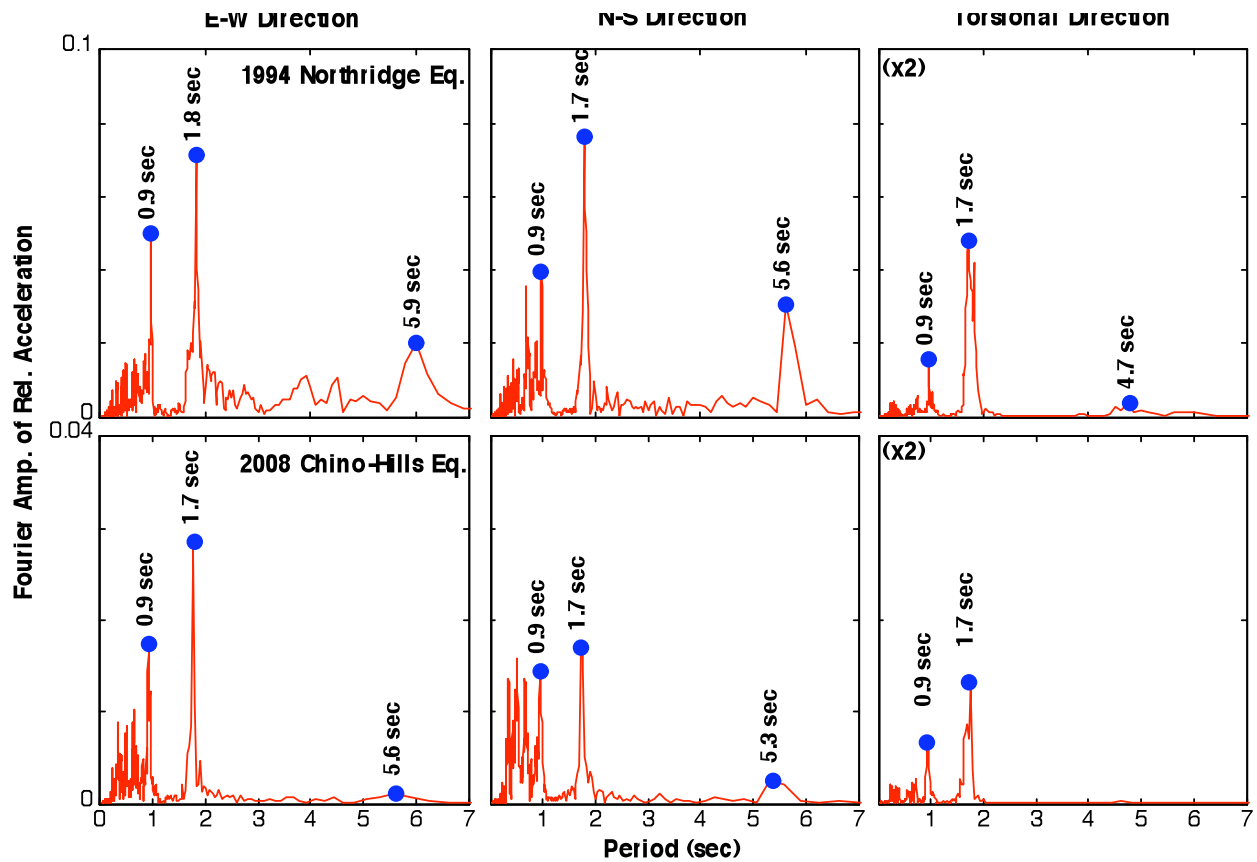


Figure 6.7 Modal damping ratios for the 19-story building.



**Figure 6.8** Comparison of observed and computed floor displacements in two horizontal directions of the 19-story building at different floor levels; recorded data is from the M6.7 1994 Northridge earthquake. The excellent agreement between the computed (OpenSees) and recorded displacements indicates that the computer model is adequate.



**Figure 6.9** Identification of natural periods for the 52-story building using recorded relative motion at the roof level (for E-W and N-S directions) and 49<sup>th</sup> floor level (for torsional direction) during the 1994 Northridge (upper-panels) and 2008 Chino-Hills (lower-panels) earthquakes.

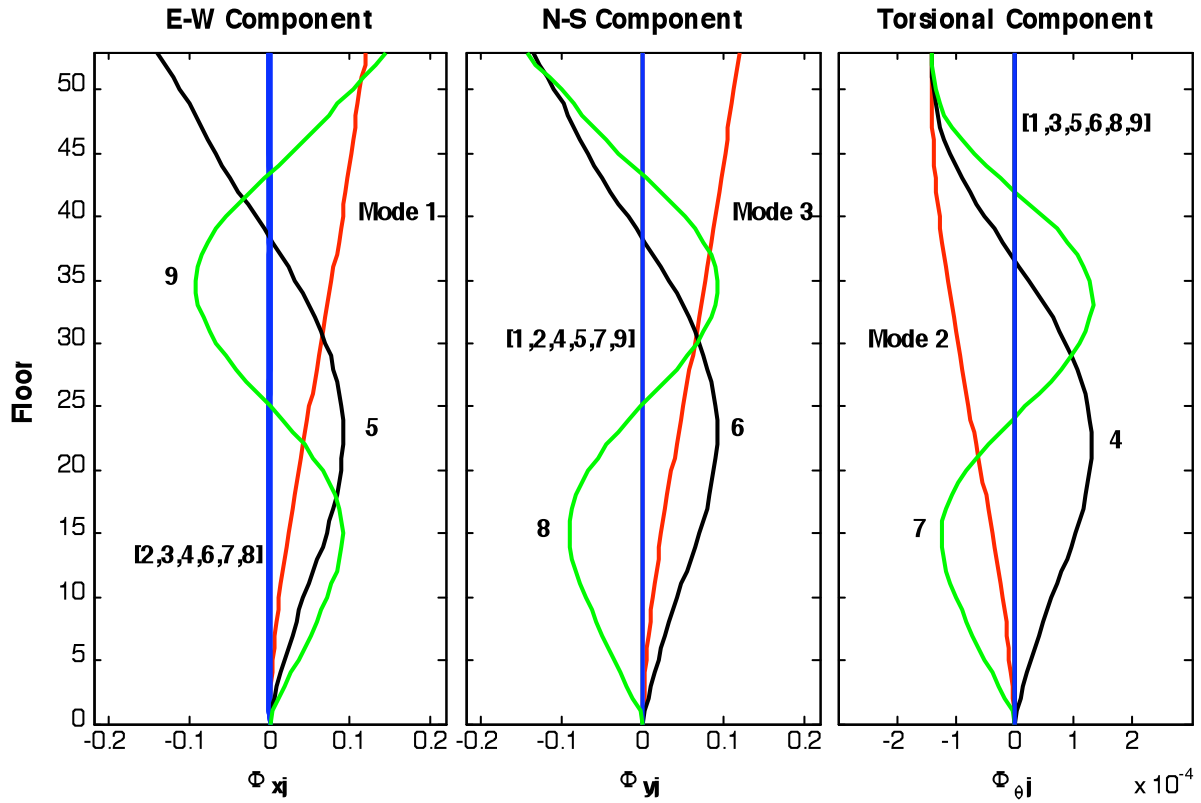


Figure 6.10 Natural vibration modes of the 52-story building.

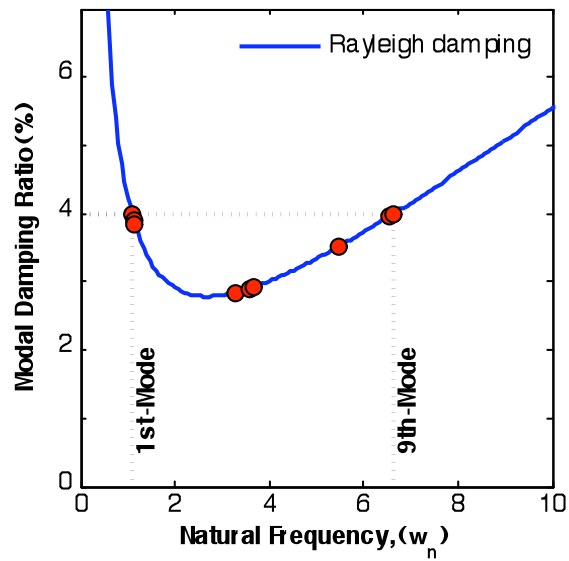
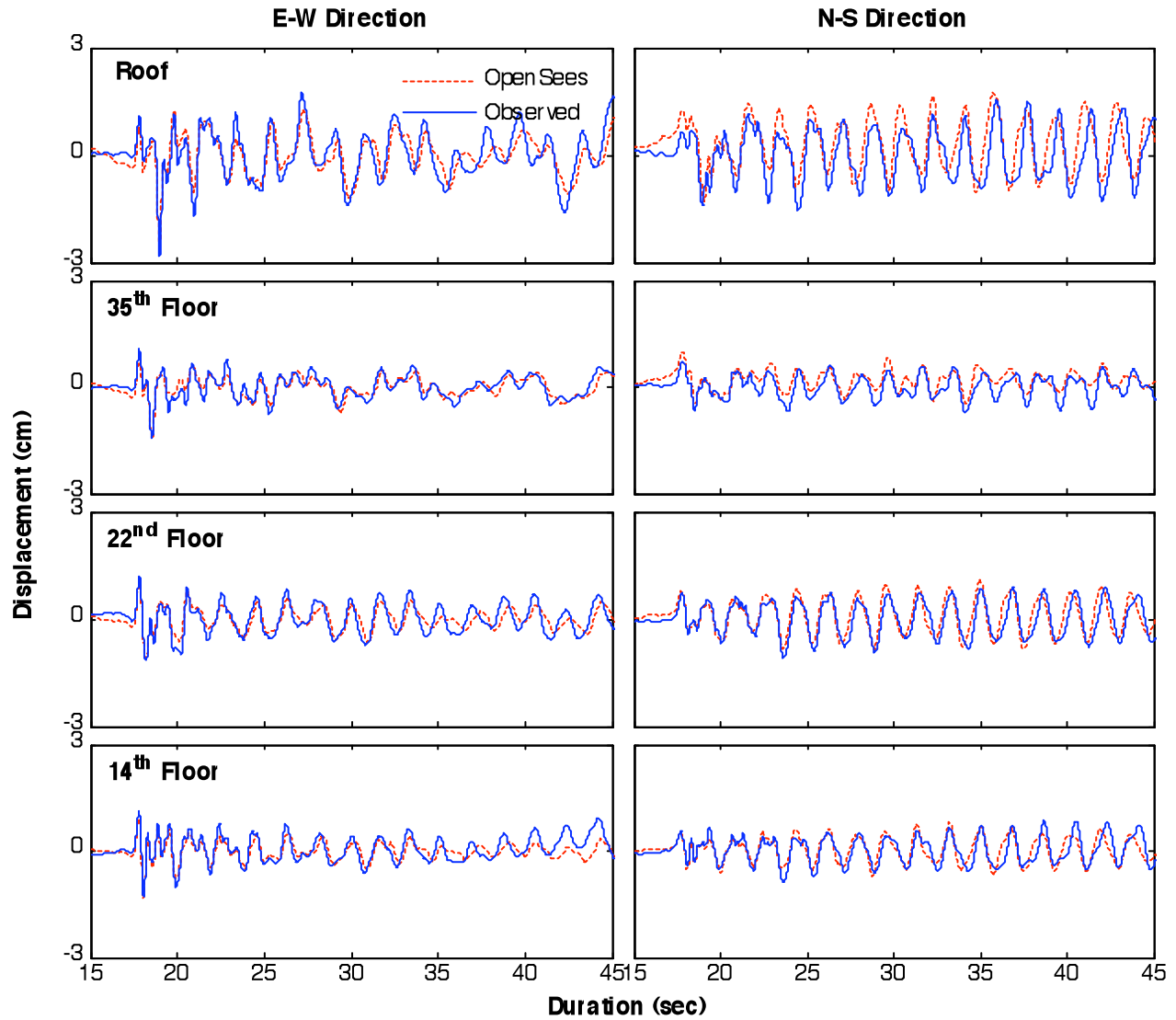
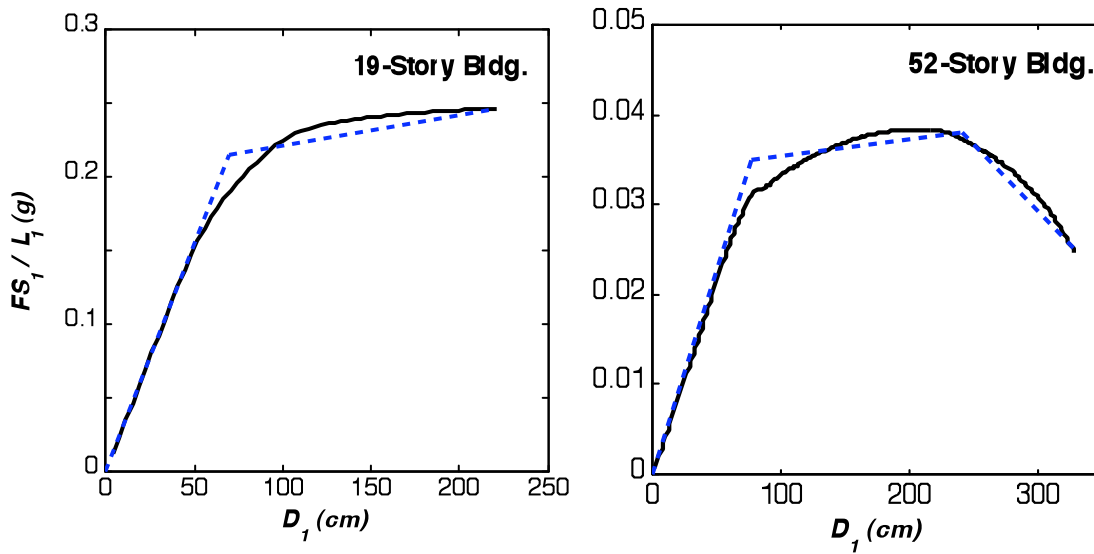


Figure 6.11 Modal damping ratios for the 52-story building.



**Figure 6.12** Comparison of recorded and computed floor displacements in two horizontal directions of the 52-story building at different floor levels; recorded data is from the M5.4 2008 Chino-Hills earthquake. The excellent agreement between the computed (OpenSees) and recorded displacements indicates that the computer model is satisfactory.



**Figure 6.13** Comparison of first-“mode” pushover curve (solid line) and its idealized model (dashed line) for the 19- and 52-story buildings. For the 19-story building, a bilinear hysteretic force-deformation relation is found to be adequate, while for the 52-story building, the hysteretic force-deformation relation is idealized by the peak-oriented model with the monotonic curve idealized as tri-linear.

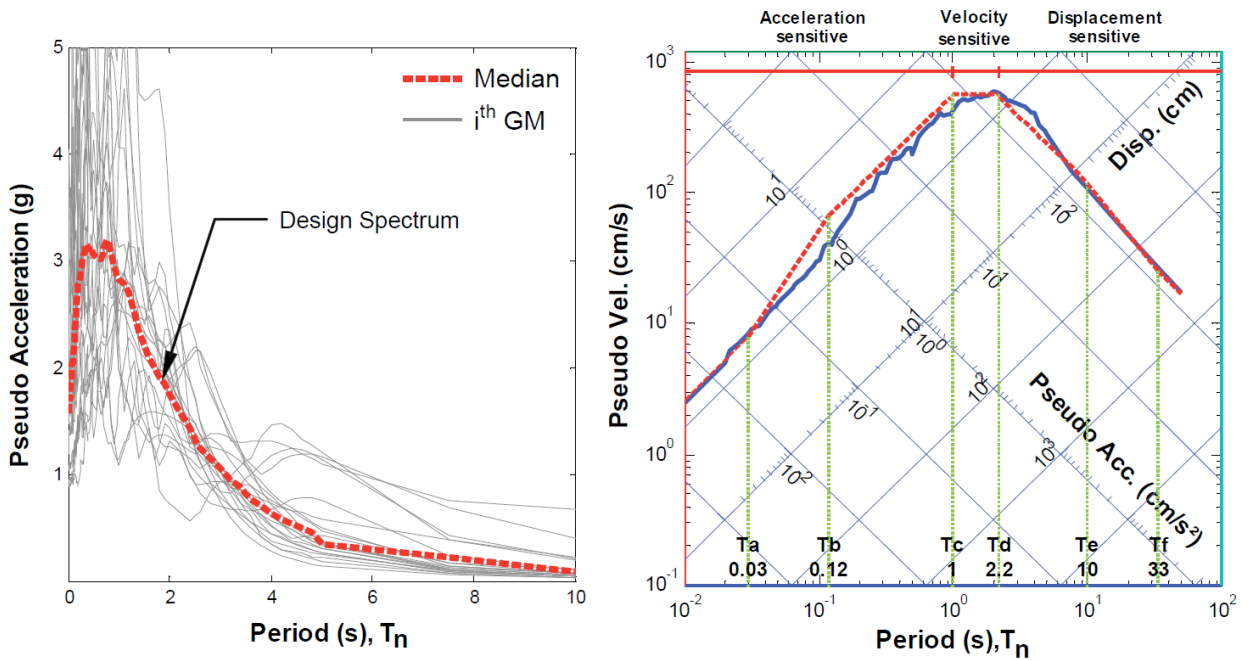


**Figure 6.14** (Left) Individual response spectra for twenty-one “unscaled” ground motions and their median response spectrum taken as the “design spectrum”; (Right) Median elastic response spectrum for the selected ensemble of ground motions shown by a solid line, together with its idealized version in dashed line; spectral regions are also identified; nearly constant velocity region is unusually narrow, which is typical of near-fault ground motions. Damping ratio,  $\zeta = 5\%$ .

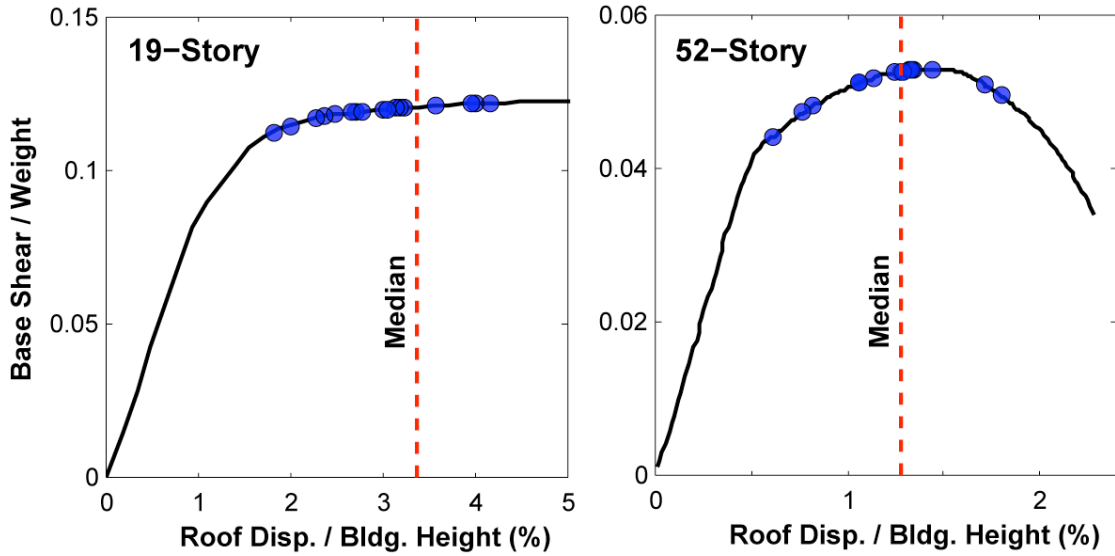


**Figure 6.15** Roof displacements determined by nonlinear RHA of the 19- and 52-story buildings for twenty-one ground motions identified on first-“mode” pushover curves. The median deformation exceeds the yield deformation by factors of 3.3 and 2.6, respectively for the 19- and 52-story buildings.

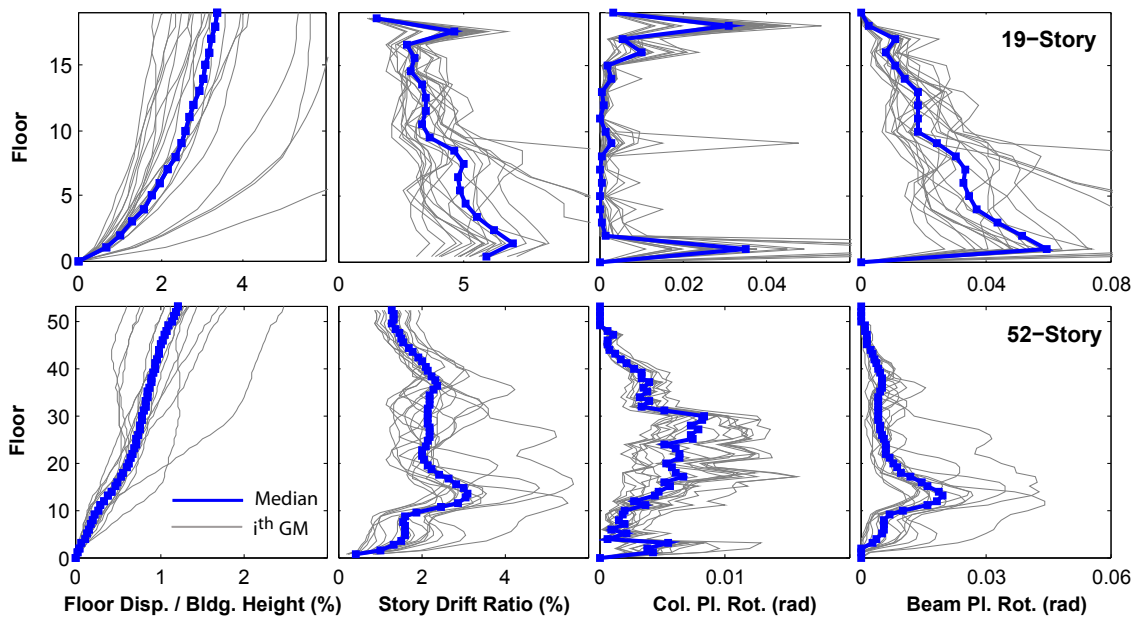


**Figure 6.16** Median values of EDPs determined by nonlinear RHA of 19- (top row) and 52-story (bottom row) buildings for twenty-one “unscaled” ground motions; results for individual ground motions are also included to show significant record-to-record variability.

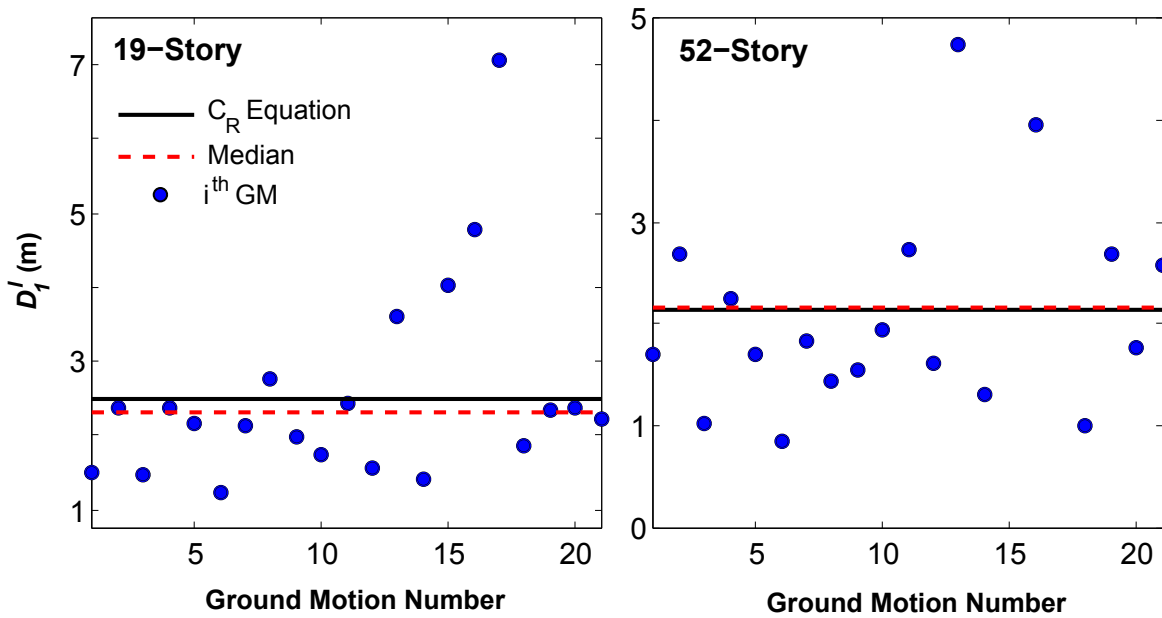


**Figure 6.17** Peak deformation  $D_1^I$  values of the first-“mode” inelastic SDF system for twenty-one “unscaled” ground motions for the 19- and 52-story buildings; “exact” target value of deformation  $\bar{D}_1^I$  is identified by horizontal dashed line; horizontal continuous line indicates target value of deformation  $\bar{D}_1^I$  established by the  $C_R$  equation. The empirical equation for  $C_R$  overestimates “exact” value of  $\bar{D}_1^I$  by only 8% for the 19-story building, and underestimates “exact” value of  $\bar{D}_1^I$  by only 1% for the 52-story building.

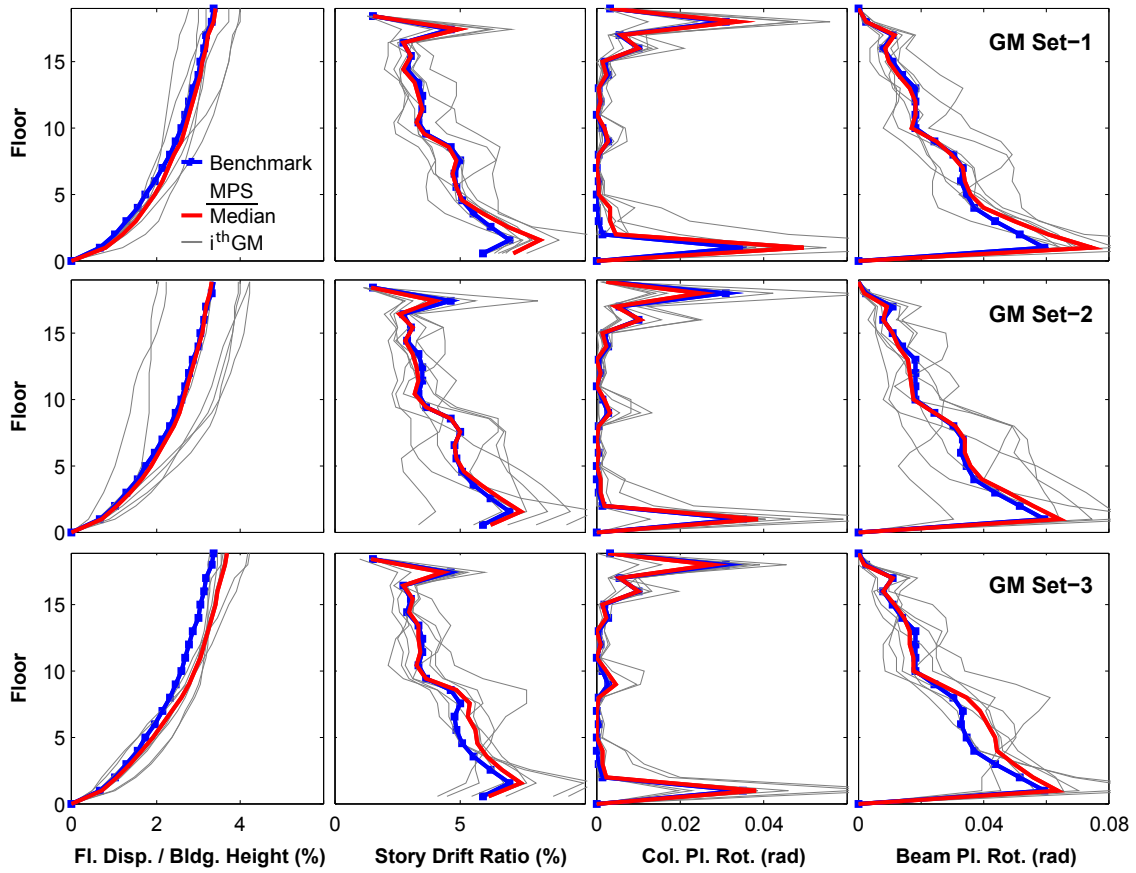


**Figure 6.18** Comparison of median EDPs based on the MPS procedure with benchmark EDPs for the 19-story building; individual results for each of the seven scaled ground motions are also presented.

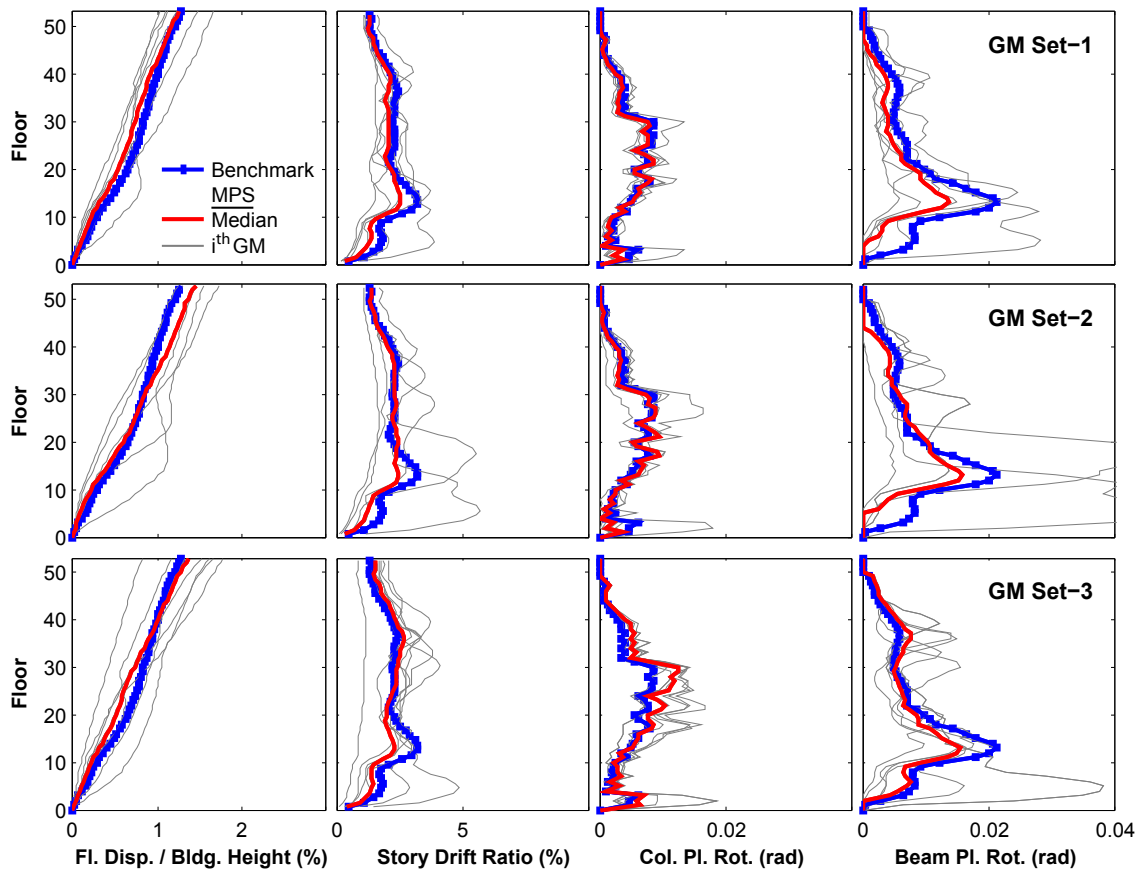


**Figure 6.19** Comparison of median EDPs based on the MPS procedure with benchmark EDPs for the 52-story building; individual results for each of the seven scaled ground motions are also presented.

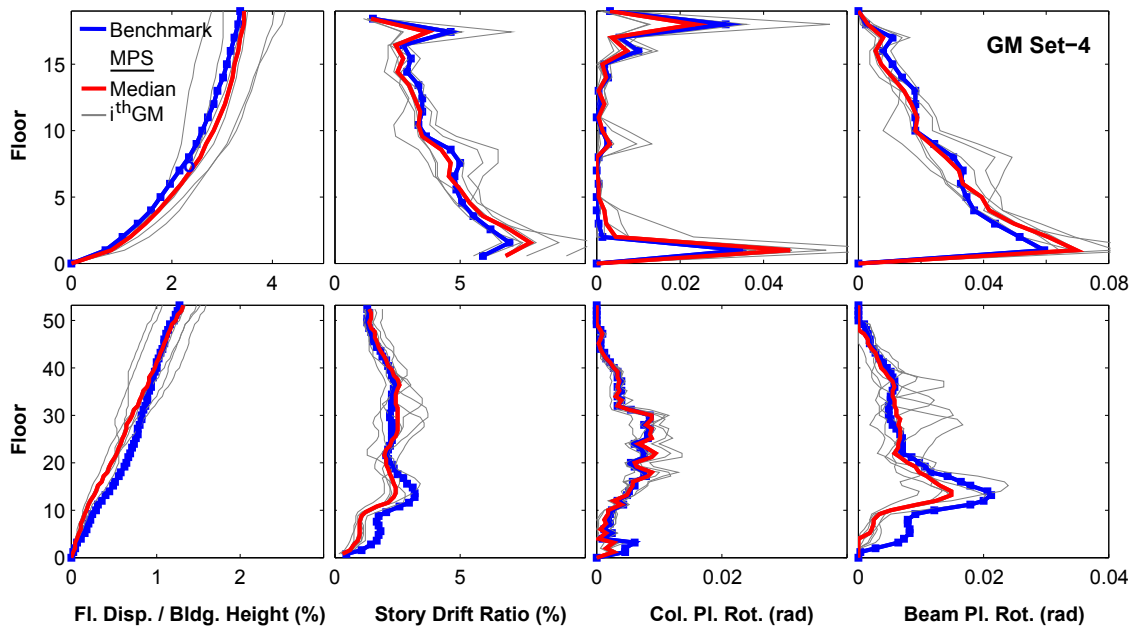


**Figure 6.20** Comparison of median EDPs for Ground Motion Set 4 scaled according to MPS procedure with benchmark EDPs; individual results of seven scaled ground motions are also presented. Results are for the 19- (top row), and 52-story building (bottom row).

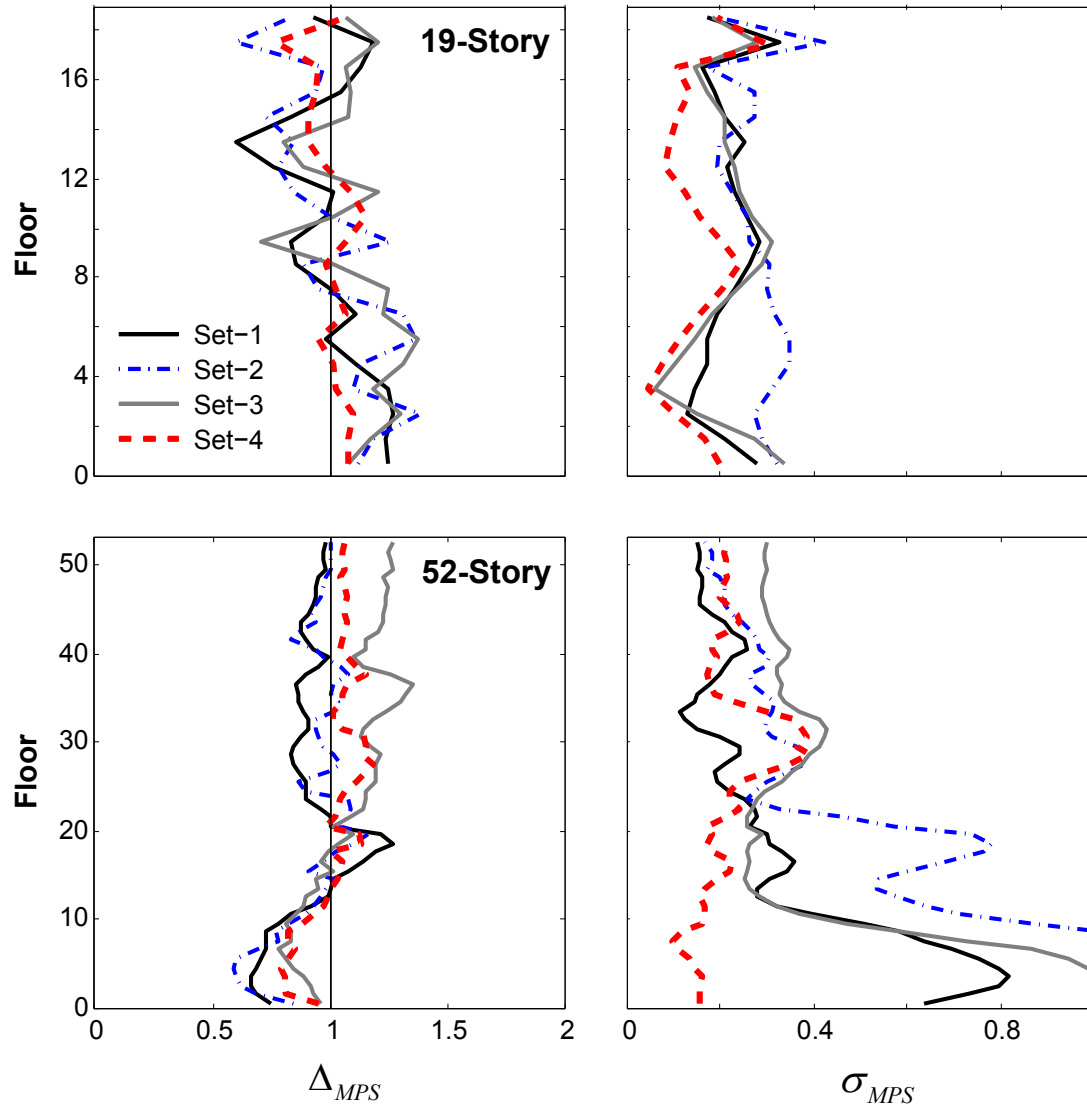
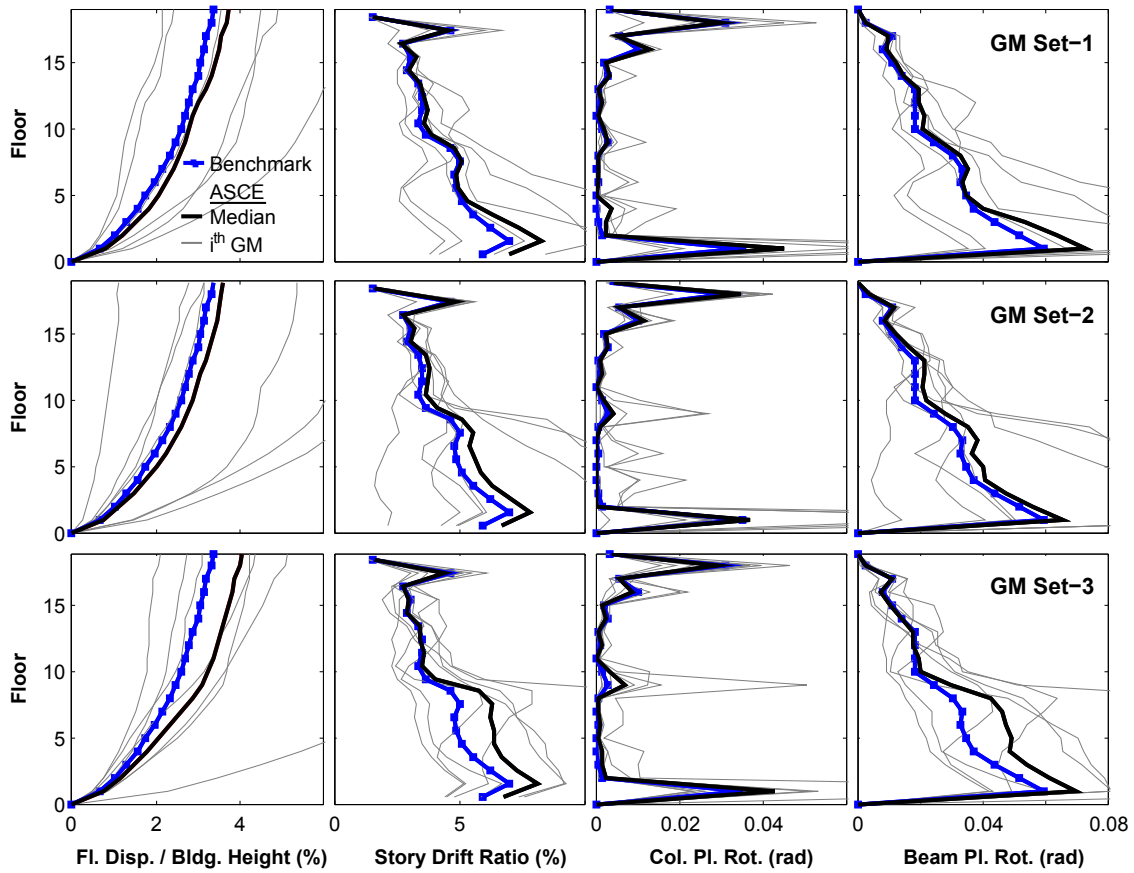
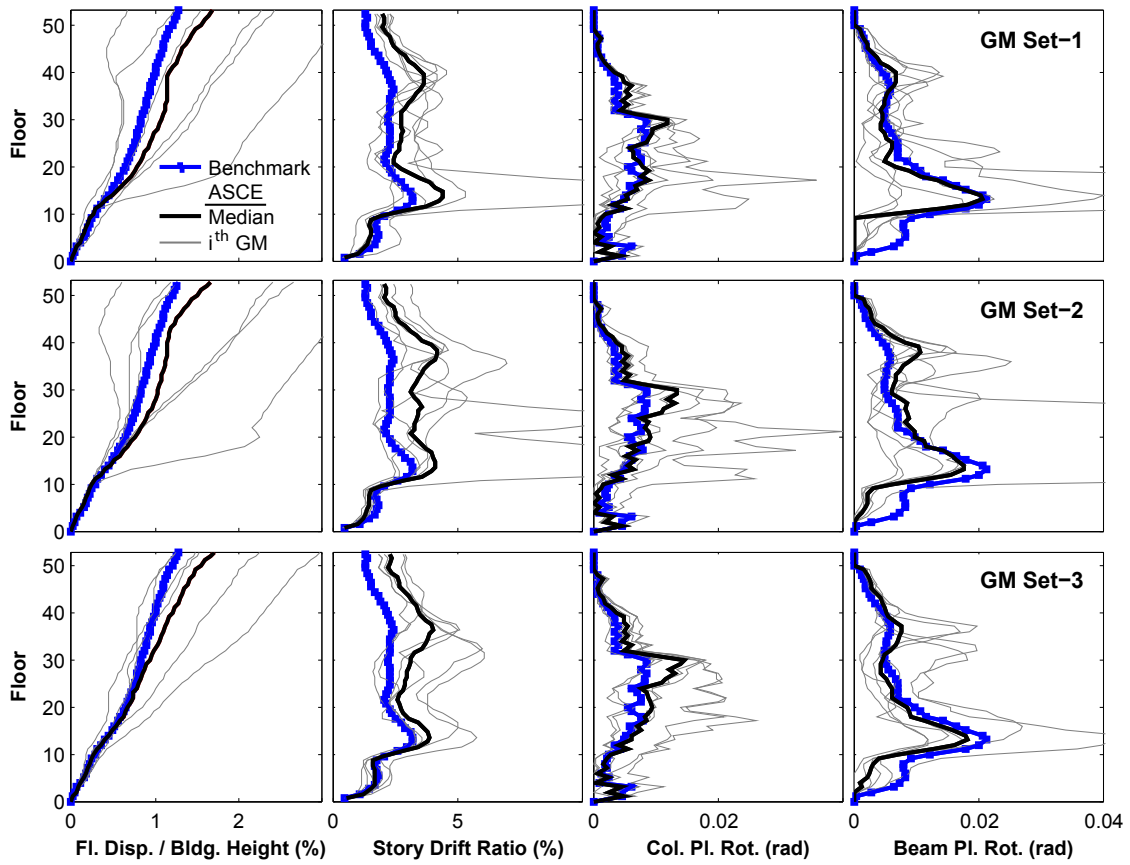


Figure 6.21 Median  $\Delta_{MPS}$  and dispersion  $\sigma_{MPS}$  of story drift ratios for four ground motions sets and for 19-story and 52-story buildings.



**Figure 6.22** Comparison of median EDPs based on the ASCE/SEI 7-05 ground motion scaling procedure with benchmark EDPs for the 19-story building; individual results for each of the seven scaled ground motions are also presented.



**Figure 6.23** Comparison of median EDPs based on the ASCE/SEI 7-05 ground motion scaling procedure with benchmark EDPs for the 52-story building; individual results for each of the seven scaled ground motions are also presented.

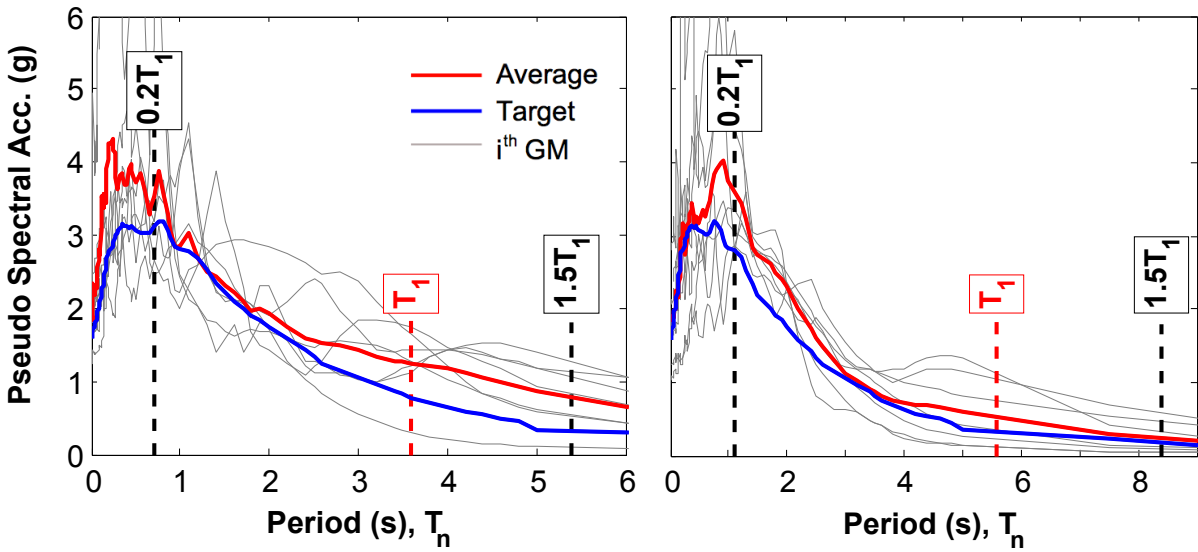


**Figure 6.24** Comparison of design spectrum with the average spectrum of seven scaled ground motions (GM Set 5) based on the ASCE/SEI 7-05 scaling method; individual response spectra are also presented. Spectral plots are for the 19- (left), and 52-story building (right). The average values of  $A(T_1)$  and  $A(T_2)$  from seven scaled records are much larger than the design spectrum values at these periods.

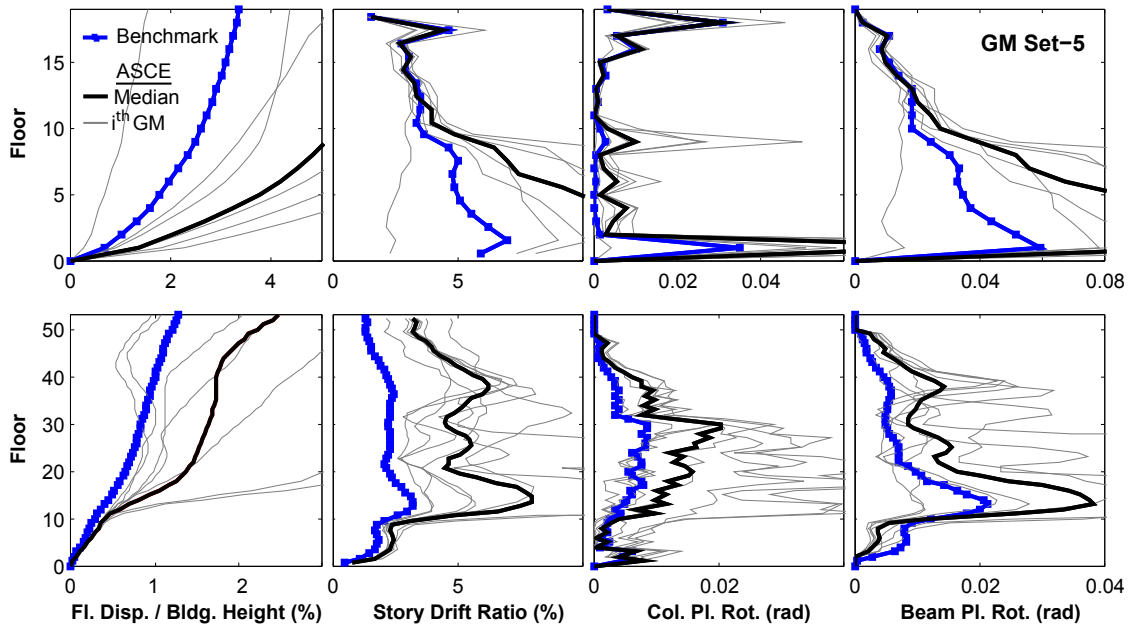


**Figure 6.25** Comparison of median EDPs for Ground Motion Set 5 based on the ASCE/SEI 7-05 ground motion scaling procedure with benchmark EDPs for the 19-, and 52-story buildings; individual results for each of seven scaled ground motions are also presented. Results are for the 19- (top row), and 52-story building (bottom row).

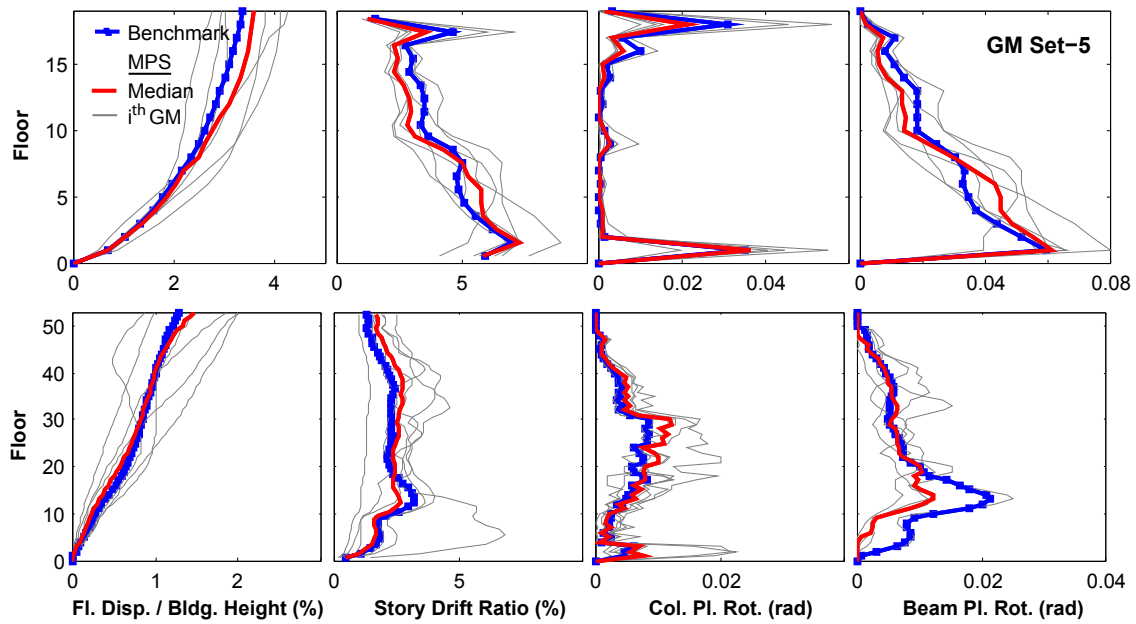


**Figure 6.26** Comparison of EDPs for Ground Motion Set 5 scaled according to MPS procedure (considering first-“mode” only) with benchmark EDPs; individual results for each of seven scaled ground motions are also presented. Results are for the 19- (top row), and 52-story building (bottom row).

## 7. EVALUATION OF MPS PROCEDURE: SHORT - PERIOD BUILDING

The efficiency and accuracy of the MPS procedure were established in previous sections considering structures with first-“mode” vibration period ranging from 1.0 to 5.6 sec. This chapter further assesses the MPS procedure considering a building with a shorter first-“mode” vibration period ( $T_1 = 0.6$  s). The short period range ( $T_1 \ll 1.0$  s) has a particular importance in predicting the inelastic target displacement values because the equal displacement rule is often violated in this range meaning that inelastic displacement values become larger than the elastic ones.

### 7.1 BUILDING DETAILS AND ANALYTICAL MODEL

The 4-story building (fig. 7.1), located in Watsonville, California is selected for the assessment of the MPS procedure. It was originally designed and constructed in 1948 as a three-story building and the fourth story was added in 1955. Its vertical carrying system consists of concrete slabs supported by composite concrete-steel columns. The lateral load system consists of concrete shear-walls in both directions. The foundation system consists of spread footings below the shear walls.

The building was instrumented in 1983 with 13 strong motion sensors on three levels; the instrumentation lay out is shown in figure 7.2. During the 1989 Loma Prieta earthquake, peak horizontal accelerations of 0.66 g at the ground level and 1.24 g at the roof level were recorded in this building. This recorded data is used to calibrate the 3-D computer model developed in OpenSees (2009). Centerline dimensions were used in element modeling. The beams, columns, and shear walls were modeled with nonlinear-beam-column element based on fiber sections containing confined concrete, unconfined concrete and steel reinforcing bars. This material model enabled capturing of the rapid strength loss after the building’s peak strength is exceeded. The crushing strain of the unconfined concrete was selected to be equal to 0.004 and that for confined concrete was selected to be that corresponding to the rupture of confining steel based on the Mander’s model (Mander and others, 1998). The strength of concrete and steel was selected based on the values specified in the structural drawings. Nodes at each floor were constrained to have the same lateral displacement to simulate rigid diaphragm behavior. The estimated floor mass and mass moment of inertia were lumped at the centre of mass at each

floor. The P- $\Delta$  effects in the global system level were included in modeling. Also considered in the model is the foundation flexibility at the base as per the FEMA-356 (ASCE/SEI, 2000) recommendations by attaching six linear springs—three along the x-, y-, and z-translation, two about the x- and y-rocking, and one about the z-torsion because the lateral load resisting system of the building consists of shear walls in both directions.

## 7.2. FIRST-“MODE” SDF-SYSTEM PARAMETERS

The force-deformation relation  $F_{S1}/L_1 - D_1$  for the first-“mode” SDF system is determined from the base shear – roof displacement relation defined by first-“mode” pushover curve by utilizing  $F_{s1}/L_1 = V_{b1} / M_1^*$  and  $D_1 = u_{r1} / \Gamma_1 \phi_{r1}$ . Only the E-W direction is considered in the pushover analyses. The resulting force-deformation relation for the first-“mode” SDF system is shown in figure 7.3 where the hysteretic force-deformation relation is idealized as tri-linear.

## 7.3. EVALUATION OF MPS PROCEDURE

Similar to the other buildings, the efficiency and accuracy of the MPS procedure will be evaluated for each of three ground motion sets (table 5.1), separately by comparing the median values of EDPs determined by nonlinear RHA of 4-story building under seven scaled records against the benchmark EDPs. Nonlinear RHAs under unscaled records indicates significant nonlinearity as shown in figure 7.4, where the resultant peak roof displacement values are identified on the first-“mode” pushover curve; and their median values are marked as vertical dashed line. Benchmark EDPs are presented in figure 7.5; also included are the results from individual records to demonstrate the large dispersion.

In the MPS procedure, a target value of deformation,  $\bar{D}_1'$  is estimated through the empirical  $C_R$  equation (Step 6 of the procedure - Chapter 2.1). Figure 7.6 compares the “exact” target value of deformation,  $\bar{D}_1'$  (dashed horizontal line) with the estimated target value of deformation,  $\bar{D}_1'$  (continuous horizontal line) using the  $C_R$  equation;  $D_1'$  values from individual records are also included to show its record-to-record variability. Notably, “exact” target value of deformation,  $\bar{D}_1'$  is determined as the median value of  $D_1'$  from twenty-one ground motions

based on first-“mode” inelastic SDF system. Estimated value of  $\bar{D}_1'$  underestimates the “exact” target value of deformation by only 6%. Once  $\bar{D}_1'$  is estimated, an appropriate scale factor for each record is determined based on the inelastic first-“mode” SDF systems (fig. 7.7) by implementing Steps 7-8 of the MPS procedure. The EDPs determined by nonlinear RHAs due to three sets of seven ground motions scaled according to the MPS and ASCE/SEI 7-05 methods are compared against the benchmark EDPs. Figures 7.7 and 7.8 present such comparisons considering the three sets of ground motions. As shown, the median values of the peak floor displacement, story drift ratio and column plastic rotations are better estimated (difference is less than 10%) using the MPS procedure; same applies for beam and column plastic rotations. The dispersion of the EDP values due to the seven scaled records is reduced as compared to the dispersion associated with the original records (fig. 7.6), but this reduction is less at the first floor.

Similar to the previous chapters, an alternative way of comparing MPS and ASCE/SEI 7-05 scaling methods is based on the ratio of the EDP value due to a scaled record and the benchmark value. The deviation of the median,  $\Delta$  of this ratio from unity is an indication of the error or bias in estimating the median EDP value, and the dispersion,  $\sigma$  of this ratio (assuming log-normal distribution) is an indication of the scatter in the individual EDPs, determined from the scaled ground motions. Figure 7.9 presents the median,  $\Delta$  of the EDP ratio for story drifts determined from records scaled according to the MPS and ASCE/SEI 7-05 scaling methods. Comparing these  $\Delta$  values against 1.0, it is apparent that the MPS and ASCE/SEI 7-05 methods have the same accuracy for the 4-story (short-period) building. The bias in the MPS methods is generally less than 30%, except in the case the Ground Motion Set-2 at upper level and Set-3 at the first floor. Figure 7.10 presents the dispersion of the EDP ratio for story drifts determined from records scaled according to the MPS and ASCE/SEI 7-05 scaling methods. It is apparent that the dispersion associated with both methods is similar. Comparison of these sets implies that dispersion varies significantly from one set to other; this observed variation for short period building was not as large as for the other buildings studied herein, which have  $T_1 > 1.0$  sec.

**Table 7.1 Scale factors computed for three sets of seven ground motions**

No.	Earthquake	Year	Station	Set	
				No.	Scale Factor
1	Superstition Hills	1987	Parachute Test Site	1	0.95
2	Northridge	1994	Jensen Filter Plant	1	0.78
3	Northridge	1994	Sylmar - Converter Sta East	1	0.69
4	Kobe, Japan	1995	Takatori	1	0.90
5	Chi-Chi, Taiwan	1999	TCU065	1	0.73
6	Chi-Chi, Taiwan	1999	TCU102	1	0.95
7	Kocaeli, Turkey	1999	Yarimca	1	1.84
1	Erzincan, Turkey	1992	Erzincan	2	1.19
2	Imperial Valley	1979	EC Meloland Overpass FF	2	2.06
3	Kobe, Japan	1995	Port Island	2	1.85
4	Northridge	1994	Sylmar - Converter Sta	2	0.97
5	Tabas, Iran	1978	Tabas	2	0.78
6	Chi-Chi, Taiwan	1999	TCU052	2	1.29
7	Chi-Chi, Taiwan	1999	TCU084	2	0.42
1	Duzce, Turkey	1999	Duzce	3	0.90
2	Imperial Valley	1979	El Centro Array #7	3	0.99
3	Loma Prieta	1989	LGPC	3	0.59
4	Northridge	1994	Rinaldi Receiving Sta	3	0.46
5	Northridge	1994	Sylmar - Olive View Med FF	3	0.76
6	Chi-Chi, Taiwan	1999	TCU068	3	1.00
7	Northridge	1994	Newhall - W Pico Canyon Rd	3	1.29



**Figure 7.1** Overview of the 4-story RC building in Watsonville, CA.

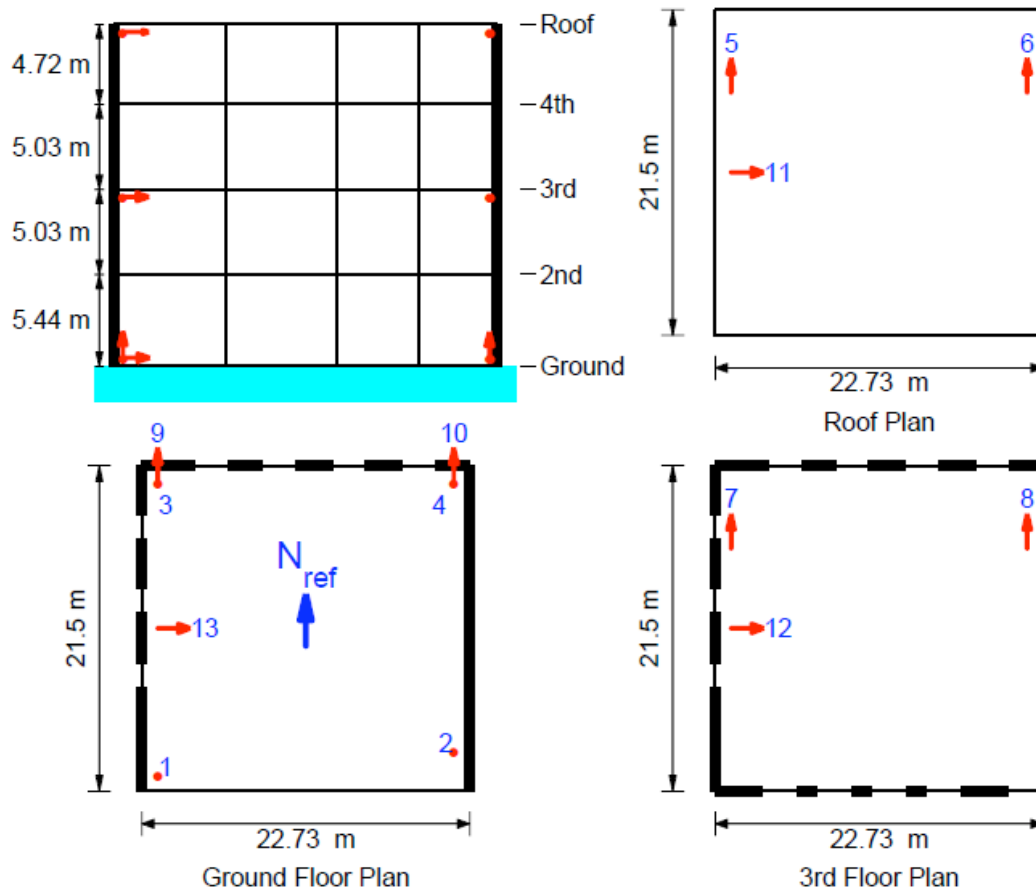


**Figure 7.2** Instrumentation lay out of the 4-story RC building.

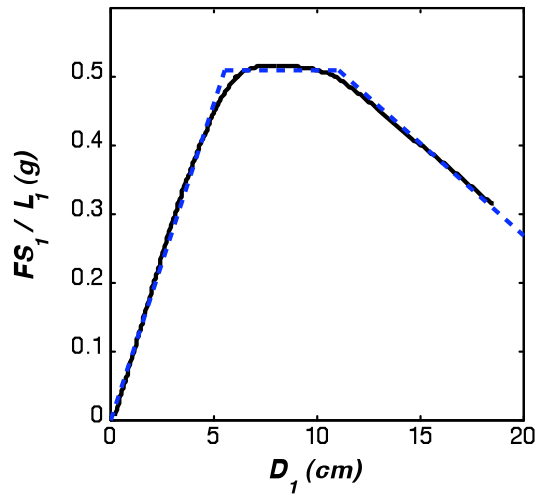


**Figure 7.3** Comparison of first-“mode” pushover curve (solid line) and its idealized model (dashed line) for the 4-story RC building.

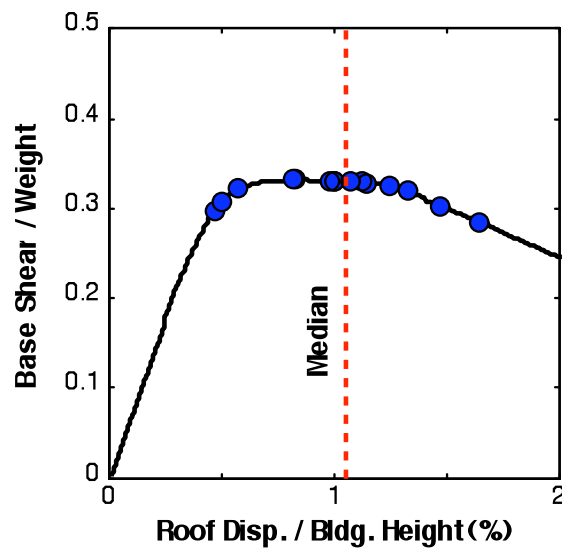


**Figure 7.4** Roof displacements determined by nonlinear RHA of the 4-story RC building for twenty-one ground motions identified on first-“mode” pushover curve.

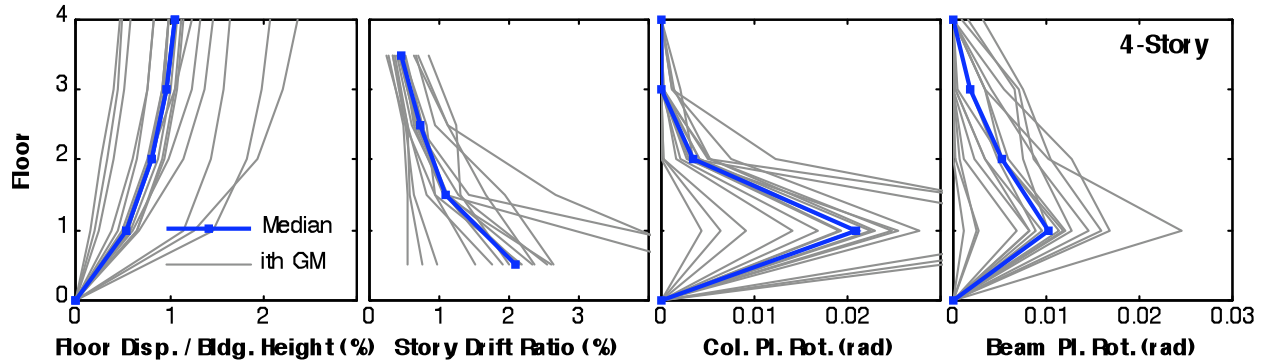


Figure 7.5 Median values of EDPs determined by nonlinear RHA of 4-story RC building for twenty-one ground motions; results for individual ground motions are also included.

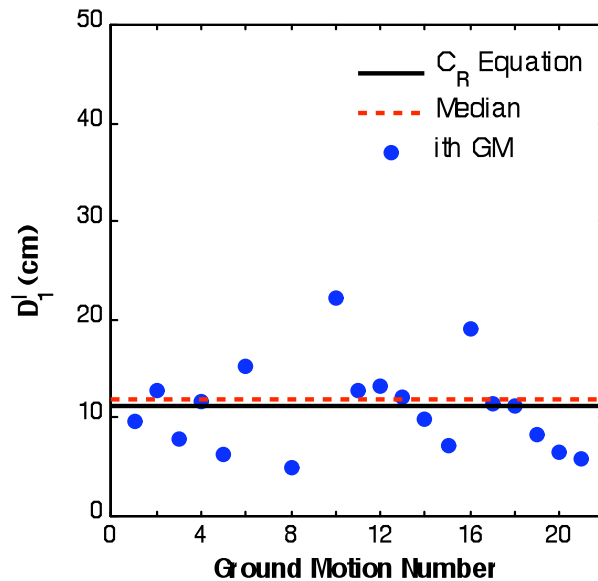
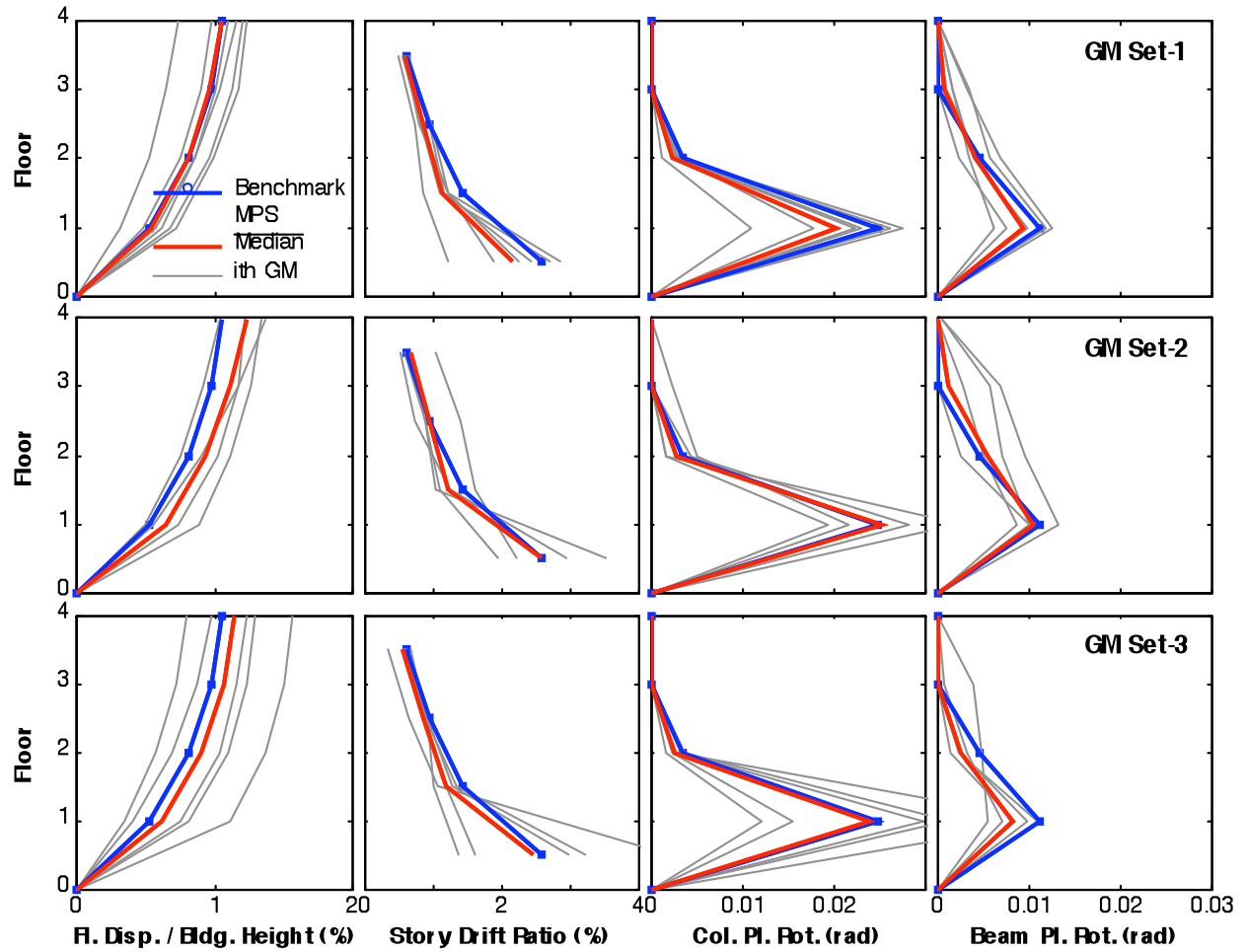
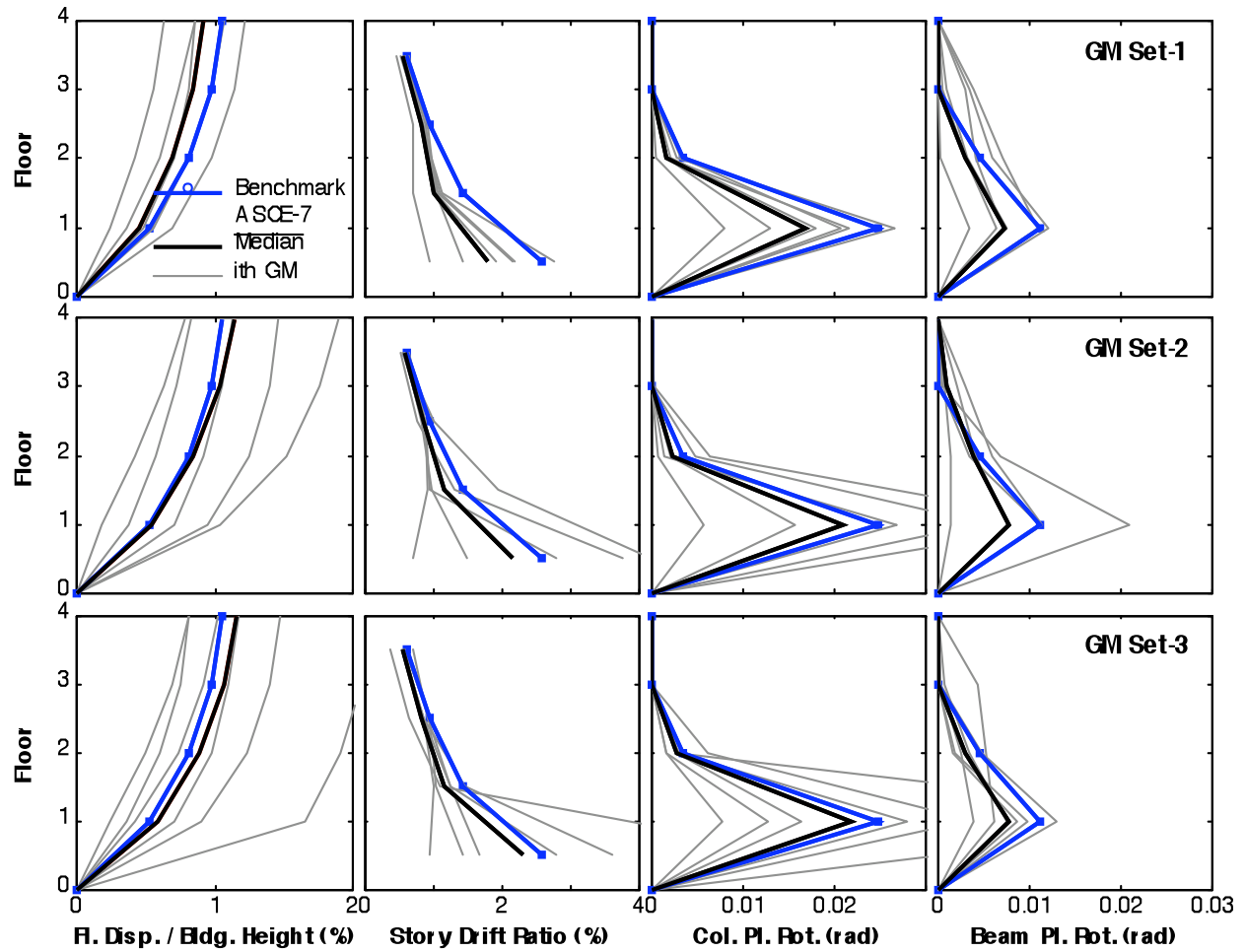


Figure 7.6 Peak deformation  $D_1^I$  values of the first-“mode” inelastic SDF system for twenty-one ground motions; “exact” target value of deformation  $\bar{D}_1^I$  is identified by horizontal dashed line; horizontal continuous line indicates target value of deformation  $\bar{D}_1^I$  established by  $C_R$  equation.



**Figure 7.7** Comparison of median EDPs based on the MPS procedure with benchmark EDPs for the 4-story building; individual results for each of the seven scaled ground motions are also presented.



**Figure 7.8** Comparison of median EDPs based on the ASCE/SEI 7-05 ground motion scaling procedure with benchmark EDPs for the 4-story building; individual results for each of the seven scaled ground motions are also presented.

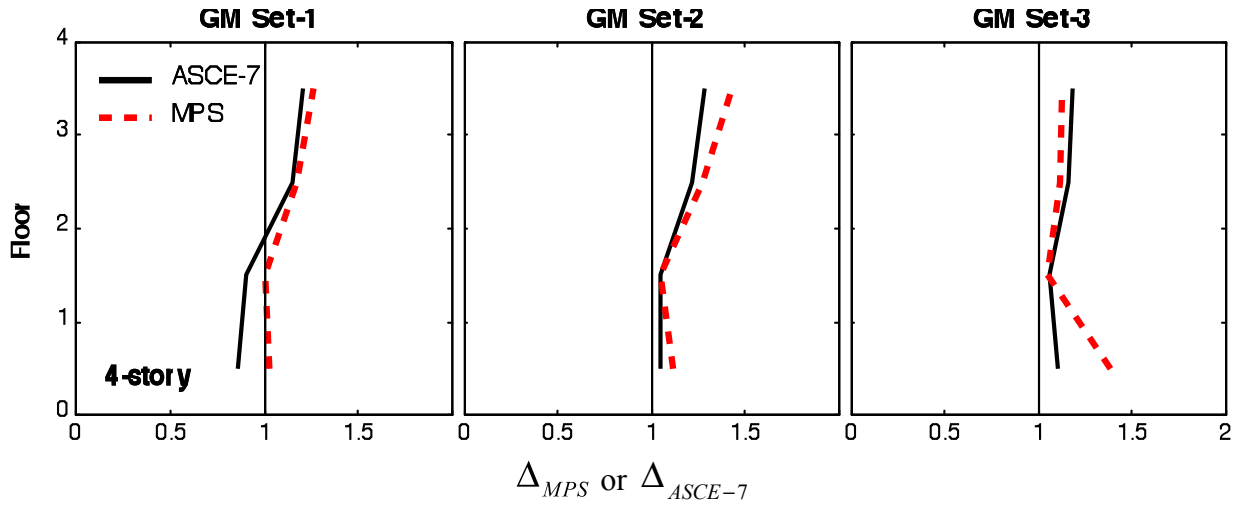


Figure 7.9 Median story drift ratios  $\Delta_{MPS}$  and  $\Delta_{ASCE-7}$  for three ground motions sets.

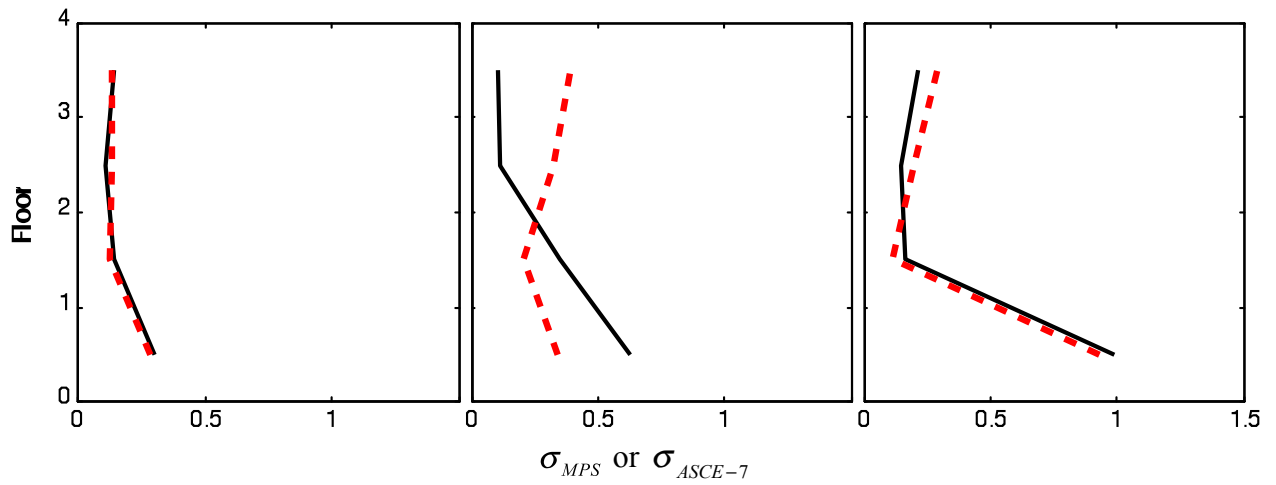


Figure 7.10 Dispersion of story drift ratios  $\sigma_{MPS}$  and  $\sigma_{ASCE-7}$  for three ground motions sets.

## **8. EVALUATION OF MPS PROCEDURE: “ORDINARY STANDARD” BRIDGES**

Current highway bridge design practice in California is governed by the Seismic Design Criteria, SDC-2006 (Caltrans, 2006), which allows equivalent static analysis and linear elastic dynamic analysis for estimating the displacement demands, and pushover analysis for establishing the displacement capacities for “Ordinary Standard” bridges. For a bridge to be considered as an “Ordinary Standard” bridge, (1) the span length should be less than 90 m, (2) the bridge should be constructed with normal weight concrete, (3) foundations must be supported on spread footings, pile caps with piles or pile shafts, and (4) the soil is not susceptible to liquefaction or lateral spreading during strong shaking (Caltrans, 2006). More than 99% of bridges in California are “Ordinary Standard” bridge (Mark Yashinsky, oral commun.).

For “Ordinary Standard” bridges, analysis methods based on linear-elastic assumption may be appropriate in low-seismic regions. In high-seismic regions however, near-fault static (surface displacement) and dynamic effects (dominant velocity pulse) may impart significant seismic demand to bridges and drive them into inelastic range, invalidating the linear-elastic assumption (Goel and Chopra, 2008). To fully portray the “true” nonlinear behavior of bridges to near-fault ground motions, nonlinear RHA may be required.

### **8.1 DESCRIPTION OF BRIDGES AND ANALYTICAL MODELS**

Two types of existing “Ordinary Standard” bridges in California were considered: single-bent overpass and multi-span bridge (fig. 8.1).

#### **8.1.1 SINGLE-BENT OVERPASS**

The selected bridge with a two-span continuous deck and single-bent composed of two octagonal columns is representative of an overcrossing designed according to post-Northridge Caltrans specifications. Figure 8.2 shows the elevation, deck and column dimensions and column section detailing. The bridge has stub wall abutments, which are restrained in the longitudinal and transverse directions as a result of end diaphragm and wing wall interaction with the soil.

The computer model of the bridge was created in OpenSees (2009). Due the abutments, the bridge was assumed to be fixed against vertical, translation and rotation about the longitudinal axis of the superstructure but longitudinal and transverse displacements were permitted. The column bent footings were supported on translational and rotational springs in each direction. The stiffness of the translational springs to model the abutments was determined in accordance with SDC-2006. The abutment stiffness in the longitudinal direction was computed as:

$$K = (K_i w h) / 1.7 \quad (8.1)$$

where  $K_i$  is the initial stiffness of the abutment taken as 11.5 kN/mm per meter;  $w$  and  $h$  are the width and height of the abutment's diaphragm. For the abutment stiffness in the transverse direction and foundation stiffness in both translational directions, an empirical value of 7,000 kN/m per pile was used to account for soil flexibility.

The finite element model of the bridge is represented by 3-D frame elements passing through the mid-depth of the superstructure and 3-D frame elements passing through the geometric centre and mid-depth of the columns and the cap beam. Fiber-discretized, nonlinear beam-column elements were used to model columns (fig. 8.3). The deck elements were assumed to remain elastic. Since the cross-section of the superstructure is uniform, it was deemed sufficient to use eight nodes within each span. The mass of each member was equally distributed to its end nodes. The seismic weight of the bridge was approximated to be 11.5 MN. The box-girder was assumed to be integral with the bent, thus full continuity was employed at the superstructure-bent connection. The characteristic strength of unconfined concrete ( $f'_c$ ) was assumed to be 28 MPa with an ultimate strain of 0.005, while the yield strength of both longitudinal and spiral reinforcement was specified as 413 MPa. The characteristic strength and ultimate strain of confined concrete were computed to be 41.6 MPa and 0.0169 using the model proposed by Mander and others (1988). A bilinear model with a post-yield stiffness of 1% of the initial stiffness was used to model reinforcing steel. For simplicity, the columns were modeled as circular columns with a diameter of 1.65 m. The diameter of the equivalent circular column was selected such that both core and cover concrete areas of the original octagonal column are equal to those of the equivalent circular column.

### 8.1.2 MULTI-SPAN BRIDGE

The bridge selected is representative of typical multi-span, single-frame prestressed concrete bridges built according to post-Northridge Caltrans design specifications. Figure 8.4 shows the bridge elevation, deck and column dimensions, and column section detailing. The bents of the bridge consist of single double-spiral columns.

The bridge was modeled as an elastic superstructure sitting on nonlinear columns on elastic foundation. The assumption of elastic superstructure was based on the capacity design approach employed by the SDC-2006. An overview of the computer model of the bridge is shown in figure 8.5. Fiber-discretized, nonlinear beam-column elements were used to model columns; the deck elements were assumed to remain elastic. The compressive strength of unconfined concrete and the yield strength of longitudinal reinforcement were taken as 28 MPa and 413 MPa, respectively. The compressive strength and ultimate strain of confined concrete were computed as 40.2 MPa and 0.0157 using Mander's model. A bilinear model with a post-yield stiffness of 1% of the initial stiffness was used to model reinforcing steel.

The columns of the bridge rest on shallow foundations. Six elastic springs in 3 translational and 3 rotational directions were used to model the soil effect. The approximate expressions in the ASCE/SEI 41-6 guidelines (ASCE/SEI, 2007) were used to compute properties of the corresponding spring constants. Seat type abutments are used at both ends of the bridge. Spring systems were used to model the dynamic stiffness of the abutments. In the transverse direction, shear keys are designed to break off during a strong ground motion. Hence, seat type abutments do not possess any stiffness in the transverse direction. In the vertical direction, the movement of the bridge is prevented at the abutments in both upward and downward directions. Thus, the abutments were modeled as restrained supports in the vertical direction. In the longitudinal direction, the bridge is free to move in the opposite direction of the abutment at each end. Towards the abutment there is a certain amount of gap before the deck makes contact with the abutment. When the deck and the abutment are in contact, the stiffness of the abutment is computed as:

$$K = (K_i w h) / 5.5 \quad (8.2)$$

where  $K_i$  is taken to be equal to 3.5 kN/mm per meter. A spring which has no stiffness in tension and remains elastic in compression with an initial stiffness of 10,060 kN/m and with a 10 cm gap was used to model the abutment behavior in the longitudinal direction.

## **8.2 FIRST-“MODE” SDF-SYSTEM PARAMETERS**

Figure 8.6 shows the first two modes of vibration and their periods for both bridges. For the single-bent overpass, the first mode (0.54 s) involves a transverse translation of the deck and the second-“mode” (0.52 s) involves a longitudinal translation of the superstructure. The multi-span single-frame bridge has the first mode (2.47 s) in the translational direction and second-“mode” (1.06 s) in the longitudinal direction. The transverse direction is more flexible for both bridges.

Modal pushover curves for two bridges were developed in the transverse and longitudinal directions separately. Similar to the modal pushover analyses procedure for buildings (Chopra, 2007), the distribution of lateral forces was determined from the shape of the fundamental transverse mode, and fundamental longitudinal mode, multiplied by tributary mass. For each direction, the resultant pushover curves for both bridges are demonstrated in figure 8.7 with a thick solid line. In the same figure, bilinear idealization of pushover curves is shown in thick dashed line. For the single-bent overpass, the pushover curves are quite similar in the longitudinal and transverse directions.

## **8.3 EVALUATION OF MPS PROCEDURE**

The accuracy of the MPS procedure was evaluated by comparing the median (defined as the geometric mean) value of an EDP due to three sets of randomly selected seven scaled ground motions against the benchmark value, defined as the median value of the EDP due to the twenty-one unscaled ground motions. A scaling procedure is considered to be accurate if the median values of an EDP due to the seven scaled ground motions are close to benchmark value; it is considered to be efficient if the dispersion of an EDP due to the set of seven scaled ground motions is small.

### 8.3.1 BENCHMARK RESULTS

Figure 8.8 shows the benchmark EDPs for the two bridges together with results from individual records to show the large record-to-record variability. EDPs adopted are global response parameters: peak value of deck drift ratio (deck displacement  $\div$  height of bent or column) and bent/column plastic rotation. The MPS procedure based only on the first-“mode” of vibration (Section 2.1) is applied to estimate response in transverse direction. The peak values of deck drift ratios due to the twenty-one unscaled ground motions range from 1% to 5%, and column plastic deformations range from less than 0.01 rad to over 0.05 rad. The deck drift ratios are identified on the first-“mode” pushover curves together with their median values in figure 8.9 to indicate that all of the excitations drive both bridges well into the inelastic range.

### 8.3.2 TARGET VALUE OF INELASTIC DEFORMATION

In evaluation of the MPS procedure, “exact” target value of deformation  $\bar{D}_1^I$  was assumed to be unknown and it was estimated (Step 6 of Section 2.1) by the  $C_R$  equation (Chopra and Chintanapakdee, 2004) using post-yield stiffness ratio and yield-strength ratio. Yield-strength ratio  $R_y$  was determined (Step 4 of Section 2.1) as 3.10 and 3.46, respectively for the single-span overpass and multi-span bridge. Alternatively, “exact” target value of deformation  $\bar{D}_1^I$  was computed by nonlinear RHAs of the first-“mode” inelastic SDF system for twenty-one unscaled records. Figure 8.10 compares the estimated target value of deformation using the  $C_R$  equation against its “exact” value; values from individual records are also included to show its record-to-record variability. The  $C_R$  equation overestimates “exact” value of  $\bar{D}_1^I$  by 12%-14%.

### 8.3.3 COMPARISONS AGAINST BENCHMARK RESULTS

The benchmark results indicated that both bridges are first-“mode” dominated, thus Step 7 and 8 of the MPS procedure are implemented to determine an appropriate scale factor for each record. The scale factors established for each bridge in each of the three sets are presented in table 8.1; the scaling factors obviously differ with the bridge. The EDPs determined by nonlinear RHAs of bridges due to three sets of seven ground motions scaled according to MPS procedure are

compared against the benchmark EDPs. Figures 8.11 and 8.12 exhibit these comparisons respectively for the single-span overpass and multi-span bridge. To quantify the accuracy of the MPS procedure, ratio of median value of EDPs due to the MPS procedure and benchmark value is computed and listed in table 8.2 for each bridge and for each set of ground motions. For the single-bent overpass, maximum deviation of median value of EDPs due the MPS procedure relative to the benchmark value is 18% for the deck drift ratio and 21% for the column plastic rotation for Set 1; Set 2 and 3 provided more accurate results. For the multi-span bridge, median deck drift ratios due to the MPS procedure overestimate the benchmark value by %14 for deck drift ratio and %19 for column plastic rotation for Set 2. For this bridge, Set 1 and 3 resulted in slightly better accuracy.

As evident in Figures 8.11 and 8.12, the dispersion of EDPs due to scaled records is significantly reduced as compared to the dispersion due to the unscaled records (fig. 8.8). To quantify this reduction, the standard deviation ( $\sigma$ ) of ratio of the EDP value from individual ground motion and its median value was tabulated in table 8.3 for each bridge and for each set of ground motions. Larger  $\sigma$  means higher dispersion. For the single-bent overpass,  $\sigma$  of EDPs due to the unscaled records are reduced by 40% to 77% by the MPS procedure, and for the multi-span bridge the reduction in  $\sigma$  is in the range of 33% to 66%.

Utilizing “exact” value of the target inelastic deformation, the median inelastic deformation value in figure 8.10, resulted in improved accuracy of the MPS procedure (referred as MPS-“Exact”) for both bridges as shown in figures 8.13 and 8.14. For the single-bent overpass and for Set 2, maximum deviation of median EDPs due the MPS-“Exact” procedure from the benchmark value is 15% for the deck drift ratio and 16% for the column plastic rotation (see table 8.2); better accuracy was obtained by Set 1, and excellent match with the benchmark value was achieved by Set 3. For the multi-span bridge, median value of EDPs due to the three sets of ground motions perfectly matches with the benchmark value (maximum deviation is only 6%). As shown in table 8.3, the dispersion in EDPs was further reduced by utilizing the “exact” value of the target inelastic deformation for both bridges.

These results demonstrate that the MPS procedure leads to scaled ground motions that yield accurate estimate of median EDPs with significantly reduced dispersion compared to the

unscaled ground motions. Further examination of the MPS procedure for curved and skew bridges are currently underway.

**Table 8.1 Scale factors computed for ground motion records considering MPS and MPS-“Exact” for single-bent overpass and multi-span bridge**

No.	Earthquake	Station	Set	MPS *		MPS-"Exact" **	
				Single-Bent Overpass	Multi-span Bridge	Single-Bent Overpass	Multi-span Bridge
1	Superstition Hills	Parachute Test Site	1	1.10	1.07	1.05	0.96
2	Northridge	Jensen Filter Plant	1	0.87	1.06	0.80	0.96
3	Northridge	Sylmar - Converter Sta East	1	1.44	1.54	1.37	1.39
4	Kobe, Japan	Takatori	1	0.92	1.04	0.89	0.94
5	Chi-Chi, Taiwan	TCU065	1	1.28	0.96	1.17	0.90
6	Chi-Chi, Taiwan	TCU102	1	1.58	1.38	1.47	1.24
7	Kocaeli, Turkey	Yarimca	1	2.56	2.04	2.52	1.90
1	Erzincan, Turkey	Erzincan	2	1.14	1.26	1.11	1.16
2	Imperial Valley	ECMeloland Overpass FF	2	2.05	1.30	1.94	1.18
3	Kobe, Japan	Port Island	2	1.42	1.20	1.35	1.09
4	Northridge	Sylmar - Converter Sta	2	0.80	1.14	0.73	1.01
5	Tabas, Iran	Tabas	2	1.17	1.14	1.11	1.05
6	Chi-Chi, Taiwan	TCU052	2	1.33	0.98	1.29	0.87
7	Chi-Chi, Taiwan	TCU084	2	0.38	1.00	0.35	0.89
1	Duzce, Turkey	Duzce	3	1.96	1.45	1.86	1.34
2	Imperial Valley	El Centro Array #7	3	1.27	1.21	1.19	1.17
3	Loma Prieta	LGPC	3	1.57	0.87	1.52	0.81
4	Northridge	Rinaldi Receiving Sta	3	0.63	1.14	0.57	1.03
5	Northridge	Sylmar - Olive View Med FF	3	1.23	1.60	1.20	1.46
6	Chi-Chi, Taiwan	TCU068	3	1.33	0.67	1.24	0.62
7	Northridge	Newhall - W Pico Canyon Rd	3	0.94	0.79	0.91	0.72

\* Target inelastic deformation is computed by  $C_R$  equation

\*\* "Exact" value of target inelastic deformation is utilized

**Table 8.2 Comparison of EDP ratios considering MPS and MPS-“Exact” for single-bent overpass and multi-span bridge**

EDP Ratio (MPS Median ÷ Benchmark)	Single-bent Overpass					
	MPS			MPS- "Exact"		
	Set-1	Set-2	Set-3	Set-1	Set-2	Set-3
Deck Drift	1.18	0.93	1.08	1.08	0.85	1.00
Column Plastic Rotation	1.21	0.93	1.10	1.10	0.84	1.01

EDP Ratio (MPS Median ÷ Benchmark)	Multi-span Bridge					
	MPS			MPS- "Exact"		
	Set-1	Set-2	Set-3	Set-1	Set-2	Set-3
Deck Drift	1.12	1.14	1.10	1.04	1.00	1.02
Column Plastic Rotation	1.17	1.19	1.13	1.06	1.00	1.04

**Table 8.3 Comparison of dispersion measure ( $\sigma$ ) considering MPS and MPS-“Exact” for single-bent overpass and multi-span bridge**

Dispersion Measure ( $\sigma$ )	Single-bent Overpass						
	Benchmark	MPS			MPS- "Exact"		
		Set-1	Set-2	Set-3	Set-1	Set-2	Set-3
Deck Drift	0.52	0.12	0.31	0.22	0.13	0.29	0.21
Column Plastic Rotation	0.56	0.13	0.34	0.24	0.14	0.32	0.23

Dispersion Measure ( $\sigma$ )	Multi-span Bridge						
	Benchmark	MPS			MPS- "Exact"		
		Set-1	Set-2	Set-3	Set-1	Set-2	Set-3
Deck Drift	0.40	0.26	0.21	0.14	0.21	0.17	0.14
Column Plastic Rotation	0.45	0.30	0.27	0.16	0.28	0.22	0.15



**Figure 8.1** Bird's eye views for single-bent overpass [Left] and multi-span bridge [Right].

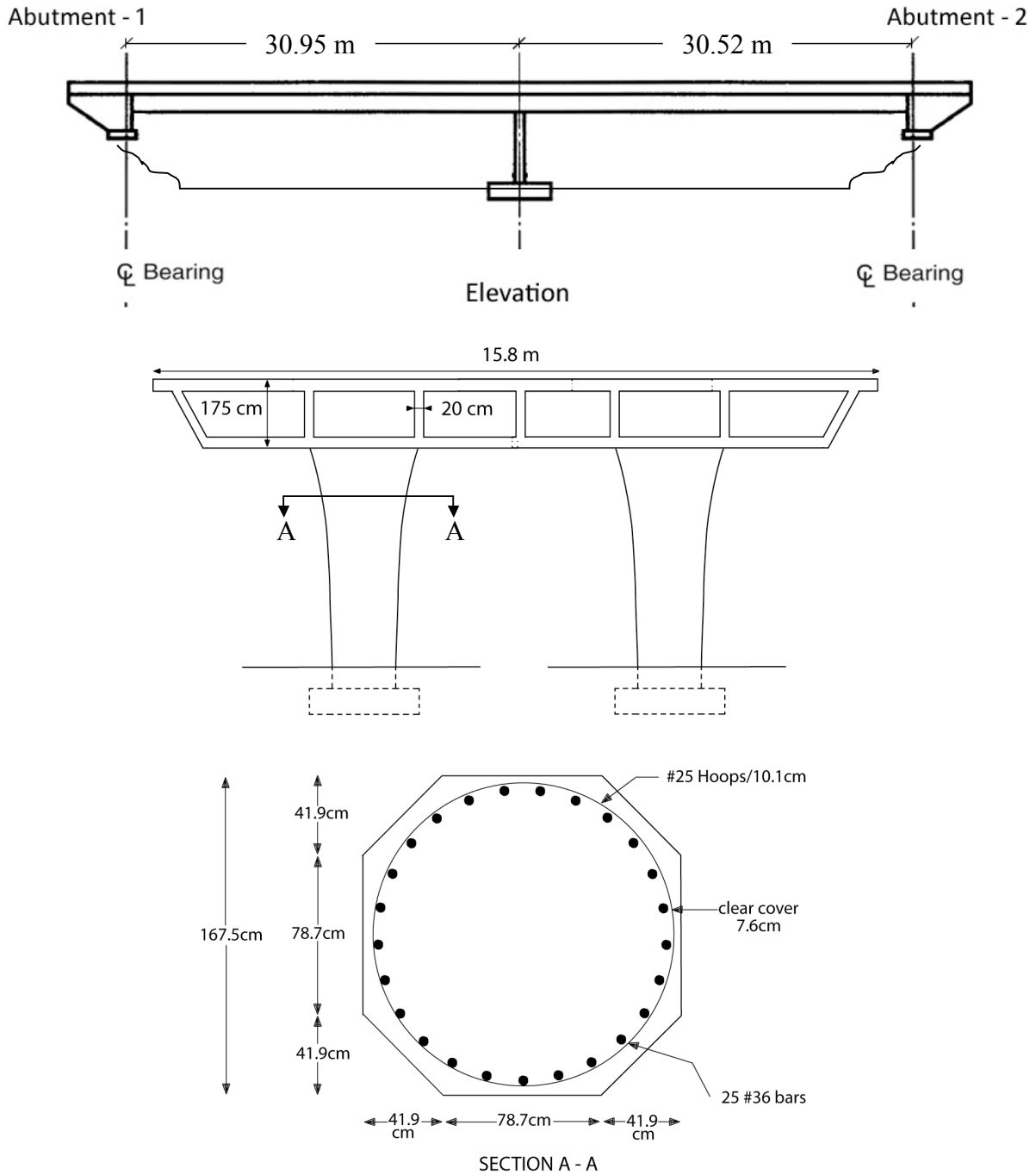


**Figure 8.2** Elevation, deck and column dimensions, and column section details of single-bent overpass.

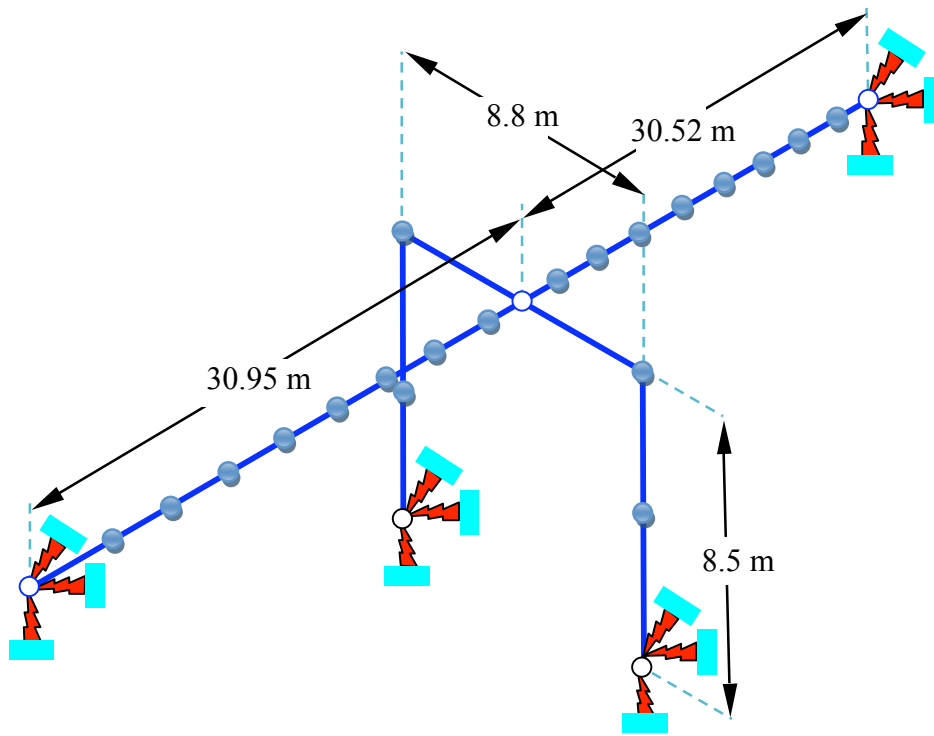


**Figure 8.3** Computer model of single-bent overpass.

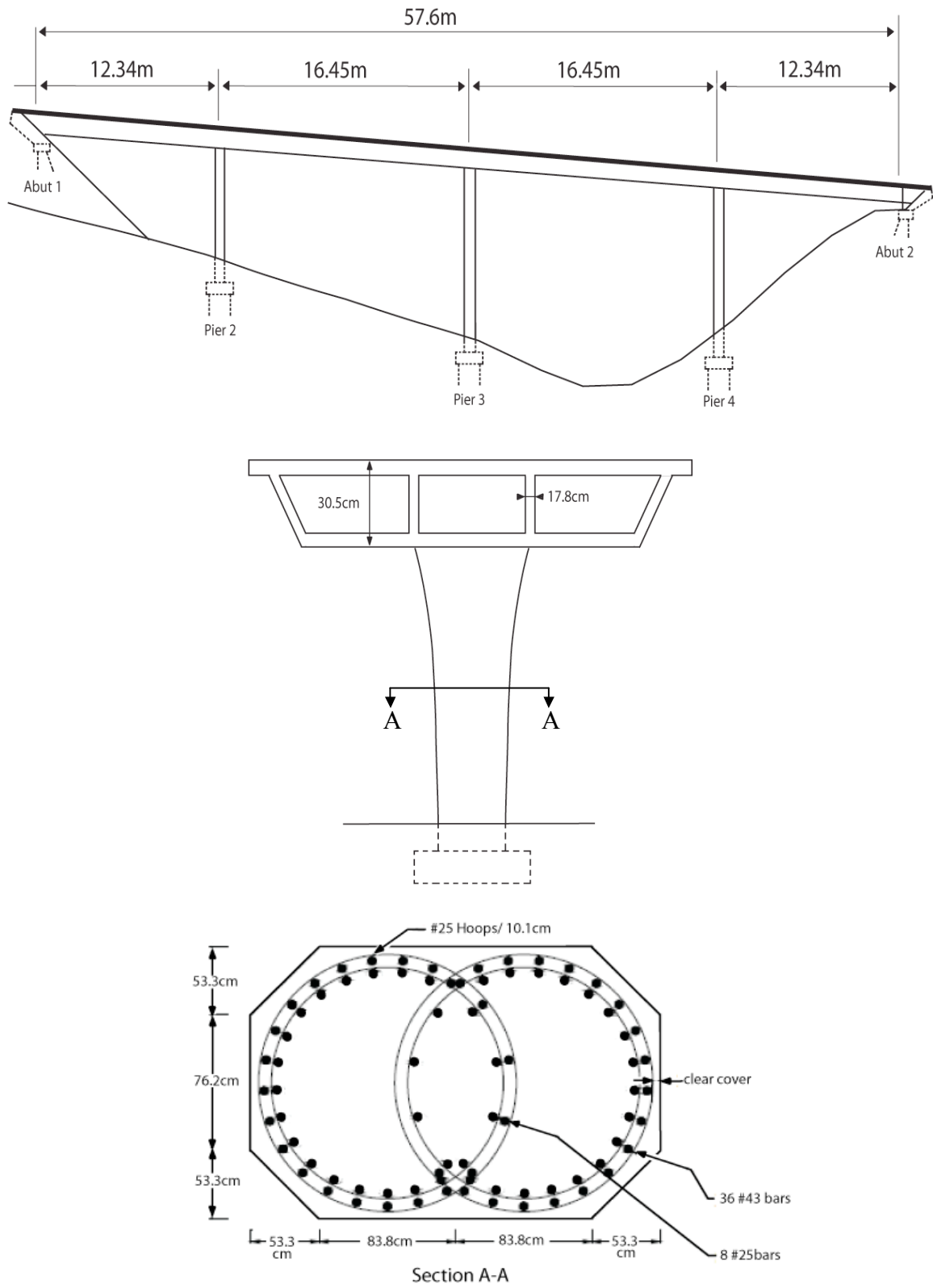


**Figure 8.4** Elevation, deck and column dimensions, and column section details of multi-span bridge.

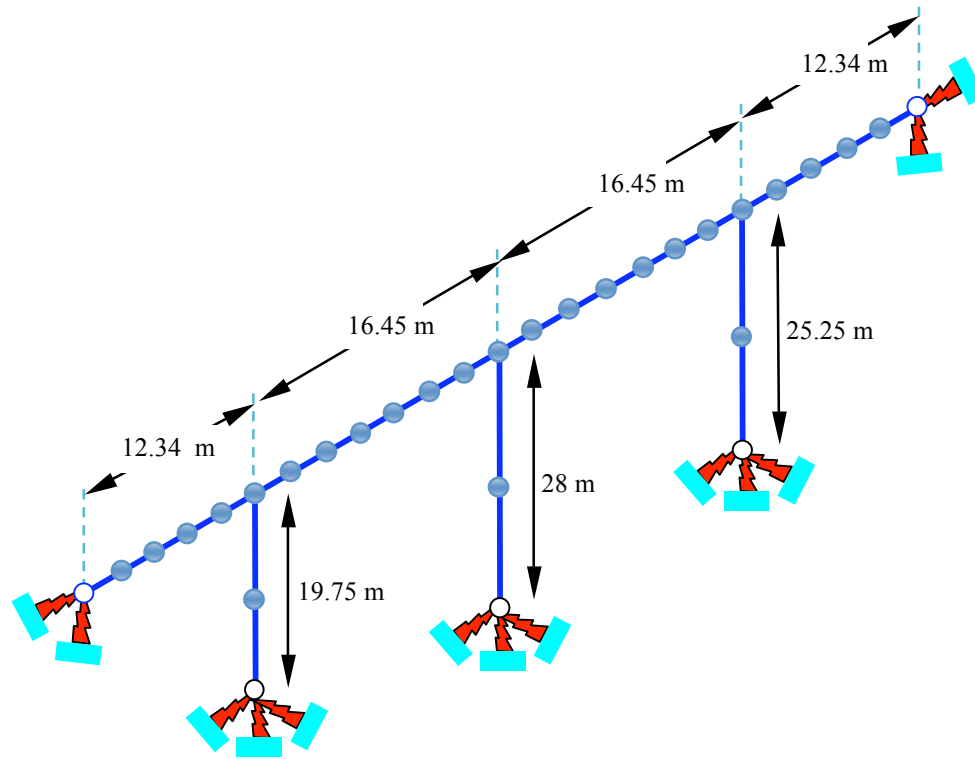


Figure 8.5 Computer model of multi-span bridge.

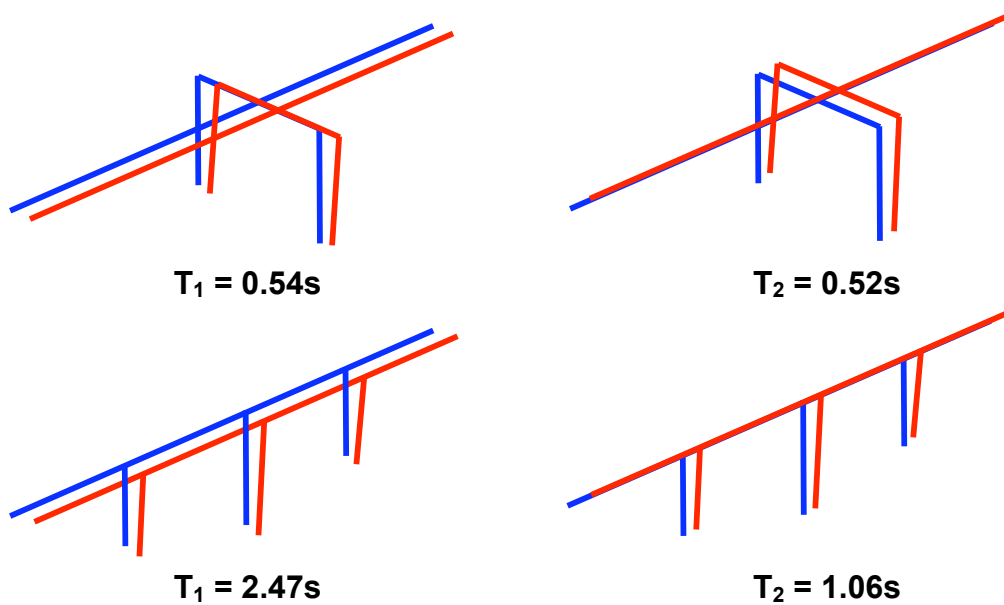
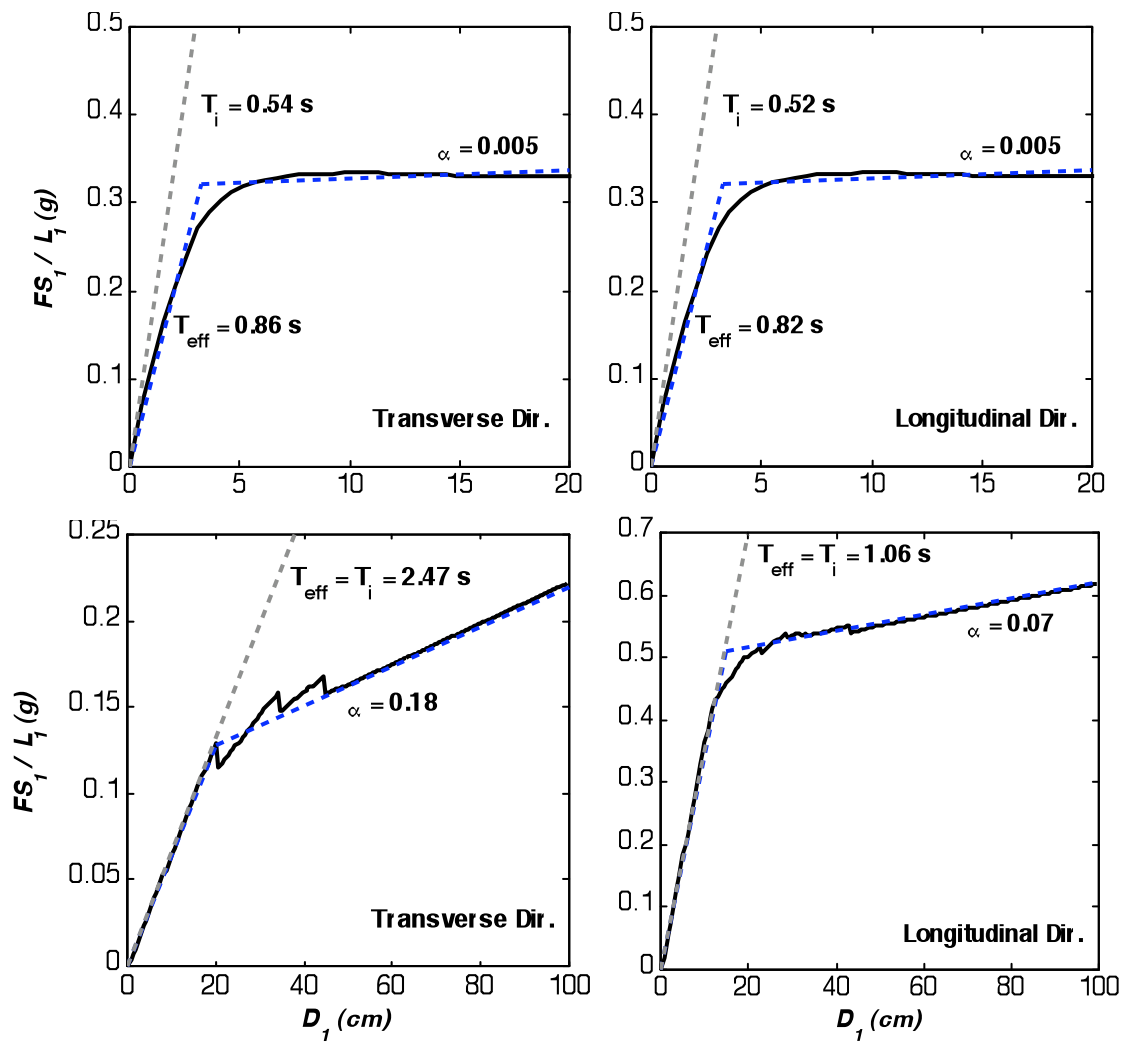
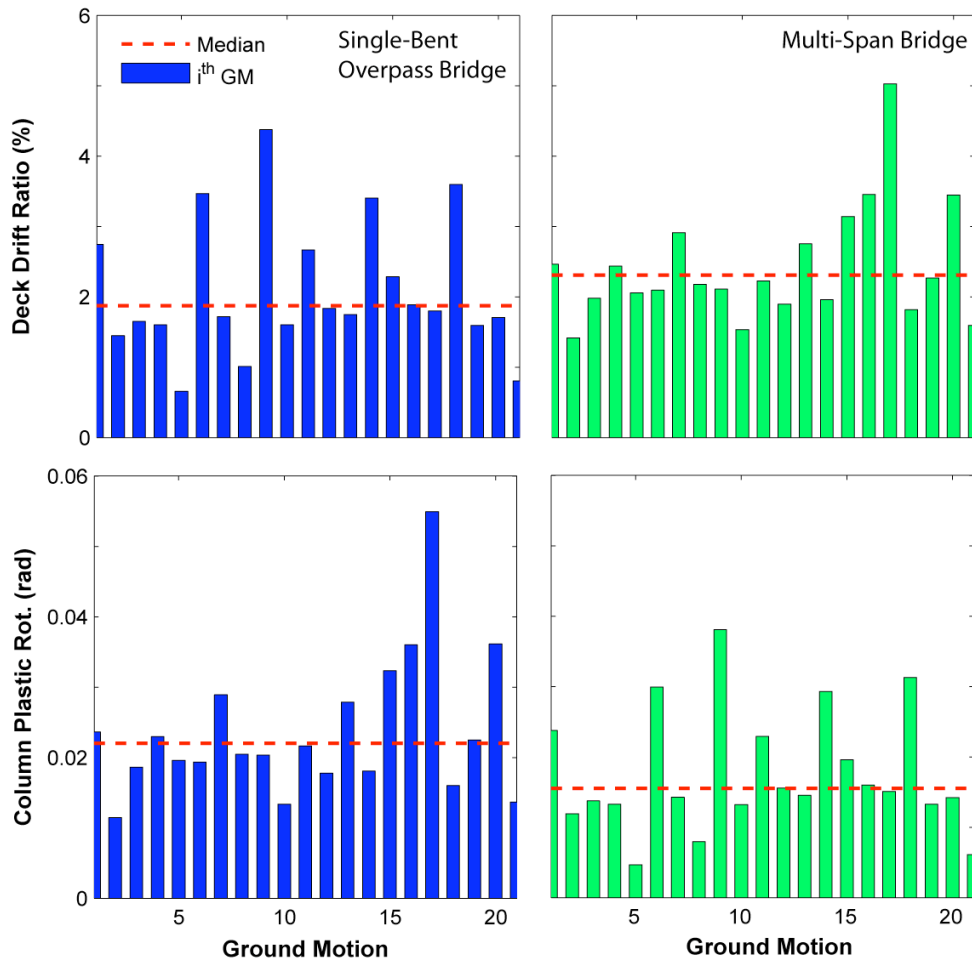


Figure 8.6 First two modes of vibration and their periods for single-bent overpass [top-row] and multi-span bridge [bottom-row].



**Figure 8.7** First-“mode” pushover curve (solid line) and its idealized bilinear model (dashed line) in transverse and longitudinal directions for single-bent overpass [top-panels]; multi-span bridge [bottom-panels].



**Figure 8.8** Median values of benchmark EDPs in transverse direction determined by nonlinear RHA of single-bent overpass [left-panels], multi-span bridge [right-panels] due to twenty-one ground motions; results for individual ground motions are also included.

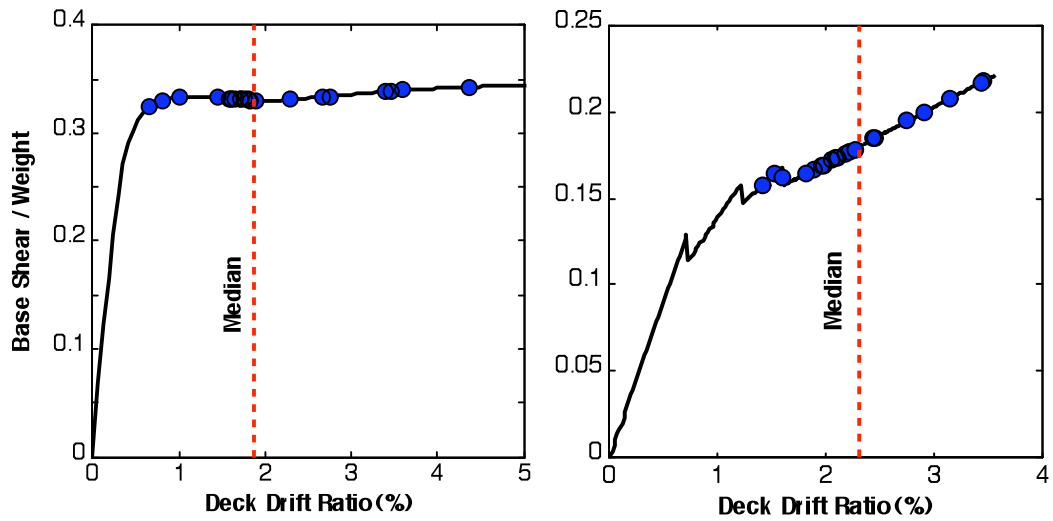


Figure 8.9 Deck drift ratios in transverse direction determined by nonlinear RHA of single-bent overpass [left] and multi-span bridge [right] for twenty-one ground motions identified on first-“mode” pushover curve.

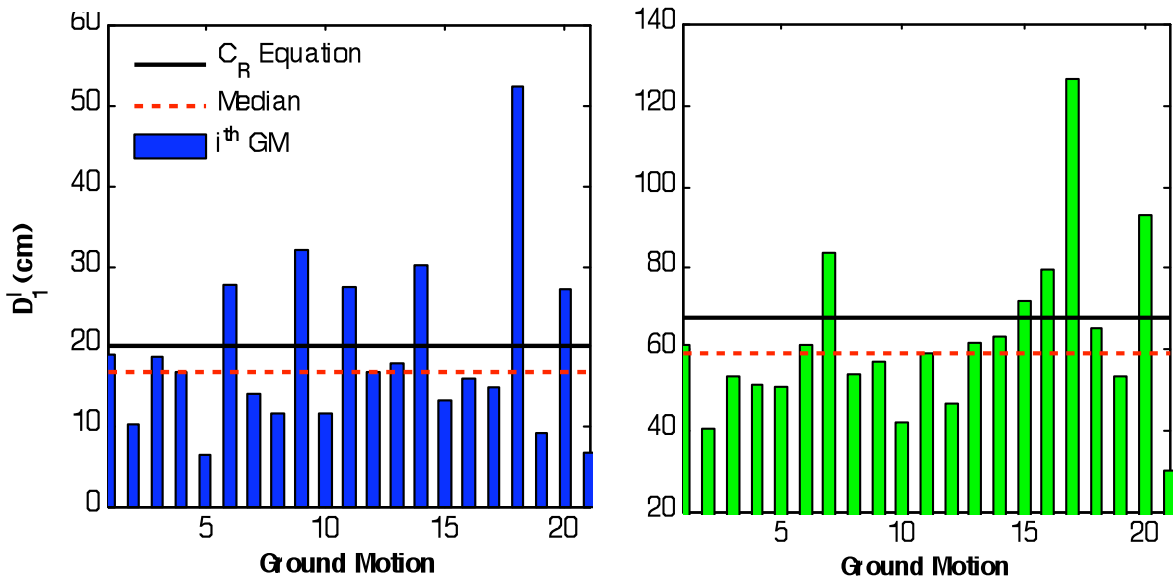


Figure 8.10 Peak deformation  $D_1^l$  values of the first-“mode” inelastic SDF system for twenty-one ground motions for single-bent overpass [left] and multi-span bridge [right]; “exact” target value of deformation  $\bar{D}_1^l$  is identified by horizontal dashed line; horizontal continuous line indicates target value of deformation  $\bar{D}_1^l$  established by  $C_R$  equation.

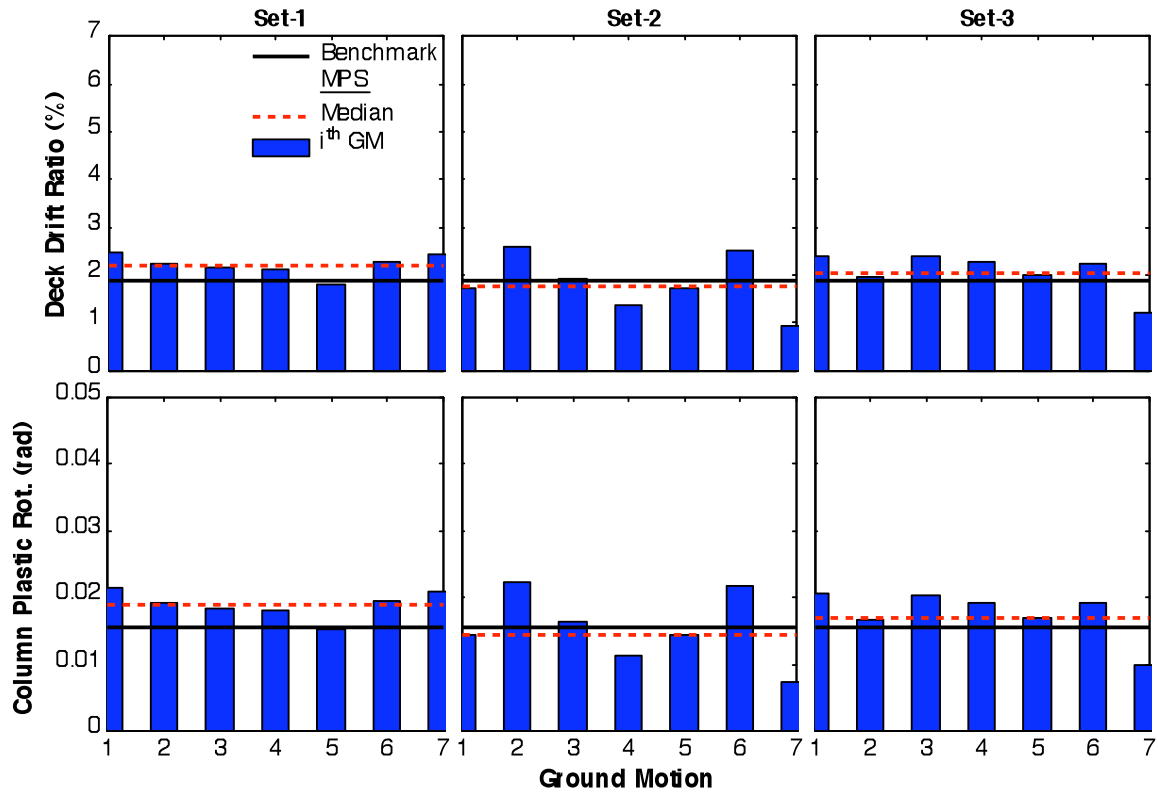


Figure 8.11 Comparison of median EDPs based on the MPS with benchmark EDPs for the single-bent overpass; individual results for each of the seven scaled ground motions are also presented.

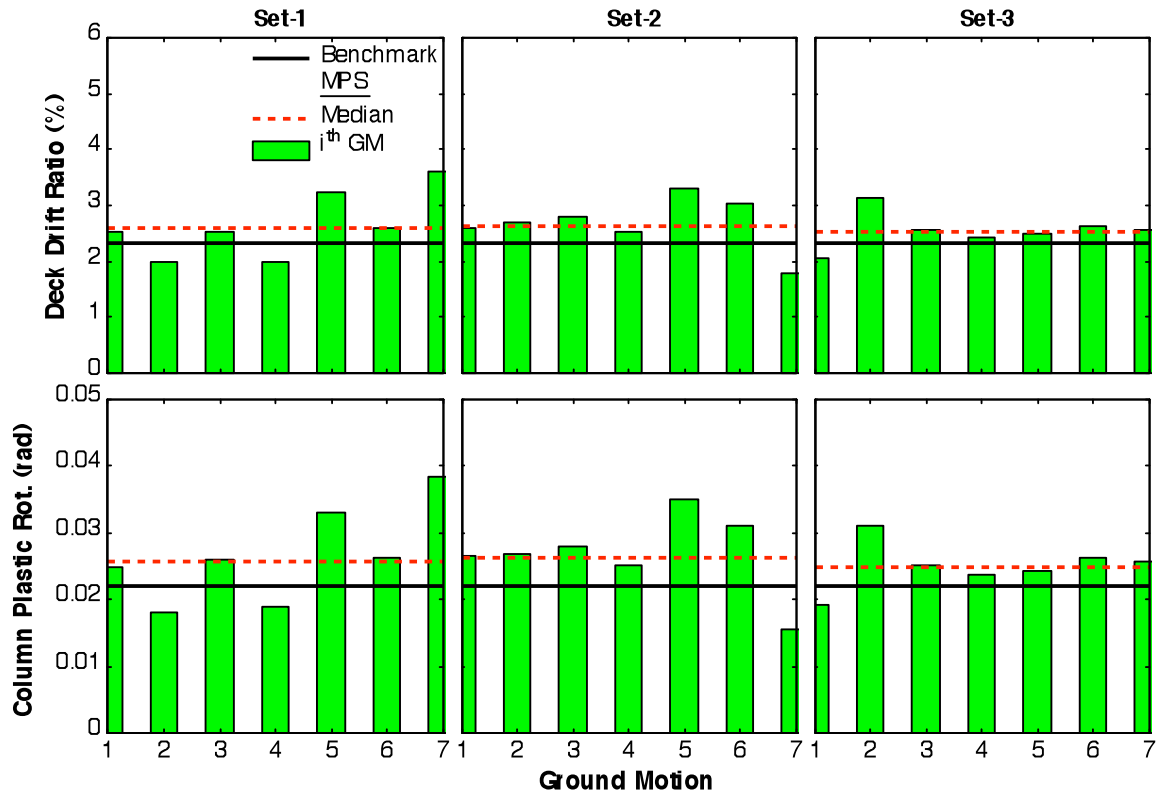


Figure 8.12 Comparison of median EDPs based on the MPS with benchmark EDPs for the multi-span bridge; individual results for each of the seven scaled ground motions are also presented.

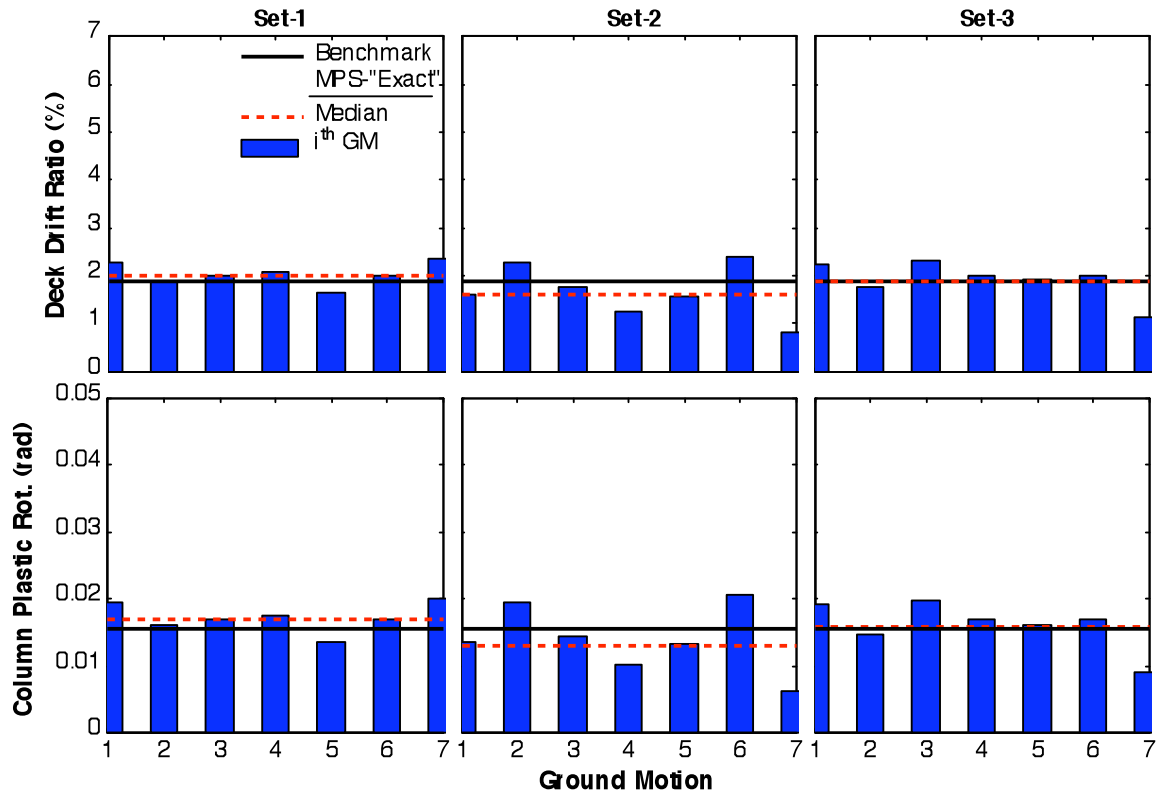


Figure 8.13 Comparison of median EDPs based on the MPS-“Exact” with benchmark for the single-bent overpass; individual results for each of the seven scaled ground motions are also presented.

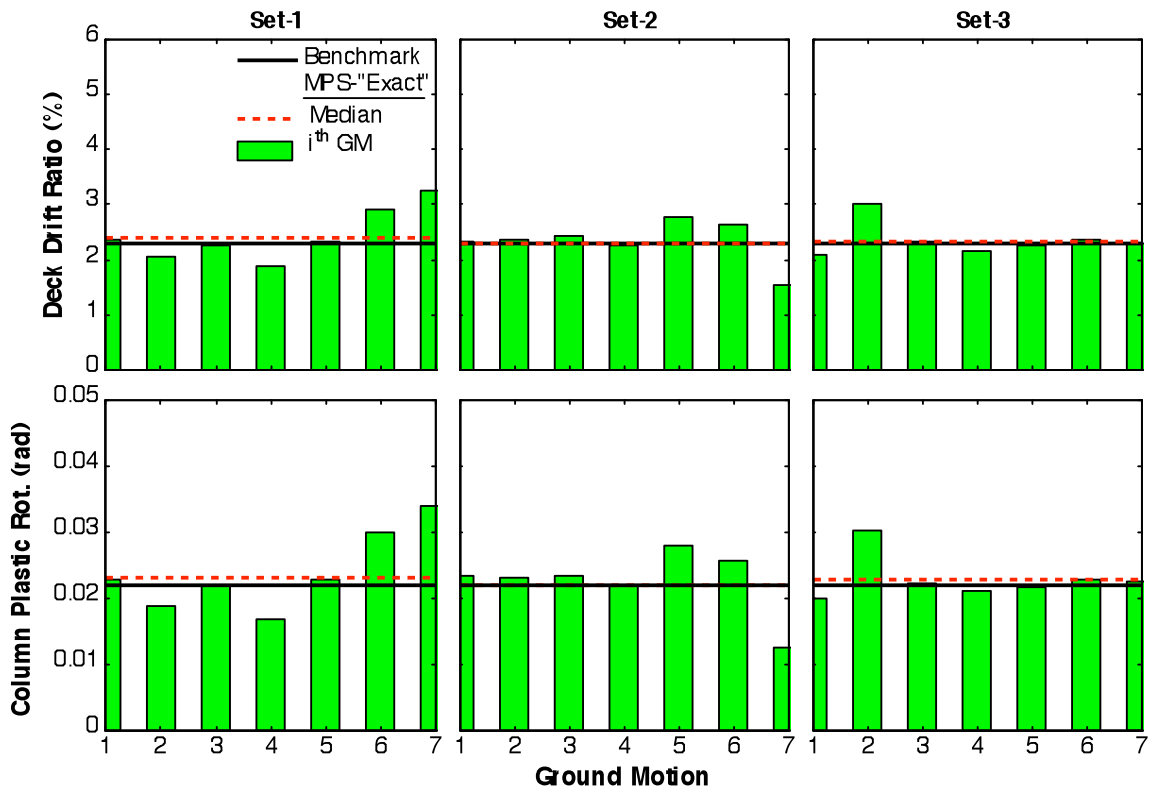


Figure 8.14 Comparison of median EDPs based on the MPS-‘Exact’ with benchmark EDPs for the multi-span bridge; individual results for each of the seven scaled ground motions are also presented.

## 9. SUMMARY & CONCLUSIONS

A modal-pushover-based scaling (MPS) method has been developed to scale ground motions for use in nonlinear response history analysis (RHA) of buildings and bridges. In the MPS method, the ground motions are scaled to match (to a specified tolerance) a target value of the inelastic deformation of the first-“mode” inelastic SDF system—its properties determined by first-“mode” pushover analysis—and the elastic deformation of second-“mode” SDF systems are considered in selecting a subset of the scaled ground motions to account for higher-mode effects.

Six building structures with a fundamental period ranging from 0.6 to 5.6 sec representing low-, mid-, and tall building types in California, as well as two bridges were utilized for testing the MPS procedure. For each structure, the median values of engineering demand parameters (EDPs) due to three sets of seven ground motions scaled by the MPS method were computed by nonlinear RHA and compared against the benchmark values of EDPs, determined by nonlinear RHA of the structure for twenty-one unscaled records. The ASCE/SEI 7-05 procedure was also applied to buildings in order to compare its performance in predicting the median EDPs and reducing their dispersion with the MPS procedure. Such comparison led to the following conclusions:

1. Even for the most intense near-fault ground motions, which represent severe tests, the MPS method estimates the median value of seismic demands to a good degree of accuracy (within 25% of the benchmark value). In contrast, the ASCE/SEI 7-05 scaling method overestimates the demand by 20 to 50% for 4-, and 6-story steel buildings, and its overestimation exceeds 50% for the 13-story building. For the 19-, and 52-story buildings, bias (overestimation or underestimation) associated with the ASCE/SEI 7-05 scaling method reaches over 25%; for the MPS, the bias remained under 20% except for the 52-story building for ground motion Set-3 which resulted in 25% of overestimation at certain floors. For bridges, the average discrepancy of 12% in deck drift ratios (relative to the benchmark values) is achieved by scaling seven records according to the MPS procedure. Maximum discrepancy is within 18% of the benchmark value for the single-bent overpass, and within 14% of the benchmark value for the multi-span bridge. These results demonstrate that the MPS procedure leads to scaled ground motions that yield accurate estimate of median EDPs.

2. The dispersion of responses due to ground motion scaled by the MPS method is much smaller compared to the ASCE/SEI 7-05 scaling method; in the latter method, dispersion is unacceptably large for some combinations of buildings and ground motions sets. Significant reduction of dispersion compared to the unscaled ground motions and ASCE/SEI 7-05 procedure indicates that the MPS procedure is efficient.
3. Using the “exact” value of target deformation, defined as the median deformation of the first-“mode” inelastic SDF system for a large ensemble of unscaled records determined by nonlinear RHA, leads to the most accurate and efficient version of the MPS method. Because this rigorous approach is not suitable for practical application, the target deformation may be estimated from the deformation of the corresponding linear system, available from the design spectrum, and empirical equations for the inelastic deformation ratio. The increase in bias and dispersion resulting from this approximation is small. The resulting practical version of the MPS method uses attenuation relations for elastic spectral ordinates that are currently available; new attenuation relations for inelastic spectral deformation are not required.
4. For first-“mode” dominated structures, scaling earthquake records to the target value of the inelastic deformation is sufficient in producing accurate estimates of median EDPs and in reducing the dispersion of EDPs due to individual ground motions. For mid-rise and tall buildings where higher vibration modes are known to contribute significantly to the seismic response, the MPS method requires an additional step to rank the scaled ground motions based on the closeness of the elastic deformation of second-“mode” elastic SDF systems to their target values. Selecting a subset of highest-ranked ground motions leads to a method that is more accurate and efficient for estimating seismic demands for taller buildings.
5. The ASCE/SEI 7-05 scaling method is seriously deficient if the records selected based on earthquake magnitude, distance and site geology are such that their scaled spectral acceleration at  $T_1$  and  $T_2$  significantly exceed the design spectrum values at these periods. However, the MPS procedure is effective in scaling even such records with spectral shape significantly different than the design spectrum.

This study has focused on developing the MPS method for scaling ground motions and its evaluation based on low-, mid-, and tall buildings in regular plan, and two “ordinary standard” bridges. In all models, stable force deformation relations were considered.

## 10. REFERENCES CITED

- Abrahamson, N.A., and Silva, W.J., 1997, Empirical response spectral attenuation relations for shallow crustal earthquakes: *Seismological Research Letters*, v. 68, p. 94-127.
- Alavi, B., and Krawinkler, H., 2000, Consideration of near-fault ground motion effects in seismic design: *Proceedings of the 12th World Conference on Earthquake Engineering*, Paper No. 2665, Auckland, New Zealand.
- Alavi, B., and Krawinkler, H., 2004, Behavior of moment-resisting frame structures subjected to near-fault ground motions: *Earthquake Engineering and Structural Dynamics*, v. 33, no. 6, p. 687-706.
- American Society of Civil Engineers, 2005, *ASCE/SEI 7-05 - Minimum design loads for buildings*: Reston, VA.
- American Society of Civil Engineers, 2007, *ASCE 41-6 Guidelines: Seismic Rehabilitation of Existing Buildings*: Reston, VA.
- Anderson, Journal, and Bertero, V.V., 1991, Seismic performance of an instrumented six-story steel building: *Earthquake Engineering Research Center, University of California, Berkeley*, Report no. 1991-11, 134 p.
- Báez, JournalI., and Miranda, E., 2000, Amplification factors to estimate inelastic displacement demands for the design of structures in the near field: *Proceedings of the Twelfth World Conference on Earthquake Engineering*: Paper No. 1561, Auckland, New Zealand.
- Baker, JournalW., and Cornell, A.C., 2006, Spectral shape, epsilon and record selection: *Earthquake Engineering and Structural Dynamics*, v. 35, no. 9, p. 1077-1095.
- Bazzurro, P., 1998, *Probabilistic Seismic Demand Analysis*: Ph.D. thesis, Dept. of Civil and Env. Engineering, Stanford University, CA. (Available online at <http://www.stanford.edu/group/rms/Thesis/index.html>; last accessed on 06/2008).

- Bazzurro, P., and Luco, N., 2004, Parameterization of Non-Stationary Acceleration Time Histories: Lifelines Program Project 1G00 Addenda, Pacific Earthquake Engineering Research (PEER) Center, University of California: Berkeley, CA, 83 p.
- Bazzurro, P., and Luco, N., 2006, Do scaled and spectrum-matched near-source records produce biased nonlinear structural responses: Proceedings of the 8th National Conference on Earthquake Engineering, Paper no. 1029, San Francisco, CA.
- Bolt B. A. and Gregor N. Journal, 1993, Synthesized strong ground motions for the seismic condition assessment of the eastern portion of the San Francisco bay bridge: Report UCB/EERC-93/12, University of California, Earthquake Engineering Research Center, Berkeley, CA.
- Bozorgnia, Y., and Mahin, S. A., 1998, Ductility and strength demands of near-fault ground structure-specific scalar intensity measures 389 motions of the Northridge earthquake: Proceedings of the 6th U.S. National Conference on Earthquake Engineering, Seattle, WA.
- Caltrans, 2006, Seismic Design Criteria: Version 1.4, California Department of Transportation, Sacramento, CA (Available online at <http://www.dot.ca.gov>; last accessed on 01/2010).
- Carballo Journal E. and Cornell C. A., 2000, Probabilistic seismic demand analysis: Spectrum matching and design: Department of Civil and Environmental Engineering, Stanford University, Report no. RMS-41.
- Chopra, A. K., 2007, Dynamics of structures: Theory and applications to earthquake engineering, Prentice Hall, Englewood Cliffs, N.J.
- Chopra, A. K., and Chinatanapakdee, C., 2004, Inelastic deformation ratios for design and evaluation of structures: Single-degree-of-freedom bilinear systems: Journal of Structural Engineering (ASCE), v. 130, no. 9, p. 1304-1319.
- Cordova, P. P., Deierlein, G. G., Mehanny, S. S. F., and Cornell, C. A., 2000, Development of a two-parameter seismic intensity measure and probabilistic assessment procedure: Proceedings of the 2nd U.S.-Japan Workshop on Performance-Based Seismic Design Methodology for Reinforced Concrete Building Structures, PEER Report 2000/10, Pacific Earthquake Engineering Research Center, University of California, Berkeley, CA.
- Goel, R.K., and Chopra, A.K., 2008, Estimating seismic demands for “ordinary” bridges crossing fault-rupture zones: Earthquake Engineering Research Center, University of California at Berkeley, Report no. UCB/EERC-2008/01.

- Graizer V., and Kalkan, E., 2009, Prediction of Response Spectral Acceleration Ordinates based on PGA Attenuation: *Earthquake Spectra*, v. 25, no. 1, p. 36 – 69.
- Gupta, B., and Kunnath, S.K., 1998, Effect of Hysteretic Model Parameters on Inelastic Seismic Demands. *Proceedings of 6th US National Conference on Earthquake Engineering*, Seattle, published by EERI.
- International Conference of Building Officials, 2006, *International Building Code*, Whittier, CA.
- International Conference of Building Officials, 2007, *California Building Code*, Whittier, CA.
- Krawinkler, H., and Al-Ali, A., 1996, Seismic demand evaluation for a 4-story steel frame structure damaged in the Northridge earthquake: *The Structural Design of Tall Buildings*, v. 5, no. 1, p. 1-27.
- Kennedy, R.P., Short, S.A., Merz, K.L., Tokarz, F. *Journal*, Idriss, I.M., Power, M.S., and Sadigh, K., 1984, Engineering characterization of ground motion-task 1: Effects of characteristics of free-field motion on structural response: NUREG/CR-3805, U.S. Regulatory Commission, Washington, D.C.
- Kurama, Y., and Farrow, K., 2003, Ground motion scaling methods for different site conditions and structure characteristics: *Earthquake Engineering and Structural Dynamics*, v. 32, no. 15, p. 2425-2450.
- Lew, M., Naeim F., Hudson M.B., Korin B.O., 2008, Challenges in Specifying Ground Motions For Design of Tall Buildings in High Seismic Regions of the United States, *Proceedings of the 14th World Conference on Earthquake Engineering*, Beijing, China.
- Luco, N., and Cornell, A.C., 2007, Structure-Specific Scalar Intensity Measures for Near-Source and Ordinary Earthquake Ground Motions: *Earthquake Spectra*, v. 23, no. 2, p. 357–392.
- Malhotra, P.K., 2003, Strong-Motion Records for Site-Specific Analysis: *Earthquake Spectra*, v. 19, no. 3, p. 557-578.
- Mander, Journal B., Priestley M.J.N and Park, R., 1998, Theoretical stress–strain model for confined concrete: *Journal of Structural Engineering (ASCE)*, v. 114, no. 8, p.1804–26.
- Mehanny, S.S.F., 1999, Modeling and Assessment of Seismic Performance of Composite Frames with Reinforced Concrete Columns and Steel Beams: Ph.D. thesis, Dept. of Civil and Env. Engineering, Stanford University, CA.
- Miranda, E., 1993, Evaluation of site-dependent inelastic seismic design spectra: *Journal of Structural Engineering (ASCE)*, v. 119, no. 5, p. 1319–1338.

- Naeim, F., Alimoradi, A., and Pezeshk, S., 2004, Selection and scaling of ground motion time histories for structural design using genetic algorithms: *Earthquake Spectra*, v. 20, no. 2, p. 413-426.
- Naeim, F., 1997, Performance of Extensively Instrumented Buildings during the January 17, 1994 Northridge Earthquake - An Interactive Information System, Report 7530.68/97, John A. Martin and Associates.
- Nau, Journal, and Hall, W., 1984, Scaling methods for earthquake response spectra: *Journal of Structural Engineering (ASCE)*, v. 110, no. 91-109.
- Neuenhofer, A., and Filippou, F.C., 1998, Geometrically nonlinear flexibility-based frame finite element: *Journal of Structural Engineering (ASCE)*, v. 124, no. 6, p. 704-711.
- OpenSees. Open Source finite element platform for earthquake engineering simulations, 2009. University of California Berkeley, Pacific Earthquake Engineering Center. (Available online at <http://OpenSees.berkeley.edu/>; last accessed on 06/2009).
- Petersen, M.D., Frankel, A.D., Harmsen, S.C., Mueller, C.S., Haller, K.M., Wheeler, R.L., Wesson, R.L., Zeng, Y., Boyd, O.S., Perkins, D.M., Luco, N., Field, E.H., Wills, C. J., and Rukstales, K.S., 2008, Documentation for the 2008 Update of the United States National Seismic Hazard Maps: U.S. Geological Survey Open-File Report 2008-1128, 61 p. (Available online at: <http://pubs.usgs.gov/of/2008/1128/>; last accessed on 06/2008).
- Power, M., Chiou, B., Abrahamson, N., and Roblee, C., 2006, The Next Generation of Ground Motion Attenuation Models” (NGA) project: An overview,” *in* Proceedings of the Eighth National Conference on Earthquake Engineering, Paper No. 2022, San Francisco, CA.
- Ruiz-Garcia, Journal, and Miranda, E., 2002, Inelastic displacement ratios for evaluation of existing structures: *Earthquake Engineering and Structural Dynamics*, v. 31, no. 3. p. 539-560.
- Silva W. and Lee K., 1987, State-of-the-art for assessing earthquake hazards in the United States; Report 24, WES RASCAL Code for Synthesizing Earthquake Ground Motions 1987. Miscellaneous Paper S-73-1: U.S. Army Engineer Waterways Experiment Station, Vicksburg, MS.
- Shome, N., and Cornell, A.C., 1998, Normalization and scaling accelerograms for nonlinear structural analysis: Prof. of the 6th U.S. National Conference on Earthquake Engineering, Seattle, WA.

- Shome, N., Cornell, C.A., Bazzurro, P., and Carballo, Journal E., 1998, Earthquakes, records, and nonlinear responses: *Earthquake Spectra*, v. 14, no.3, p. 469–500.
- Shome, N., and Cornell, C.A., 1999, Probabilistic Seismic Demand Analysis of Nonlinear Structures, Reliability of Marine Structures Program Report No. RMS-35, Dept. of Civil and Env. Engineering, Stanford University, CA. (Available online at <http://www.stanford.edu/group/rms/Thesis/index.html>; last accessed on 06/2009).
- Tothong, P., and Cornell, A.C., 2008, Structural performance assessment under near-source pulse-like ground motions using advanced ground motion intensity measures: *Earthquake Engineering and Structural Dynamics*, v. 37, no. 7, p. 1013-1037.
- Veletsos, A.S., and Newmark, N.M., 1960, Effect of inelastic behavior on the response of simple systems to earthquake motions: *Proceedings of the Second World Conference on Earthquake Engineering*, Tokyo, Japan, v. II, p. 895–912.
- Ventura, C.E. and Ding, Y., 2000, Linear and nonlinear seismic response of a 52-storey steel frame building: *The Structural Design of Tall Buildings*, v. 9, no. 1, p. 25-45
- Vidic, T. Fajfar, P., and Fischinger, M., 1994, Consistent inelastic design spectra: Strength and displacement: *Earthquake Engineering and Structural Dynamics*, v. 23, no. 5, p. 507-521.
- Youngs, R. Power, M., Wang, G., Makdisi, F., and Chin, C.C., 2007, Design Ground Motion Library (DGML) – Tool for Selecting Time History Records for Specific Engineering Applications (Abstract): SMIP07 Seminar on Utilization of Strong-Motion Data, p. 109 – 110. (Available online at [http://www.conservation.ca.gov/cgs/smip/docs/seminar/SMIP07/Pages/Paper8\\_Youngs.aspx](http://www.conservation.ca.gov/cgs/smip/docs/seminar/SMIP07/Pages/Paper8_Youngs.aspx); last accessed on 06/2008).

## 11. NOTATION

The following symbols are used in this report:

$a$	=	Parameter in empirical formula for $C_R$
$A$	=	Pseudo-spectral acceleration
$\bar{A}_n$	=	Target pseudo-spectral acceleration
$b$	=	Parameter in empirical formula for $C_R$
$c$	=	Parameter in empirical formula for $C_R$
$C_R$	=	Ratio of peak deformations of inelastic and corresponding elastic SDF systems for systems with known yield-strength reduction factor
$d$	=	Parameter in empirical formula for $C_R$
$\bar{D}_n$	=	Target value of nth mode elastic deformation
$\bar{D}_1^I$	=	First-“mode” target value of inelastic spectral displacement
$D_n(t)$	=	Deformation of a SDF system
$D_1^I$	=	Peak deformation of inelastic SDF system
$D_n$	=	Peak deformation of elastic SDF system
$D_{I,y}$	=	Yield deformation of inelastic SDF system
$F_{s1}$	=	System resisting force under first-“mode” pushover
$L_R$	=	Deformation ratio $C_R$ for zero-period system
$\mathbf{m}$	=	Mass matrix of a MDF system
$M$	=	Moment magnitude of earthquake
$M^*$	=	Effective modal mass
$n$	=	Mode sequence number
$R_y$	=	Yield-strength reduction factor
$R_{cl}$	=	Closest distance to co-seismic rupture plane
$\mathbf{s}_n^*$	=	Load vector of modal pushover analysis
$SF$	=	Ground motion scaling factor
$T_a$	=	Period defined in Newmark-Hall smooth design spectrum (fig. 4.5)
$T_b$	=	Period defined in Newmark-Hall smooth design spectrum (fig. 4.5)
$T_c$	=	Period separating the acceleration- and velocity-sensitive regions
$T_d$	=	Period separating the velocity- and displacement-sensitive regions
$T_e$	=	Period defined in Newmark-Hall smooth design spectrum (fig. 4.5)
$T_f$	=	Period defined in Newmark-Hall smooth design spectrum (fig. 4.5)
$T_n$	=	Elastic natural vibration period
$u_{r1}$	=	Roof displacement of a MDF system under first-“mode” pushover

$\ddot{u}_g$	=	Earthquake ground acceleration
$V_{b1}$	=	Base shear under first-“mode” pushover
$V_{b1y}$	=	Global yield strength under first-“mode” pushover
$V_{S30}$	=	Average shear-wave velocity within 30 m depth from surface
$\alpha$	=	Ratio of post-yield and initial stiffness
$\zeta$	=	Damping ratio
$\Gamma$	=	Modal participation factor
$\phi$	=	Mode shape
$\iota$	=	Influence vector
$\Delta$	=	Geometric mean
$\sigma$	=	Dispersion
$\Delta_n$	=	Norm used for ranking scaled records considering nth mode

## 12. APPENDIX A: COMPUTATION OF MINIMUM SCALE FACTOR

Although not explicitly stated in the ASCE/SEI 7-05 scaling procedure, it is desired to scale records with scale factors close to unity. To obtain a scale factor close to unity for each of seven records, residuals between the scaled spectrum of record and target spectrum is minimized between  $0.2T_I$  and  $1.5T_I$  through a method of least square whereby the square of sum of the residuals is expressed as

$$\lambda = \sum_{i=1}^n [\bar{A}_i - (SF \cdot A_i)]^2 \quad (\text{A.1})$$

in which  $\bar{A}_i$  and  $A_i$  are respectively the target spectral acceleration and record's (unscaled) spectral acceleration at  $i^{th}$  spectral period.  $n$  is the number of periods (log spaced) covered between  $0.2T_I$  and  $1.5T_I$ .  $SF$  is the scaling factor minimizing  $\lambda$ , that is,  $d\lambda / dk \cong 0$ ; and it is computed from

$$k = \left( \sum_{i=1}^n (x_i y_i) \right) / \left( \sum_{i=1}^n (x_i x_i) \right) \quad (\text{A.2})$$

Note that Eq. (A.2) yields an optimal scaling factor to ensure that the record's scaled spectrum matches closely the target spectrum between  $0.2T_I$  and  $1.5T_I$ . Occasionally, the average spectrum of seven scaled records may fall below the target spectrum in this period range and violates the ASCE/SEI 7-05 requirement. If this situation is encountered, each record needs to be further amplified with the same factor of the ratio of maximum difference.